JUUSO POHJOLA
BOROSILICATE SCAFFOLD PROCESSING FOR BONE TISSUE
ENGINEERING

Master of Science Thesis

ABSTRACT

Tissue engineering utilizes artificial porous structures, scaffolds, to temporarily replace parts of tissues or organs in order to enhance the healing process. Scaffolds for bone tissue repair should fulfill several structural, mechanical and chemical criteria. Bioactive glasses and biodegradable polymers are typical materials used in scaffold fabrication for bone tissue engineering. Bioactive glasses have remarkable biological performances but suffer from poor mechanical properties and processability. Whereas biodegradable polymers have a wide variety of processing options but generally have low strength and biological activity. In his study, borosilicate glasses were utilized to produce 3D scaffolds. In a first time, the aim was to produce mechanically strong scaffolds without significant crystalline phase which could lead to loss of bioactivity. The reactivity of the scaffolds in aqueous solution was studied in the light of the scaffolds´ morphologies. In a second time, the potential for developing porous glass/polymer scaffolds was investigated.

In this study, borosilicate glasses were under investigation and calcium was substituted by magnesium and/or strontium to enhance the hot working domain while providing therapeutic effect. Structures and thermal properties of the glasses were determined. Glass scaffolds were prepared via the porogen burn-off method and robocasting using sintering temperatures enabling viscous flow without significant crystallization. Composite scaffolds were produced using supercritical carbon dioxide processing by adding glass powder to poly(lactide-co-ε-caprolactone) matrix. The scaffolds´ morphologies, mechanical properties and *in vitro* behavior were analyzed.

Based on the results, it was concluded that both magnesium and strontium substitution enhanced the sinterability of the base glass but had a decreasing effect on reactivity. Utilized production methods yielded promising scaffold morphologies that seemed to be suitable for clinical applications. Robocasted scaffolds were found to have slightly higher reactivities than the scaffolds produced via porogen burn-off method, which was suspected to be due to higher interconnectivity of the pore network. Addition of glass particles into polymeric matrix was found to promote the polymer´s biological properties.

TIIVISTELMÄ

JUUSO POHJOLA: Luukudosteknologisten borosilikaattiskaffoldien valmistus
Tampereen teknillinen yliopisto
Diplomityö, 86 sivua, 20 liitesivua
Lokakuu 2017
Materiaalitekniikan diplomi-insinöörin tutkinto-ohjelma
Pääaine: Polymeerit ja biomateriaalit
Tarkastajat: Apulaisprofessori, akatemiatutkija Jonathan Massera, Tutkijatohtori Amy Nommeots-Nomm

Avainsanat: bioaktiivinen lasi, biohajoava polymeeri, *in vitro*, kiteytyminen, komposiitti, luukudosteknologia, sintraaminen, skaffoldi

Kudosteknologiassa hyödynnetään huokoisia rakenteita, skaffoldeja, korvaamaan väliaikaisesti vaurioituneita osia kudoksista tai elimistä paranemisen tehostamiseksi. Luukudosteknologiset skaffoldit joutuvat vastaamaan moniin rakenteellisiin, mekaanisiin ja kemiallisiin vaatimuksiin. Bioaktiiviset lasit ja biohajoavat polymeerit ovat yleisesti käytettyjä materiaaleja näissä sovelluksissa. Bioaktiivisilla laseilla on erinomaiset biologiset ominaisuudet, mutta ne kärsivät puutteellisista mekaanisista ominaisuuksista ja prosessoitavuudesta. Biohajoavia polymeerejä taas voidaan prosessoida monin eri menetelmin, mutta ne ovat yleisesti ottaen mekaanisesti heikkoja ja eivät biologisesti aktiivisia. Tässä työssä valmistettiin 3D-skaffoldeja borosilikaattilaseista. Tavoitteena oli tuottaa lujia skaffoldeja ilman kiteytymistä, joka voisi heikentää bioaktiivisuutta. Skaffoldien reaktiivisuutta vesiliuoksissa tutkittiin niiden rakenteen pohjalta. Lisäksi tutkittiin mahdollisuuksia valmistaa huokoisia lasi-polymeerikomposiitteja.

Työssä tutkittiin borosilikaattilaseja, joissa kalsiumia korvattiin osittain magnesiumilla ja/tai strontiumilla lämpökäsittelymahdollisuuksien ja terapeuttisten efektien parantamiseksi. Laseista tutkittiin niiden rakennetta ja termisiä ominaisuuksia. Lasiskaffoldeja valmistettiin hyödyntämällä huokoistusainetta tai 3D-tulostusta. Sintraus suoritettiin lämpötiloissa, jotka sallivat viskoosin virtauksen, mutta eivät johtaneet merkittävään kiteytymiseen. Komposiittiskaffoldeja valmistettiin ylikriittisellä hiilidioksidimenetelmällä lisäämällä lasijauheita poly(laktidi-ko-ε-kaprolaktoni) –matriiseihin. Skaffoldien morfologiaa, mekaanisia ominaisuuksia ja *in vitro* –käyttäytymistä tutkittiin.

Tulosten pohjalta voitiin päätellä, että magnesium ja strontium parantavat referenssilasin sintrautuvuutta mutta samanaikaisesti hidastavat sen reaktiivisuutta. Hyödynnettyjen prosessointimenetelmien avulla oli mahdollista tuottaa skaffoldirakenteita, jotka vaikuttivat sopivilta kliinisiin käyttökohteisiin. 3D-tulostettujen skaffoldien reaktiivisuus vaikutti olevan suurempi kuin huokoistusaineen avulla tuotettujen skaffoldien, minkä epäiltiin aiheutuvat suuremmasta huokoisten keskinäisestä yhdistymisestä. Lasipartikkelien lisääminen polymeerimatriisiin paransi polymeerin biologisia ominaisuuksia.

PREFACE

This study was conducted in Biomaterials and Tissue Engineering research group of the Institute of Biosciences and Medical Technology (BioMediTech) at the Tampere University of Technology. Part of the experiments were conducted in Structure-Property Relationship in Glasses group during a researcher exchange to Otto-Schott Institute of Materials Research of Friedrich Schiller University Jena, Germany.

I want to express my gratitude to Assoc. Prof, Academy Research Fellow Jonathan Massera for offering me a possibility to work in this interesting and meaningful project. In addition, I want to thank both him and Dr. Amy Nommeots-Nomm (the jolliest post-doc at TUT) for all their valuable guidance and insights regarding both the experimental and theoretical part of this work. I owe my lifetime gratitude to several colleagues for their support and help during this project. In no specific order, I hereby thank Jenna, Viivi, Henriikka, Inari and Ayush. In addition, the whole Biomaterials and Tissue Engineering research group has my gratitude for providing a pleasant and supportive working environment.

I also want to express my gratitude to Prof. Dr. Delia Brauer for providing a warm welcome to her research group during my researcher exchange. Thilo, Juliane and Roland deserve my honest thanks for helping me during my visit and for making it so pleasant.

My family and friends also deserve my thankfulness for their support and for showing interest in my studies and tasks. Most of all, I want to express my deepest gratitude to Salla for her endless support regarding all aspects of life.

Tampere, 19.10.2017

Juuso Pohjola

CONTENTS

APPENDIX A: SBF REAGENTS AND IONIC CONCENTRATIONS

APPENDIX B: DTA CURVES

APPENDIX C: TGA CURVES

APPENDIX D: ICP-OES RESULTS

APPENDIX E: FTIR SPECTRA

APPENDIX F: SEM IMAGES

LIST OF SYMBOLS AND ABBREVIATIONS

B	Boron
BO	Bridging oxygen
Ca	Calcium
CaO	Calcium oxide
CaP	Calcium phosphate
DTA	Differential thermal analysis
EDX	Energy dispersive X-ray spectroscopy
FDA	Food and Drug Administration
FTIR	Fourier transform infrared spectroscopy
H	Hydrogen
HA	Hydroxyapatite ($Ca_{10}(PO_4)_6(OH)_2$)
HSM	Hot-stage microscopy
Mg	Magnesium
Na	Sodium
Na_2O	Sodium oxide
NBO	Non-bridging oxygen
OH^-	Hydroxide ion
P	Phosphorus
PO_4^{3-}	Phosphate
P_2O_5	Phosphorus pentoxide
PGA	Polyglycolide
PCL	Poly(ε-caprolactone)
PE	Polyethylene
PEG	Poly(ethylene glycol)
PHBV	Poly(β-hydroxybutyrate-co-β-hydroxyvalerate)
PLA	Polylactide
PLCL	Poly(lactide-co-ε-caprolactone)
PLLA	Poly(L-lactide)
PDLLA	Poly(DL-lactide)
PLGA	Poly(lactide-co-glycolide)
PMMA	Poly(methyl methacrylate)
PU	Polyurethane
$scCO_2$	Supercritical carbon dioxide
SEM	Scanning electron microscope
Si	Silicon
SiC	Silicon carbide
SiO_2	Silica
Si-OH	Silanol
Sr	Strontium
Q^n	Number of bridging oxygen species in silicon tetrahedron
T_g	Glass transition temperature
TGA	Thermogravimetric analysis
TMC	Poly(trimethylene carbonate)
T_p	Crystallization peak temperature
T_x	Onset of crystallization temperature

1. INTRODUCTION

For a long time, grafts have been used to repair and replace tissues or organs that have been damaged or lost due to diseases, trauma or aging. However, the shortage of grafts and their possible adverse side effects such as pain, rejection and disease transmission are a major problem. Bone tissue engineering is an interdisciplinary field focusing upon the development of alternative methods of treatment. A common approach in tissue engineering is to guide and enhance tissue regeneration with an artificial porous three-dimensional construct, a scaffold. Scaffold can be implanted to the damaged site to replace the lost tissue. The aim of the scaffold is that the tissue grows inside the structure and simultaneously the scaffold degrades, leaving a naturally healed tissue to the implantation site. Tissue engineering approach can be very effective, but its complex nature puts serious demands on the materials and scaffold processing methods. (Rahaman *et al.* 2011; Burg *et al.* 2000).

Bioactive glasses were first discovered by Professor Larry Hench in 1969. Since then, they have gained great interest because of their ability to bond to both soft and hard tissue. They promote bone growth and healing through the formation of a hydroxyapatite (HA) layer that resembles the mineral phase of bones. However, the traditional silica based bioactive glasses are difficult to process with thermal processing methods without inducing extensive crystallization, which may limit their bioactivity and ability to sinter properly (Filho *et al.*1996; Massera *et al.* 2012a). In addition, bioactive glasses suffer from the same brittleness as normal glass materials. These undesirable properties have limited the commercial applications to granules and pastes. The thermal processing window and other properties, such as dissolution rate, can be improved by altering the composition of the commercially used 45S5 or S53P4 glasses. This has resulted in the extensive study of different substitutes such as boron (B), magnesium (Mg) and strontium (Sr). (Fu *et al.* 2011a; Massera & Hupa 2014; Jones 2013).

Biodegradable polymers are a diverse class of polymeric materials with great variation in properties, which has made them suitable for several biomedical applications such as plates, screws and drug delivery devices. They can possess excellent processing characteristics but their use is limited due to the lack of bioactivity and low strength. The limitations of a single material type can be overcome by fabricating composite structures, which combine the desired properties of different materials. For instance, by embedding bioactive glass particles to a biodegradable polymer matrix, a strong and bioactive material can be obtained. (Nair & Laurencin 2007; Rich *et al.* 2002).

In this thesis, a previous study (Tainio 2016) is continued. Tainio´s work showed that the substitution of boron, magnesium and strontium for the original components of the S53P4 glass was found to improve the glass hot forming region, thus resulting in glasses that seemed to be suitable for scaffold production. In this study, bioactive glasses from the previously studied compositions are used to fabricate 3D scaffolds via different processing methods. In addition, pertaining to the beneficial effect of bioactive glasses on cell behavior, composite scaffolds are also produced. The scaffold performance are then tested *in vitro*. The purpose of this study is to further evaluate the processability of previously studied glass compositions and reveal the effects of different fabrication methods on the scaffold structure and dissolution *in vitro*. If scaffolds with promising properties and structures are proven possible to be manufactured, this study can have an important contribution to the development of bioactive glass and/or composite scaffolds for bone tissue engineering.

2. THEORETICAL BACKGROUND

This chapter presents the necessary background information for understanding the science behind this thesis and reason for its importance. First, the biological aspect of bones and their common treatments are presented. Then an alternative approach of tissue engineering is introduced and the possibilities and limitations related to it are considered.

2.1 Bone tissue engineering

The inadequacy of current orthopedic treatments causes economical, technical and ethical issues. This has given rise to an interdisciplinary field called tissue engineering which focuses on finding alternative methods that could overcome the limitations of current conventional treatments. (Sultana 2013, p. 1; Jones 2013).

2.1.1 Anatomy and physiology of bone

Human skeletal system contains over 200 bones. Together they provide structural support, protect organs and enable locomotion. Bones also contain bone marrow and store calcium and phosphate ions. (Amini *et al.* 2012; Florencio-Silva *et al.* 2015). Depending on the location in the body, as well as on the lifestyle and age of a person, there are structural and compositional differences between bones. In general, bone is a connective tissue that consists of calcium phosphate mineral (mainly hydroxyapatite), organic matrix, cells and water. The mineral hydroxyapatite, with the chemical formula $Ca_{10}(PO_4)_6(OH)_2$, accounts for around 65 % of the weight of the bones and gives bone its rigidity. The organic matrix, which makes around 25 % of the weight, is mainly composed of type I collagen and provides elasticity and tensile strength. The remaining 10 % of bone weight is water, which enhances the toughness. (Hollinger *et al.* 2004, p. 92; Ralston 2013; Olszta *et al.* 2007).

Bone tissue can be categorized into two groups; cortical and trabecular bone (Amini *et al.* 2012). Cortical bone is dense and forms the outer lining of all bones. It is formed from cylindrical structures called Haversian systems, which contain blood vessels and are aligned parallel to the bone axis. Trabecular bone, also called cancellous bone or spongy bone, has a porous structure with open interconnected pores larger than 500 μm in size (Jones 2013). High porosity gives trabecular bone lower density but higher surface area with respect to cortical bone. It is present in the entire inner portion of ribs and vertebrae, but also forms parts of other bones, such as the epiphyses of long bones. (Reznikov *et al.* 2014). The empty spaces within the interconnected network of bony trabeculae are filled with bone marrow. The structure of bone is illustrated in Fig. 1. (Ralston 2013).
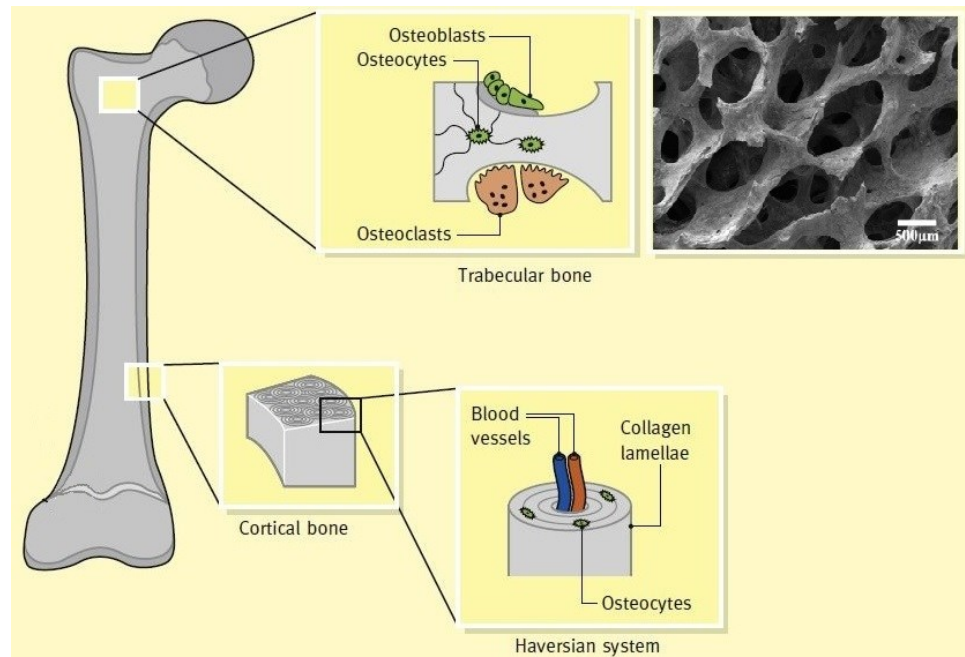
Figure 1. *Structure of cortical and trabecular bone and their common locations. Modified from (Ralston 2013, Fu et al. 2009).*

Structural and compositional differences between cortical and trabecular bone result in significantly different mechanical properties, which are summarized in Table 1. For example, trabecular bone contains less mineral than cortical bone, which accounts for lower Young´s Modulus (Hollinger *et al.* 2004, p. 93). (Fu *et al.* 2011a; Reznikov *et al.* 2014).

Table 1. *Characteristic mechanical properties of bone (Fu et al. 2011a).*

Property	Cortical bone	Trabecular bone
Compressive strength (MPa)	100–150	2-12
Flexural strength (MPa)	135–193	10–20
Tensile strength (MPa)	50–151	1–5
Young´s Modulus (GPa)	10–20	0.1–5
Fracture toughness (MPa·m$^{1/2}$)	2–12	0.1-0.8
Porosity (%)	5–10	50–90

Bone remodels constantly throughout life and has remarkable capability to repair itself (Zreiqat *et al.* 2015, p. 120). Remodeling is a process in which old bone is being replaced by new. It occurs when bone adapts to mechanical stresses but also as a part of growing, healing and calcium homeostasis. The dominant cellular components in remodeling are osteoclasts and osteoblasts, which are also presented in Fig. 1. (Hollinger *et al.* 2004, p. 55). Both rise from stem cell precursors as a response to hormones and other regulatory molecules such as growth factors. Remodeling begins when osteoclasts arrange to form a tight layer over the bone surface and secrete hydrochloric acid and enzymes that cause bone resorption. After sufficient level of resorption is reached, osteoclasts detach from

bone surface and go through a programmed cell death called apoptosis. New bone material is formed by osteoblasts when they migrate to the resorbed site and start depositing organic bone matrix, which later calcifies and forms mineralized bone. Osteoblasts become entrapped within the matrix and differentiate to osteocytes that connect to each other via cytoplasmic processes and to cells on the bone surface. When deposition of bone matrix ends, the osteoblasts remaining on bone surface become bone lining cells. Bone lining cells function in osteoblast differentiation and protect bone surface from unwanted resorption. (Ralston 2013; Florencio-Silva *et al.* 2015).

When osteoclast and osteoblast activity is in balance, bone remodels normally without mass loss or gain. Continuous imbalance between these processes leads to abnormal bone remodeling and is a characteristic feature in numerous diseases. For example, osteoporosis and osteoarthritis lead to excessive bone resorption. Local increased resorption may also cause bone metastases (Ralston 2013). When these defects are substantial, the body´s healing capacity may be exceeded and medical treatments are required. (Hollinger *et al.* 2004, p. 55; Zreiqat *et al.* 2015, p. 120).

2.1.2 Conventional medical treatments

Bone is, after blood, the most transplanted tissue. Need for bone repair and regeneration may arise from diseases, traumas, tumor removal or aging. (Jones 2013). In 2011, there were over 6 million bone fractures, 10 % of which suffered from incomplete recovery, and 10 million people suffering from osteoporosis in the United States alone. Conventionally severe defects have been treated using grafts and it is estimated that there are 2.2 million bone graft procedures performed around the world annually. (Fu *et al.* 2011).

There are two common approaches for bone grafting. Autologous bone tissue is harvested from the patient, usually from the pelvis. The limited supply of tissue available brings a significant limitation to the autograft procedure. Other major drawbacks are donor site pain and possible morbidity. Another option is to use allografts, which are osseous tissues taken from another individual and transferred to the patient. This approach may provide additional tissue but, in addition to high costs, bears risks related to disease transfer and adverse immunological responses. Bone cements as space filling agents have also been used but they possess contamination risks. (Burg *et al.* 2000; Fu *et al.* 2011a; Zreiqat *et al.* 2015, p. 169).

Synthetic bioinert materials, which often are metals and polymers, are widely available and have been used to replace or fix tissues. However, they are not well tolerated in the body and may trigger chronic inflammation, which eventually results in the formation of a fibrous tissue capsule around the implant as body tries to isolate and remove it. The fibrous capsule is typically not tightly bonded to the material and thus the lack of stable interface hinders the performance of the implant. (Kasper *et al.* 2012, p. 133). Their inert

nature and lack of bonding with tissue may result in need for revision surgeries and implant removals, which brings additional costs and further discomfort to patient. (Jones 2013; Nair & Laurencin 2007). Mechanical properties of the materials commonly used in orthopedic applications also do not match with the properties of bone. This mismatch may limit the use of e.g. some polymers in load-bearing applications or in the case of metals, lead to stress shielding and deterioration of the tissue. (Fu *et al.* 2011; Burg *et al.* 2000).

2.1.3 Tissue engineering approach

Tissue engineering, in the field of regenerative medicine, tries to overcome the problems of conventional treatments through a different approach; by combining materials science, biology and biochemistry. Understanding the structure and function of tissues forms the basis of tissue engineering (Sultana 2013, p. 1). This knowledge is used to design porous and biodegradable three-dimensional constructs, scaffolds, which mimic the structure and properties of the tissues that are being replaced. When implanted to the defect site, scaffolds guide cell growth and temporarily supports the tissue until healing is complete. (Fu *et al.* 2011a)

The repair and regeneration of tissues can further be enhanced by growing cells within the scaffold prior to implantation and by embedding biomolecules such as growth factors into the scaffold. In the case of bone regeneration, growth factors may e.g. induce osteoblast differentiation and proliferation. (Rahaman *et al.* 2011; Kasper *et al.* 2012, p. 264–267). The concept of tissue engineering relies on inducing the body´s own healing mechanisms to repair the damages and, because of the biodegradable nature of the scaffold, eventually result only in naturally healed tissue. In addition to bone, other tissues such as skin and cartilage have also been regenerated. (Fu *et al.* 2011a; Jones 2013).

2.2 Materials in tissue engineering

Biomaterials are defined as materials that are intended to interface with biological systems to evaluate, treat, augment or replace any tissue, organ or function of the body (Nair & Laurencin 2007). It is essential that a biomaterial used in tissue engineering is also biocompatible. Biocompatibility is the ability of a material to perform its function without inducing any adverse side effects (Kasper *et al.* 2012, p. 118). In a narrower sense, it can be understood as the capability to support normal cellular activity without causing any negative local or systemic side effects such as cytotoxicity, cell death. Biocompatibility does not require the material to be degradable and thus inert bioceramics and some metals such as titanium are regarded as biocompatible materials too. (Velasco *et al.* 2015; Barone *et al.* 2010).

Biodegradability is desired in tissue engineering scaffolds and is one of the most crucial requirements when suitable materials are chosen. It differs from bioresorbability due to

the differences in its degradation products. Whereas biodegradation only requires the material to be broken down into smaller molecules and fragments through biological activity, bioresorption requires that the degradation products must be eliminated from the body through metabolism. (Hutmacher 2000). Even though both bioresorbability and biodegradability are used to describe scaffold materials, these terms are often used interchangeably. Several different bioresorbable materials have been used in bone tissue engineering and they include e.g. bioactive glasses and biodegradable polymers. (Velasco *et al.* 2015; Rahaman *et al.* 2011; Barone *et al.* 2010; Tomlins 2016, p. 2).

2.2.1 Bioactive glasses

Professor Larry Hench invented the first bioactive glass in 1969 after being encouraged to develop a material that would be tolerated by the human body in an improved manner compared to traditional implant materials. Hench designed a resorbable glass with a composition of 46.1 % SiO_2, 24.4 Na_2O %, 26.9 % CaO and 2.6 % P_2O_5 in mol-%. The glass was named 45S5 and later trademarked with a name Bioglass®. It was observed that the glass implant could bond so strongly with rat bone that when it was tried to be removed, the bone broke. (Jones 2013). Material´s ability to induce certain biological responses that result in the bond formation between the material and host tissue is thus defined as bioactivity. Bioactive materials can be divided to Classes A and B depending on their level of bone growth promotion. Class B bioactive materials promote bone growth only along the bone-implant interface, representing a property called osteoconductivity. In addition to being osteoconductive, bioactive glasses may also be osteoinductive Class A biomaterials which induce bone growth away from the interface to areas where bone normally is not present. (Ylänen 2011, p. 16). Hench´s discovery launched the research of bioactive ceramics, under which bioactive glasses are also categorized. (Gerhardt & Boccaccini 2010; Rahaman *et al.* 2011).
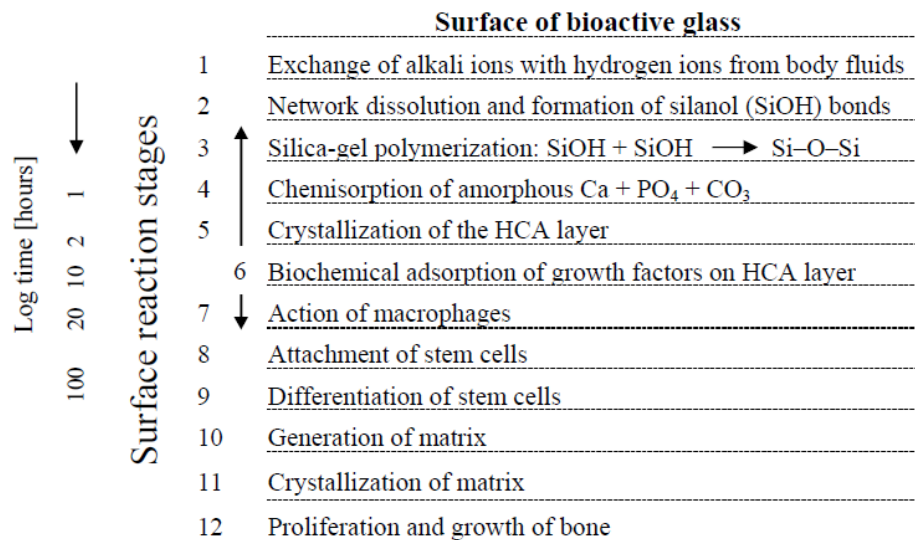
Traditional soda-lime silicate glasses consist of an amorphous three-dimensional SiO_2 network, which makes them chemically durable and biologically inert. By lowering the silica content and adding high amounts of glass network modifiers such as Na and Ca, it was possible to reduce the durability of the glass and make it degradable. In addition, high CaO/P_2O_5 ratio was required for the 45S5 glass to be bioactive. (Rahaman *et al.* 2011). Sodium and calcium as glass network modifiers disrupt the silica network by forming so-called non-bridging oxygen (NBO) species, charge balanced by the cations, as presented in Fig. 2. Increase in the amount of NBO species results in lower glass network connectivity and increased reactivity as the number of silicon-oxygen bridges decreases. Phosphorus acts as a network former by, like silicon, forming bonds with multiple oxygen atoms. (Ylänen 2011, p. 3, 4, 17). Silicon atoms in the network are present as tetrahedra and can be described by the Q^n species, where *n* presents the number of bridging oxygen (BO) connected to the silicon. By increasing the amount of alkali and alkali-earth oxides, the initial Q^4 species are converted to Q^3, Q^2 and Q^1. (Jones 2013; Serra *et al.* 2002)
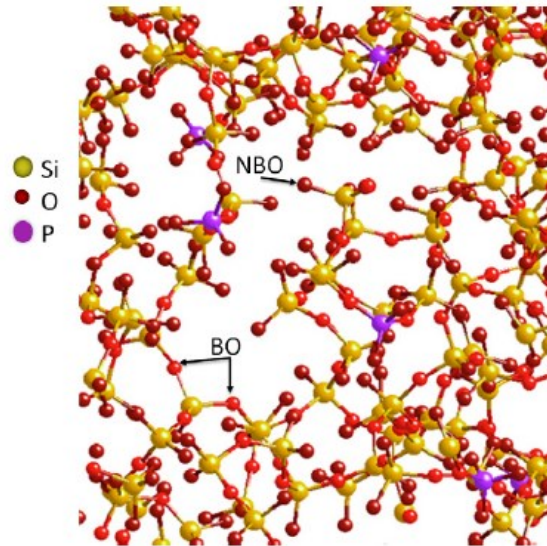
Figure 2. *Molecular structure of bioactive glass network. Network modifiers, which are not illustrated for clarity, cause the formation of non-bridging oxygen (NBO) species whereas the silica-rich network is composed mainly of bridging oxygen (BO) species. (Jones 2013).*

It is proposed that when bioactive glass is immersed to aqueous solution, the material surface goes through exchange of Na^+ ions with H^+ ions from the solution and then leaching of Ca^{2+} and soluble silica. This exchange creates silanol (Si-OH) bonds to material´s surface. This causes an increase in the pH of the solution, i.e. increase in the hydroxide ion (OH^-) concentration. The formed hydroxide ions cause further breakage of the silica bonds, resulting in dissolution of silica as silicic acid ($Si(OH)_4$) and condensation of silanol species. The silica network then repolymerizes into an as amorphous network rich in silica often called "silica gel". Ca^{2+} and PO_4^{3-} ions released into the environment and the ones migrating from the remaining glass to the surface, cause supersaturation in the local media, which leads to precipitation of an amorphous calcium phosphate layer to the glass surface. Hydroxide and carbonate (CO_3^{2-}) ions from the solution are incorporated to the calcium phosphate layer, which crystallizes and transforms to hydroxycarbonate apatite (HCA) layer. (Rahaman *et al.* 2011; Jones 2013; Ylänen 2011, p. 16).

The formed HA layer, at the surface of the bioactive glass, resembles the bone mineral phase and is responsible for the material bioactivity and its bonding to hard tissue. Proteins from physiological fluids adsorb to the layer and allow attachment of osteoprogenitor cells, which proliferate and differentiate to bone matrix-depositing osteoblasts. The biological response and glass behavior is further clarified in Fig. 3, which also illustrates the timeframe of actions taking place. New bone is formed as the material degradation proceeds and ideally the bone formation rate should match the degradation rate of the glass. In an ideal situation, all glass should be degraded and replaced by bone. (Rahaman *et al.* 2011).

Surface of bioactive glass

	Log time [hours]	Surface reaction stages		
			1	Exchange of alkali ions with hydrogen ions from body fluids
			2	Network dissolution and formation of silanol (SiOH) bonds
			3	Silica-gel polymerization: SiOH + SiOH $\longrightarrow$ Si–O–Si
	1		4	Chemisorption of amorphous Ca + PO_4 + CO_3
	2		5	Crystallization of the HCA layer
	10		6	Biochemical adsorption of growth factors on HCA layer
	20		7	Action of macrophages
			8	Attachment of stem cells
	100		9	Differentiation of stem cells
			10	Generation of matrix
			11	Crystallization of matrix
			12	Proliferation and growth of bone

Figure 3. *Surface reactions of bioactive glass and biological response to the HA layer formation. (Gerhardt & Boccaccini 2010).*

The bioactivity of a glass is traditionally studied *in vitro* by immersing materials in TRIS buffer solution or simulated body fluid (SBF). SBF is a buffer solution possessing similar ionic compositions to human blood plasma. The formation and rate at which a HA layer is formed is usually taken as an indication of the bioactivity of the material. (Ylänen 2011, p. 17).

The most commonly used bioactive glasses in biomedical applications are melt-derived (Rahaman *et al.* 2011). Their preparation involves mixing high purity raw materials, most commonly carbonates, and melting them in a furnace, typically at temperatures between 1000 and 1550 °C. Melting time varies with respect to material chemistry and batch size but commonly range between 1 and 24 hours. (Ylänen 2011, p. 6). Melting is followed by forming and shaping processes that are chosen according to the final application. Bioactive glasses are often casted and then annealed to relieve the residual stresses caused by rapid cooling. Glass can also be quenched in water in order to obtain a frit when only glass particles are needed. (Kasper *et al.* 2012, p. 200; Jones 2013).

Another glass manufacturing method is sol-gel processing, which is a chemistry-based route, involving condensation and gelation reactions of metal alkoxide raw materials. The formed gel is essentially wet silica network, which is converted to glass upon heating and drying. (Kasper *et al.* 2012, p. 201). The drying step can induce cracks to glass monoliths bigger than 1 cm in size and it is a great disadvantage when compared to melt-derived glasses. However, the sol-gel process can be conducted at room temperature and it is also a versatile process which can be modified by controlling the process chemistry. The sol-gel derived glasses are typically nanoporous, which increases their reactivity but also decreases the mechanical properties (Rahaman *et al.* 2011). Because of the high surface area, the total silica content of sol-gel- derived glasses can be as high as 90 % without the

loss of bioactivity whereas melt-derived glasses become biologically inert if their silica content is over 60 %. (Jones 2013).

Scaffold production from melt-derived bioactive glasses is achieved through sintering of glass particles. During sintering, particles are heated above their glass transition temperature (T_g) which induces local viscous flow of the glass and fuses the particles together. The process is driven by the reduction of the surface energy. (Jones 2013). Sintering starts with neck formation between adjacent particles and is followed by neck growth and densification of the structure, as illustrated in Fig. 4. (Ertuğ 2013, p. 92, 93).

Figure 4. *Illustration of sintering process. Based on (Ertuğ 2013, p. 93).*

Sintering must be conducted below the crystallization temperature (T_p) if an amorphous product is desired. The sintering window is defined as the temperature difference between the onset of crystallization (T_x) and glass transition temperature T_g, meaning that a wider sintering window is believed to favor thermal processing without crystallization. (Rahaman *et al.* 2011). Sintering temperature should be high enough to give the sintered object sufficient mechanical properties but at the same time the temperature should be limited to avoid extensive crystallization. Another important factor to be considered is the particle size. The specific surface area increases when particle size is decreased, resulting in more efficient sintering. However, one should keep in mind that typical bioactive glasses exhibit surface crystallization and such crystallization is further enhanced when the surface are to volume of particles ratio increases, due to an increase in the density of nucleation sites (Massera *et al.* 2012a; Ray *et al.* 1996; Fabert *et al.* 2017; Massera *et al.* 2015). This leads to need for a compromise. (Jones 2013).

Glass viscosity is another important parameter, which is related to thermal transitions and affects the sintering behavior of the glass. Viscous flow sintering occurs when the glass viscosity is 10^8–10^9 dPa·s and since e.g. the commercially used silica-based glass compositions 45S5 and S53P4 (also known as BonAlive®) crystallize around 10^9 dPa·s, they cannot be sintered properly without extensive crystallization. (Ylänen 2011, p. 8). The effects of glass crystallization are not yet completely understood and there are different opinions about the possible consequences. Results have shown that partial crystallization can be beneficial in enhancing the mechanical properties. (Fagerlund *et al.* 2012). In contrast, the loss of a completely amorphous structure may lead to inadequate sintering, instability and even to limited bioactivity. (Bellucci *et al.* 2010; Fu *et al.* 2011a). These factors have limited the commercial applications of silicate-based 45S5 and S53P4 glass

compositions, both of which are approved by the US Food and Drug Administration (FDA), mostly to particulates. (Massera & Hupa 2014; Jones 2013). Examples of such products are bone filler NovaBone® and PerioGlas®, used is dental applications. (Rezwan *et al.* 2006).

After the discovery of 45S5 other bioactive glass types and compositions have been designed to overcome its limitations. The other FDA approved glass S53P4 has given promising clinical results but in addition to the poor processability it has been observed that implanted S53P4 granules were not completely degraded even in 14 years after implantation (Lindfors *et al.* 2010). Controlled bioactivity and degradability are essential in medical applications and thus the development of more readily dissolving glass compositions has been necessary. For example, phosphate glasses composed of a P_2O_5 network and additional network modifiers can dissolve to greater extent in longer timescales and their dissolution rate can be modified by compositional tailoring. Another highly promising modification is to replace partly or completely the silicon in the glass network with boron. (Jones 2013; Rahaman *et al.* 2011). Boron substitution for silicon reduces the chemical durability of the glass and thus increases the dissolution and apatite formation rate, which can again be tailored by modifying the borate content. Borate and borosilicate glasses can also possess enhanced thermal processing characteristics when compared to glass compositions with high silica content. Especially the ability to sinter through viscous flow without crystallization has made boron-containing glasses interesting candidates for tissue engineering applications, i.e. for scaffold production. However, excess boron released from the glass is cytotoxic and thus static *in vitro* studies have yielded undesirable results. On the other hand, in some cases cytotoxicity was reduced in more dynamic conditions that resemble biological systems in a better manner. (Fu *et al.* 2009; Ylänen 2011, p. 115). However, despite the clear improvements of cell viability and proliferation in dynamic tests, the cell activity remains well below when compared to traditional silicate-bioactive glasses. It should be said that recently the glasses developed in (Tainio, 2016) have shown cell activity similar or higher than in typical silicate bioactive glasses (unpublished data).

Thermal processing behavior can also be modified by tailoring the network modifier and intermediate concentrations. Magnesium substitution for calcium and potassium or lithium substitution for sodium can decrease the tendency of the glass to crystallize and thus widen the thermal processing window. (Ylänen 2011, p. 8; Miguez-Pacheco *et al.* 2016). Compositional tailoring too requires compromises since e.g. magnesium substitution for calcium has a negative effect on the apatite formation rate as it strengthens the glass network (Massera & Hupa 2014). The traditional bioactive glass elements such as silicon, calcium and phosphorus have roles in bone formation, which makes them also important in the biological aspect. The modification of elemental composition does not only affect the thermal properties but also the biological behavior. Strontium, zinc and magnesium have been proven to promote bone formation and other added therapeutic ions have shown to have complimentary roles in vivo, for example; copper acts as an angiogenesis

promoting element. Even antibacterial properties can be achieved by incorporating silver into the glass structure. (Hoppe *et al.* 2011).

Even though bioactive glasses possess several desirable properties, their clinical success is currently limited by poor processing characteristics, low strength and brittleness. Recent advancements have yielded promising results when tissue engineering applications are considered but comprehensive characterization and careful optimization of glass compositions and processing parameters are necessary in future studies. (Jones 2013).

2.2.2 Biodegradable polymers

Biodegradable polymers are the most extensively used class of biodegradable materials. They are widely utilized in the biomedical field in implants, drug delivery systems and tissue engineering applications. This diverse group of materials can be divided to natural and synthetic polymers depending upon their origin, with each group showing some common properties. (Nair & Laurencin 2007).

The biodegradability results from labile bonds in the polymer chains, which can be broken in biological environments through different mechanisms. Bond breaking, i.e. chain scission reduces the molecular weight of the material and eventually results in the release of monomer or oligomer degradation products, which can be excreted or further processed by the human body. (Lendlein & Sisson 2011, p. 354, 355). Typically, natural polymers degrade enzymatically whereas most synthetic polymers degrade hydrolytically in aqueous environments. The degradation rate is greatly affected by the hydrophilicity of the material and hydrophilic polymers tend to degrade at higher rates than hydrophobic ones. (Nair & Laurencin 2007). Hydrophilic polymers degrade homogeneously via bulk degradation whereas highly hydrophobic polymers only degrade at the material surface via surface erosion (Fig. 5). Some enzymatically degradable hydrophilic natural polymers are exceptions and only degrade from the surface if the macromolecular enzyme diffusion inside the material is restricted. (Domb *et al.* 2011, p. 21, 22; Bastioli 2005, p. 4; Fernández *et al.* 2013).

Many other important factors affecting the degradation rate are related to the chemical nature of the material. Increasing the molecular weight, crystallinity and bond strength in the polymer chains reduces the degradation rate, in contrast increasing the molecular weight distribution increases it. In addition, the occurring mass loss and material elimination from the body are impacted by the solubility of the degradation products. If the degradation products are acidic or basic, they can also affect the degradation rate inside the material through autocatalysis, which is also demonstrated in Fig. 5. Several other factors affecting the degradation are also known and these should be considered when a designed material is chosen for a medical application. (Domb *et al.* 2011, p. 21, 22).
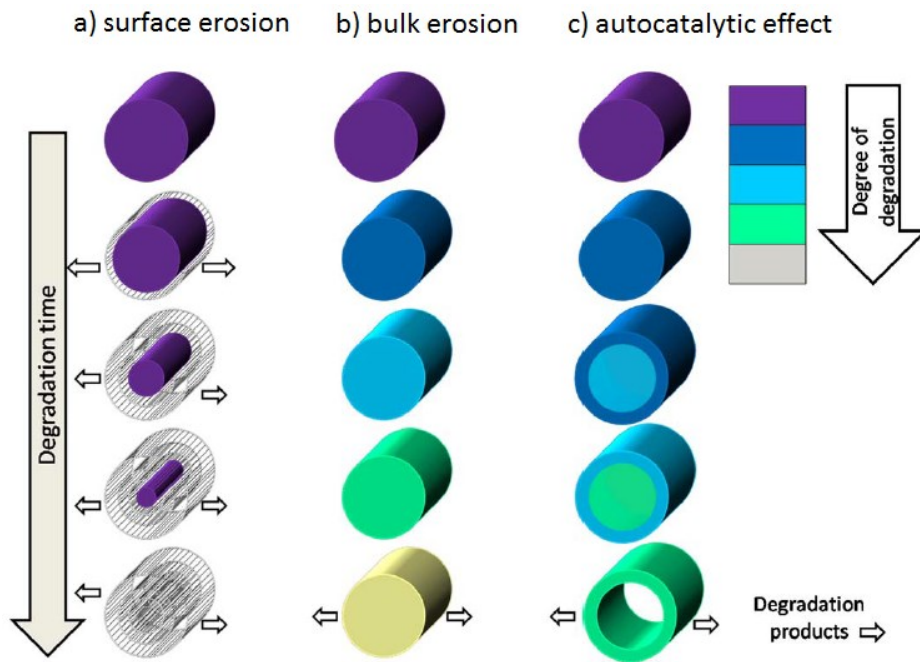
Figure 5. *Illustration of different degradation modes. Modified from (Woodruff & Hutmacher 2010).*

Natural polymers, which are derived from the plant or animal kingdom, are usually well tolerated within the human body because they may even be already present in human tissues as natural components. They include e.g. protein derivatives such as collagen and fibrin and polysaccharides such as hyaluronic acid and chitosan. Collagen´s potential in biomedical field has been extensively studied because it is present throughout the human body in high quantities. Collagen can act as a substrate for cell growth and thus it has been utilized e.g. as a skin substitute. The natural origin of these materials gives them an active role in the body and makes their remodeling and cell receptor binding possible. (Nair & Laurencin 2007). This ability to interact with innate biological systems also comes with negative sides such as the risk for pathogen transfer and immunogenicity. Natural polymers also suffer from batch-to batch variations and relatively low inherent strengths, which further decrease their reliability. Possible applications are also restricted by their poor thermal processing characteristics. (Lendlein & Sisson 2011, p. 356; Domb *et al.* 2011, p. 5).

Synthetic biodegradable polymers are currently governing the biomedical field and they are preferred over natural ones as implant materials because of their processability, tai-lorability and structural reproducibility. Of all synthetic biodegradable polymers the poly(α-ester)s are utilized most widely; they are thermoplastic and the ester bonds present in their molecular structures make them hydrolysable. (Nampoothiri *et al.* 2010). The poly(α-ester)s family includes e.g. polylactide (PLA), polyglycolide (PGA) and poly(ε-caprolactone) (PCL) polymers and the two first examples belong to the subclass of poly(α-hydroxy acid)s. Poly(α-ester)s are produced from monomer precursors via con-densation or ring opening polymerization mechanisms, depending on the monomer. The

ring opening route is highly preferred in the production of PLA and PGA after the difunctional lactic acid and glycolic acid monomers first have been converted to cyclic lactide and glycolide dimers. The cyclic precursors and resulting homopolymer structures are presented in Fig. 6. (Nair & Laurencin 2007; Domb *et al.* 2011, p. 320).
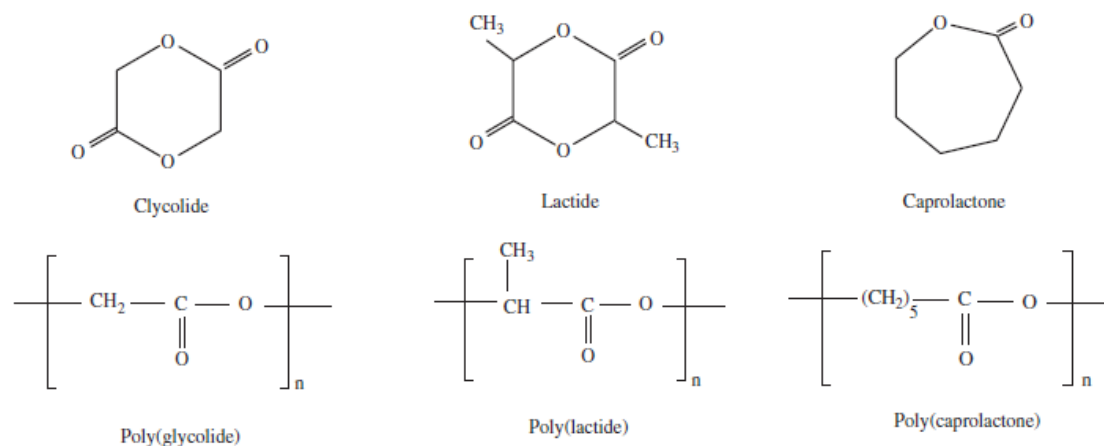
Figure 6. *Cyclic precursors and polymer structures of PLA, PGA and PCL. Modified from (Nair & Laurencin 2007).*

PLA, PGA and PCL have many common properties. In addition to being thermoplastic polymers, they all degrade mainly via bulk hydrolysis *in vivo* which causes the strength and molecular weight to drop considerably before mass loss occurs. However, their degradation rates, as well as many other properties, have great differences. Degradation time is affected by the molecular structure of the polymer and e.g. the presence of methyl groups lowers the degradation rate by increasing hydrophobicity. (Bastioli 2005, p. 290). Thus, PLA degrades at a lower rate than PGA whereas the degradation time of PCL is even longer and can be 2–4 years. On the other hand, PLA has great variation in its degradation kinetics since the lactic acid monomer is chiral and thus may be present in both L- and D-forms. (Nampoothiri *et al.* 2010; Woodruff & Hutmacher 2010). The ratio of these stereoisomers in the polymer structure greatly affects several properties and e.g. by changing from pure L-form towards the racemic DL-form the degradation rate increases. The change also lowers the crystallinity and thus poly(DL-lactide) (PDLLA) is amorphous whereas poly(L-lactide) (PLLA) is semicrystalline like PGA and PCL. (Nair & Laurencin 2007; Rezwan *et al.* 2006).

A common feature related to the degradation of PLA, PGA and PCL is that the chain scission of ester bonds produces acidic degradation products that may cause inflammation upon accumulation. However, the acidic by-products can be eliminated via physiological pathways. For example, lactic acid that is produced during PLA degradation is a natural metabolite and can be broken down to water and carbon dioxide in the citric acid cycle. (Nair & Laurencin 2007; Woodruff & Hutmacher 2010).

PCL differs greatly from PLA and PGA when mechanical and thermal properties are considered. Whereas PLA and PGA are strong and show low elongation, PCL is very ductile but possesses remarkably lower strength. Form the mechanical point of view, PLLA resembles the commercially available polystyrene (Bastioli 2005, p. 291). Another difference rises with thermal behavior since PLA and PGA can sustain relatively high temperatures in comparison to PCL, which melts around 60 °C. Some characteristic properties of these discussed polymers are summarized Table 2. (Nair & Laurencin 2007).

Table 2.   *Characteristic properties of PLA, PGA and PCL.*

Property	PLA	PGA	PCL	Reference
Degradation time	> 2 years (L-lactide), 12–16 months (D,L-lactide)	6–12 months	> 2 years	(Nair & Laurencin 2007; Woodruff & Hutmacher 2010)
Crystallinity (%)	0 (D,L-lactide), 37 (L-lactide)	45–55	50	(Nair & Laurencin 2007; Taylor & Francis Group)
T_g (°C)	60–65 (L-lactide), 55–60 (D,L-lactide)	35–40	-60	(Nair & Laurencin 2007)
T_m (°C)	175 (L-lactide)	225–230	59–64	(Nair & Laurencin 2007; Domb et al. 2011, p. 326)
Young´s Modulus (GPa)	4.8 (L-lactide) 1.9 (D,L-lactide)	7	0.9–1.5	(Domb et al. 2011, p. 327; Nair & Laurencin 2007; Taylor & Francis Group)
Tensile strength (MPa)	53	57	23	(Nair & Laurencin 2007; Nampoothiri et al. 2010; Taylor & Francis Group)
Elongation at break (%)	12–26	20–34	> 700	(Nair & Laurencin 2007; Taylor & Francis Group)

The low melting temperature of PCL allows processing and forming at low temperatures. PCL is also soluble in several organic solvents and can form miscible blends with multiple other polymers. These factors widen the possibilities related e.g. to scaffold production or property tailoring. PCL has been traditionally used as a long-term implant in drug delivery, e.g. in a contraceptive device Capronor®. However, the long degradation time has limited the use of PCL homopolymer in other applications. (Woodruff & Hutmacher 2010). PLA and PGA are usually produced via traditional melt processing including: injection and compression molding, extrusion and film blowing. These methods include e.g. injection and compression molding, extrusion and film blowing. PGA has remarkable fiber forming abilities and thus fiber drawing and spinning methods have been important manufacturing routes. (Domb *et al.* 2011, p. 325). One example of a PGA based commercial product is DEXON® suture. PLA on the other hand has been seen as an ideal material

for load bearing implants and it has found its use for example in orthopedic implants used in bone fixation. BioScrew®, Bio-Anchor® and Phantom Soft Thread Soft Tissue Fixation Screw® are examples of commercially successful products. (Nair & Laurencin 2007).

An important driving factor for the research and use of PLA, PGA and PCL is that they have all gained FDA approval. But all these homopolymers possess disadvantages such as non-ideal degradation rate or inadequate mechanical performance. Because of that there has been extensive research related to their blending and copolymerization with each other or other biodegradable polymers such as poly(trimethylene carbonate) (TMC). For example, copolymerization of different lactide isomers with glycolide yields poly(lactide-co-glycolide) (PLGA) which may possess very different mechanical properties and degradation behavior depending on the monomer content and their ratios (Lendlein & Sisson 2011, p. 8). The degradation rate of PLGA can, for instance, be tailored and it is possible to obtain degradation times as short as 1-2 months. PLGA has been used extensively in sutures but it also shows potential for use in tissue engineering applications because of sufficient cell adsorption and proliferation. Similarly, copolymerization of PCL with DL-lactide increases the degradation rate and copolymerization of PGA and PCL results in a more flexible material than pure PGA. Even though blending and copolymerization allow tailoring of properties to some extent they cannot solve all problems related e.g. to material interaction with tissue. (Nair & Laurencin 2007; Woodruff & Hutmacher 2010, Rezwan *et al.* 2006).

2.2.3 Composites

Tissue engineering puts high demands on material performance. Despite the numerous beneficial properties of bioactive glasses and biodegradable polymers, these single materials cannot fulfill all requirements. Whereas biodegradable polymers possess good processing characteristics but insufficient interaction with tissue, bioactive glasses excel in biological performance but are difficult to process. If they are used together as a composite, it is possible to combine the desired properties of the single material types. Since bone is also a composite material, this approach can even offer better mimicking of naturally occurring systems. (Ylänen 2011, p. 166; Rezwan *et al.* 2006; Kumar *et al.* 2015).

Composites are constructed of two or more distinct materials that are present in the structure as separate phases. Bioactive glass composites used in biomedical applications are typically composed of a biodegradable polymer matrix and a bioactive glass phase, which is incorporated to the matrix either in the form of particulates or fibers. A common approach with Bioglass® containing composites is to use glass particles and either PLGA or PDLLA as a matrix material. (Boccaccini & Maquet 2003). The aim is to utilize the processability and elasticity of the polymeric component and to increase the stiffness and bioactivity of the structure with bioactive glass. Other possible composite assemblies include coating porous glass structures with biodegradable polymers or coating a biodegradable polymer scaffold with bioactive glass particles. (Ylänen 2011, p. 164–166, 172).

The properties of the scaffold are not only affected by the independent material components. Volume fractions of the different phases as well as the size and shape of the filler material have tremendous effects on mechanical and biological properties. For example, it has been shown that bioactivity of the composite is enhanced when the glass particle size is reduced or more glass is incorporated to the structure. However, this also leads to a larger interfacial area between the glass and polymer, which may reduce crack resistance. The interface between different phases also greatly affects the mechanical properties and thus good interfacial bonding is desired. (Kumar *et al.* 2015). In addition to increasing the mechanical and biological properties, bioactive glass can also affect the degradation behavior of the polymer matrix. Bioactive glass increases the hydrophilicity of the structure, which can result in higher levels of water intake, leading to an increase in the degradation rate. (Rezwan *et al.* 2006). Bioactive glass can also affect the polymer´s degradation behavior, for example by buffering the pH change caused by acidic degradation products of the polymer. (Ylänen 2011, p. 166; Boccaccini & Maquet 2003). Different phases in the composite system may have dissimilar degradation rates, which leads to concerns about the possible instability of the structure after implantation. (Jones 2013).

Composite materials have become an important area of research and expectations for their future in tissue engineering are high (Rezwan *et al.* 2006). However, their nature is even more complex than their independent components´ alone, which gives great challenges for their research and development. (Jones 2013).

2.3   Scaffolds

Scaffolds are porous three-dimensional constructs that are intended to temporarily replace and support parts of tissues to promote natural healing processes. They are facing strict requirements, only some of which are related to the earlier discussed biomaterials. Other important aspects surrounded their structure, and porosity which is linked to the chosen production method. (Jones 2013, Fu *et al.* 2011a).

2.3.1   Function and property requirements

Biocompatibility of the scaffold material is essential for successful cell attachment, proliferation and differentiation. In bone tissue engineering, the goal is to create a material that is osteoconductive and bioactive to facilitate bone growth and tissue bond formation, which reduces the tendency for undesired fibrous tissue encapsulation. (Kasper *et al.* 2012, p. 199). Since bone remodeling is strongly affected by physical loading, the strength of the scaffold material should match with the strength of bone to cause sufficient mechanical stimulus but at the same time to avoid stress-shielding reactions. Depending on the patient and site of the body, bones may possess varying mechanical and physical properties, which makes it necessary to tailor the scaffold properties for different applications. (Sultana 2013, p. 6, 7; Fu *et al.* 2011a).

Cells should be able to migrate within the scaffold and form new tissue and blood vessels. This requires that fluid movement occurs within the structure so that nutrients can be delivered and cell metabolic waste disposed. Thus, the porosity and pore interconnectivity strongly affect the tissue ingrowth to the structure. (Sultana 2013, p. 6, 7). Different pore sizes favor different processes and e.g. pores smaller than 50 µm are optimal for protein and cell adhesion whereas larger pores (> 300 µm) favor vascularization, bone formation and bone ingrowth (Kasper *et al.* 2012, p. 200). However, the optimum pore size for bone formation is being debated and values ranging from 200 µm to 400 µm are suggested (Burg *et al.* 2000). Typically, the minimum requirement for adequate tissue ingrowth is at least 50 % porosity with interconnected pores larger than 100 µm (Rahaman *et al.* 2011). Whereas higher porosity is desired for enhanced biological activity, it simultaneously decreases the mechanical properties of the scaffold. For example, both Young´s modulus and tensile strength are negatively affected by increased porosity. The scaffold should also be able to carry load and support the healing tissue and thus there is need for compromises between mechanical and biological performance. (Tomlins 2016, p. 39; Jones 2013). It should be noted that in addition to porosity, both surface chemistry and structure affect cell attachment and behavior too. Whereas surface chemistry is related to material composition, the texture is a physical property. By tailoring the surface roughness, osteoblast attachment can be improved. (Sultana 2013, p. 6, 7)

Healing tissue should replace the scaffold and thus biodegradability is a crucial feature. In an ideal situation, the degradation of the scaffold would occur at the same rate as the new tissue grows. Weakening of the scaffold material´s molecular network increases the degradation rate but again results in lower mechanical strength, thus giving need for balance between faster degradation and structural rigidity. The scaffold should not degrade too fast but instead provide support for long enough to allow proper healing of the tissue. (Jones 2013, Hutmacher 2000).

Other factors are more important from the aspect of clinical use. When the scaffold is implanted infections should be avoided which gives need for sterilization. Chemical sterilization may leave residues on the scaffold surface whereas sterilization with gamma irradiation can cause breaking of molecular bonds. Thus, the material should be able to be sterilized without considerable loss of properties. (Sultana 2013, p. 7). A wide use of a certain scaffold type requires mass production in a controllable and economical manner. Especially the scalability of some production methods may be challenging because of their long cycle times or high amounts of required work. (Kasper *et al.* 2012, p. 200; Hutmacher 2000). Since no implantation site is alike, malleability and option for cutting scaffolds to suitable shapes during operation are also desired (Jones 2013, Burg *et al.* 2000).

2.3.2 Preparation methods

Since the properties of the scaffold strongly dictate the success of the treatment, it is relevant to optimize the processing conditions and raw material choice for a given application. Currently, there are no specific fabrication methods or materials that are considered ideal for all applications. The choice of material limits the possible processing methods, each of which has pros and cons. (Hutmacher 2000). Furthermore, tailoring the processing parameters for individual materials is required for balancing between several structural criteria of the scaffold. (Hollinger *et al.* 2004, p. 159, 160; Tomlins 2016, p. 30–34).

One of the early techniques developed for producing bioactive glass scaffolds is the so-called porogen burn-off method, which involves mixing glass powder with organic particles. As the mixture is heated, decomposition of the organic matter occurs, inducing porosity to the structure. (Ylänen 2011, p. 111). Usually sintering of the scaffold is conducted during the same thermal cycle. Porogen materials that have been utilized with this method include e.g. poly(methyl metacrylate) (PMMA) and polyethylene (PE) polymers and naphthalene. The porogen method has been widely utilized in the past because it enabled simple, versatile and cost-efficient scaffold production. (Brovarone *et al.* 2006). However, insufficient burning of the sacrificial material may leave residue in the structure and it can negatively affect the sintering process. When scaffolds are produced with low porogen loading, the pores typically have low interconnectivity. Additionally, due to the processing method itself, controlling the size distribution of the pores is challenging, as it is directly related to the location, size and shape of the porogen particles at the point of sintering. (Jones 2013; Chevalier *et al.* 2008).

Pore interconnectivity and the porosity of bioactive glass scaffolds can be improved by using a sacrificial polymeric foam, typically made of polyurethane (PU), instead of porogen particles and the method is called foam replication. The foam is soaked in a glass powder containing slurry, which coats the foam template. After soaking, the excess slurry is usually extracted by squeezing the foam and the green body is let to dry. The foam is then burnt out and the glass is sintered during the same thermal cycle. Since the glass particles are coating the foam, its decomposition results in a scaffold with a similar foam-like structure which usually highly resembles the human trabecular bone. However, there is a chance that the struts remain hollow after the polymer has decomposed. In addition, the porosity and pore size of foams may have great variations and thus it is important to evaluate the suitable foam type for a given process. (Dressler *et al.* 2009). Relying so heavily on the foam can be considered as one of the greatest disadvantages of this method but on the other hand, it allows production of highly porous structures with tailorable pore sizes and good interconnectivity. (Ylänen 2011, p. 111). Other important processing parameters that should be considered include: slurry composition, glass particle size and number and duration of foam soaking times. (Jones 2013). By soaking the foam multiple

times, the thickness of the glass coating on the foam and thus the strut thickness can be increased. (Chen *et al.* 2006; Fu *et al.* 2009).

Solvent casting combined with particulate leaching has been utilized in the production of porous scaffolds from polymeric materials. Organic solvents are used to dissolve the polymer and water-soluble particles, e.g. salt or sugar, are added to the solution as pore forming agents. The solvent is let to evaporate, thus yielding a polymeric template, which contains the porogen particles. The template is immersed to water, which initiates the dissolution of the water-soluble substances and thus induces pore formation. This method has similar disadvantages as the porogen method for glass processing previously discussed, i.e. it can result in low pore interconnectivity and residual porogen within the structure. (Hollinger *et al.* 2004, p. 159; Tomlins 2016, p. 30, 31). However, the process is simple, suitable for various biomaterials and also for composite scaffold production if bioactive glass particles are added to the solution (Woodruff & Hutmacher 2010, Ylänen 2011, p. 167).

Many other polymer processing techniques require high temperatures or toxic solvents. Supercritical carbon dioxide (scCO$_2$) fluid processing allows scaffold production at low temperatures and without additional chemicals. At temperatures above 31.1 °C and 73.8 bar pressure carbon dioxide assumes the form of a supercritical fluid, a state with similar density to liquid but with a gas-like viscosity. If an amorphous or semicrystalline polymer is subjected to scCO$_2$, it drastically decreases its T_g and the viscosity of the polymer whilst increasing the diffusivity. The scCO$_2$ increases the polymer chain mobility and diffuses into the structure, saturating it after a certain time. The solubility strongly depends on the processing conditions and the chemical structure of the polymer. For instance, amorphous regions are more susceptible for scCO$_2$ intake than crystalline regions. (Davies *et al.* 2008). After the saturation, depressurization is conducted and it induces nucleation inside the polymer, thus resulting in pore formation as these nuclei grow. As the gas content decreases, the T_g of the polymer simultaneously returns its nominal value, which causes the stabilization of the formed porous structure. (White *et al.* 2012). ScCO$_2$ method allows processing of thermally labile materials and incorporation of sensitive molecules such as drugs and proteins to the structure without damaging them. (Liao *et al.* 2012). The process is limited by a number of factors; scaffolds can be subject to a non-porous skin, which hinders e.g. cell migration into the structure. It also can be challenging to induce interconnected porosity and to optimize the various processing parameters, such as depressurization rate and temperature, for materials of choice. (Bhamidipati *et al.* 2013).

Recent advances in the additive manufacturing technology have provided new scaffold fabrication technologies (Sultana 2012, p. 22). These methods are often referred to as Rapid Prototyping (RP) or Solid Freeform Fabrication (SFF) techniques and can be used for a variety of materials including polymers and glasses. The processes rely on computer-aided designs (CAD), which act as models for the construction of the real objects via layer-by-layer deposition. (Hutmacher 2000). These methods are grouped under the term

3D printing but consist of various independent processes such as Fused Deposition Modeling (FDM), Selective Laser Sintering (SLS) and Direct Ink Writing (DIW), which is also known as robocasting. Whereas SLS utilizes a laser to sinter powder bed layer by layer, in robocasting viscous paste or ink is extruded to form the object, which can later be sintered. (Deliormanlı & Rahaman 2012). All these methods offer high levels of controllability of the structure, including the discrete design of the idealized porosity and pore interconnectivity. It is possible to design strong and tailored constructs for individual patients based upon their needs. However, additive manufacturing methods may apply restrictions to raw materials, their form and properties. In addition, they are typically time-consuming and require complex and expensive equipment. Especially porous scaffolds are suffering from non-uniform shrinkage during sintering, which may induce cracking. Even though these processes possess several challenges, they are expected to have great potential in the future, thus supporting the need for process optimization. (Bose *et al.* 2013; Woodruff & Hutmacher 2010; Ylänen 2011, p. 168).

3. EXPERIMENTAL PART

This chapter presents the experimental part of the thesis. First the glass production is discussed, followed by material characterization. Then scaffold preparation steps are explained and different analysis methods are presented.

The objective of this thesis was to evaluate the suitability of Mg- and Sr-containing borosilicate glasses for scaffold production and the effects of different fabrication methods on the scaffold structure and consequent *in vitro* performance.

3.1 Glass production

A reference glass for this study was designed by replacing 6.73 mol-% of SiO_2 in the commercial silicate based S53P4 glass (BonAlive®) with B_2O_3 (Fagerlund *et al.* 2012). The base glass was named B12.5. Three more glasses were produced by substituting 5 mol-% Mg and/or 10 mol-% Sr for the Ca in the base glass. Glass abbreviations and their oxide contents are reported in Table 3.

Table 3. *Abbreviations and compositions (in mol-%) of the studied glasses.*

Oxide type	B12.5	B12.5-Mg5	B12.5-Sr10	B12.5-Mg5-Sr10
SiO_2	47.12	47.12	47.12	47.12
B_2O_3	6.73	6.73	6.73	6.73
CaO	21.77	16.77	11.77	6.77
Na_2O	22.66	22.66	22.66	22.66
P_2O_5	1.72	1.72	1.72	1.72
MgO	0.00	5.00	0.00	5.00
SrO	0.00	0.00	10.00	10.00

3.1.1 Melt process

Studied glasses were prepared by mixing high purity raw materials; Belgian quartz sand (99.4 % SiO_2) and analytical grades of H_3BO_3 (CAS No. 10043-35-3), MgO (CAS No. 1309-48-4), $SrCO_3$ (CAS No. 1633-05-2), $(NH_4)H_2PO_4$ (CAS No. 7722-76-1) and Na_2CO_3 (CAS No. 497-19-8) from Sigma-Aldrich and $CaCO_3$ (CAS No. 471-34-1) from ThermoFisher GmbH.

Mixtures were melted in a platinum crucible in LHT 02/17 LB Speed electric furnace (Nabertherm GmbH, Lilienthal, Germany) in air atmosphere. All studied glasses were subjected to a similar melting procedure. First, the materials were heated from room temperature (RT) to 800 °C with a 10 °C/min heating rate. The 800 °C temperature was

maintained for 15 minutes to allow evaporation of volatile CO_2. Then the temperature was raised from 800 °C to 1300 °C at 10 °C/min and was maintained for 30 minutes to adequately homogenize the glass melt. Batch size was calculated to yield 100 g of glass.

The molten glasses were casted into a graphite mold and after a brief solidification were transferred to a pre-heated electric muffle furnace (Nabertherm L 5/11 or L 3/12) and annealed for 5 hours at temperatures approximately 40 °C below the T_g of each composition (presented in Fig. 15). Annealing was conducted to relieve the residual stresses caused by rapid cooling. After annealing, the glasses were let to cool down back to RT inside the furnace. A schematic of the thermal processing cycle of the studied glasses is presented in Fig. 7 and Table 4.
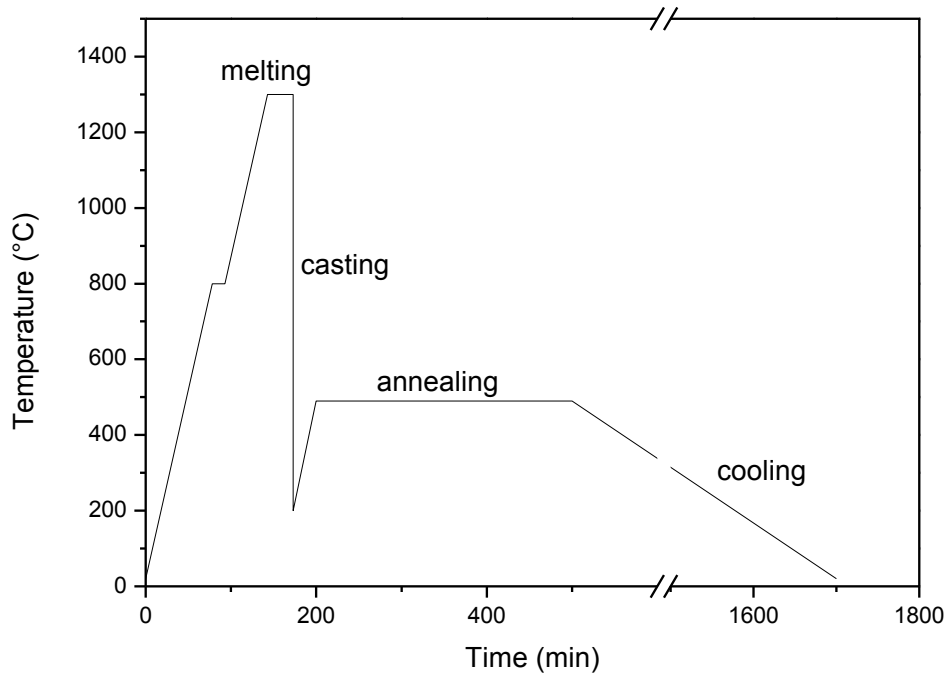
Figure 7. *Illustration of the thermal processing cycle.*

Table 4. *Thermal processing cycles of studied glasses. T_g – 40 °C annealing tempera-tures are used but other processing steps are identical between different glass compositions.*

Step	Duration	Final temperature
Heating (10 °C/min)	~ 80 min	800 °C
Holding	15 min	800 °C
Heating (10 °C/min)	50 min	1300 °C
Holding	30 min	1300 °C
Casting	~ 1 min	< 500 °C
		Glass
Annealing	5 h	B12.5 490 °C
		B12.5-Mg5 470 °C
		B12.5-Sr10 460 °C
		B12.5-Mg5-Sr10 460 °C
Cooling	overnight	RT

After cooling, the glass blocks were crushed to < 5 mm pieces in a metallic mortar. Some bigger chunks of each glass composition were saved for further investigation and polished with silicon carbide (SiC) papers (Struers Aps, Ballerup, Denmark) up to P4000 grit paper. All other glasses were milled in a Pulverisette type 05.102 planetary ball mill (Fritsch GmbH, Idar-Oberstein, Germany) to fine powder. Alumina crucibles and balls were used in the milling process and rotation speed was set to 275–300 RPM. Powders were sieved after 5-7 min milling periods with ASTM specified test sieves (Gilson Company, Inc., Ohio, USA) and powder fractions smaller than 38 μm in size were extracted. Milling was continued for the remaining fraction and ball to glass volume ratio was kept at 1:1 by adjusting the number of balls to match the remaining amount of glass. The sieved < 38 μm particles were used for thermal analysis and scaffold processing whereas the bigger chunks were saved for physical and structural characterization.

3.1.2 Physical properties

The particle size distributions of the milled and sieved powders were measured in distilled water with Mastersizer 2000 particle size analyzer combined with Hydro 2000S module (Malvern Instruments, Ltd., Worcestershire, United Kingdom). Each measurement was repeated 5 times and average distribution values were taken.

The densities of bulk glass pieces were measured by following Archimedes´ principle. The weights of glass pieces were measured both in air and immersed in distilled water at RT. The glass densities ρ_{glass} (g/cm^3) were obtained using the following equation

$$\rho_{glass} = \frac{m_{air}}{m_{air} - m_{water}} \cdot \rho_{water} \, , \qquad\qquad (1)$$

where m_{air} and m_{water} are the measured weights of glass pieces in air and distilled water, respectively, and ρ_{water} is the density of distilled water (0.997 g/cm^3 at RT) (Brauer *et al.* 2011). Three parallel measurements were conducted for each glass composition and average density values were calculated.

Molar volumes of the glasses were calculated from the obtained average density values and known glass oxide contents. Molar volume, V_m (cm^3/mol), can be calculated using the following equation

$$V_m = \frac{\sum(\chi_i \cdot M_i)}{\rho_{glass}}, \tag{2}$$

where χ_i and M_i are the molar fractions and molecular weights of the individual oxide components, respectively. (Chanshetti *et al.* 2011).

3.1.3 Structural properties

Raman spectroscopy studies were conducted on polished glass pieces to gain information about their molecular structures by observing characteristic bond vibrations in the glass networks. Measurements were conducted using an inVia™ confocal Raman microscope (Renishaw plc, Gloucestershire, United Kingdom) in the 200-1800 cm^{-1} wavenumber range. Ar-laser ($\lambda = 514$ nm and 150 W power), 50x objective and diffraction grating with 2400 grooves/mm were used in the measurements that were composed of 2 accumulations of 20 s exposure times. The obtained spectra were baseline corrected and normalized to the peak with the highest intensity.

Fourier transformation infrared spectroscopy (FTIR) measurements were conducted on glass powder (particle size < 38 μm) to gain complementary information about the glasses structures. Measurements were done with a Spectrum One FT-IR Spectrophotometer (PerkinElmer Inc., Massachusetts, USA) using the attenuated total reflectance (ATR) accessory. 8 scan accumulations scans were performed in 650–4000 cm^{-1} wavenumber range with a 4 cm^{-1} resolution. The spectra were baseline corrected and normalized to the peak with the highest intensity.

3.1.4 Thermal properties

Differential Thermal Analysis (DTA) studies were conducted to < 38 μm sized particles to gain information about the thermal transitions of the glasses. Measurements were done using a STA 449 F1 Jupiter® (Netzsch-Gerätebau GmbH, Selb, Germany). 30 mg of samples was placed in a platinum pan and heated up at 10 °C/min, from 40 to 1000 °C, in nitrogen atmosphere. The glass-transition temperature (T_g), the onset of crystallization temperature (T_x) and crystallization peak temperature (T_p) were determined for each composition from the obtained DTA curves. The T_g was taken from the minimum of the first

derivative of the heat flow curve in the vicinity of the first endothermic peak, i.e. from the inflection point. T_x was determined from the point of crossing tangents of the exothermic crystallization peak and the plateau preceding it. T_p was obtained from the highest point of the crystallization peak. The position for T_g, T_x and T_p is illustrated in Fig. 8, presenting the DTA trace of the glass B12.5 along with the first derivative.
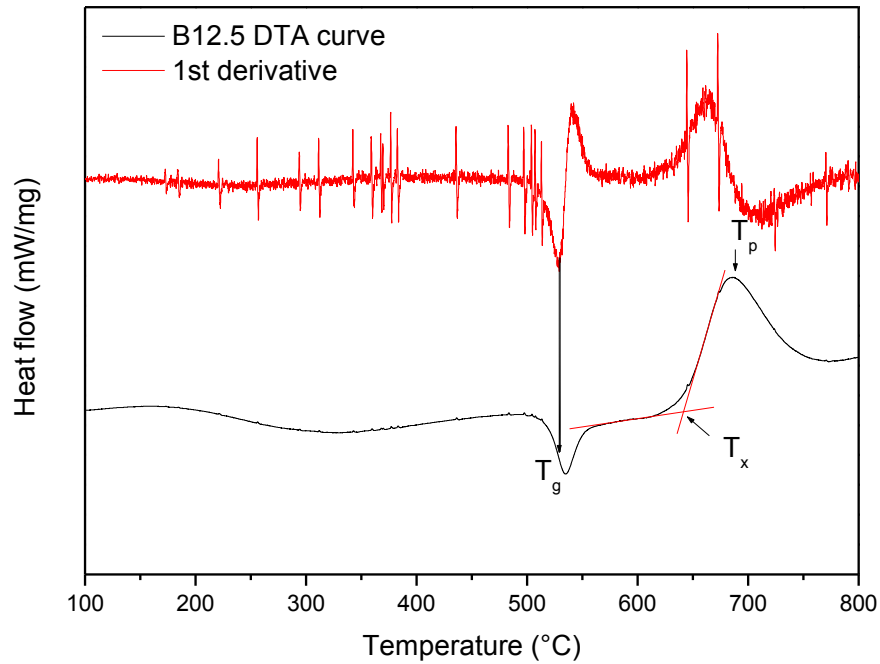
Figure 8. *DTA curve of B12.5 presenting the points of T_g, T_x and T_p.*

From the DTA thermogram, one can also define the hot forming domain ΔT ($\Delta T = T_x - T_g$). To further evaluate the ability of the glasses to sinter without extensive crystallization, the glass particles were also heat treated at various temperatures within ΔT for all compositions. Small pellets of each glass composition were compacted in a metallic mold by applying 25 MPa pressure with a hydraulic press. The intact pellets were extracted from the mold and heat-treated on a metallic plate in a Nabertherm LT 9/11/SKM electric muffle furnace. The metallic plate was coated with boron nitride spray beforehand to prevent sticking. Treatments were conducted in air atmosphere with a heating ramp of 10 °C/min from RT to 550, 575, and 600 °C. The temperatures were maintained for 1 hour, after which the samples were let to cool down to RT overnight. The heat-treated samples were crushed to fine powder in a mortar and a pestle and analyzed with a X-ray diffractometer (XRD) to reveal possible crystallization during heat treatment. Measurements were conducted in the 10-60° 2θ diffraction angle range with MiniFlex™ (Rikagu, Tokyo, Japan). Information from the XRD measurements have been used to define the maximum temperature the glass of investigation can withstand without undergoing significant crystallization.

3.2 Scaffold preparation

Different scaffold production methods were used. The aim was to evaluate the ability of attaining scaffolds with pore size and mechanical properties suitable for medical use. In a second time, the impact of the scaffold manufacturing process on the glass degradation was studied. Porogen burn-off and robocasting methods were used to produce sintered bioactive glass scaffolds while supercritical CO_2 was utilized to obtain polymer/bioactive glass composite scaffolds.

The scaffolds´ sintering temperatures were determined from the XRD results by evaluating the highest temperatures that did not induce extensive crystallization in the glasses. From the XRD and DTA data it appeared that that sintering should be conducted at $T_x -$ 95 °C for all glass compositions in order to avoid thermally induced crystals. The sintering temperatures are presented in Table 5.

Table 5. *Chosen sintering temperatures for different glass compositions.*

Temperature	B12.5	B12.5-Mg5	B12.5-Sr10	B12.5-Mg5-Sr10
$T_x - 95$ (°C)	545	554	528	542

3.2.1 Porogen burn-off method

The porogen material used in this thesis was ammonium bicarbonate, NH_4HCO_3 (Sigma-Aldrich, ≥ 99.5 %, CAS No. 1066-33-7). Scaffolds were produced by mixing < 38 μm sized glass powders and porogen particles with 30:70 volume ratios. Mixing of the components was conducted by hand in a plastic bottle. Similar volumes of all mixtures were loaded to a metallic mold that had cylindrical holes with 15 mm diameters. The powders were then compacted in the mold by applying 25 MPa pressure with a hydraulic press.

The intact compacted pellets were extracted from the mold and sintered in a Nabertherm LT 9/11/SKM electric muffle furnace and in an air atmosphere. Pellets were placed on a boron nitride coated metallic plate in the furnace. Sintering was conducted at 1 °C/min from RT to 300 °C to allow the decomposition and elimination of the porogen material. Then the temperature was raised with at 5 °C/min heating rate from 300 °C to the sintering temperatures (Table 5). The sintering temperatures were maintained for 1 hour, after which the furnace was let to cool down to RT overnight. The cooled sintered scaffolds were stored in a desiccator until further analysis.

3.2.2 Robocasting

In this study, the ink was prepared by dissolving Pluronic® F-127 (Sigma-Aldrich, CAS No. 9003-11-6) to distilled water up to 25 wt-% concentration. Dissolution of the Pluronic was done under stirring in an ice water bath overnight until the solution became

homogeneous. Sieved < 38 μm sized glass powders were added to the solution to gain inks with 35 vol-% glass concentration. Mixing was conducted in plastic pots with Vibrofix VF1 electrical shaker (IKA®-Labortechnic, Staufen, Germany) by having 4 x 1 min mixing periods. Before and between each mixing period the pots were placed in an ice water bath to reduce the ink´s viscosity. After the last mixing period, the pots were tapped to reduce the amount of bubbles in the ink. Then the inks were transferred to a plastic syringe before gelation occurred. From the plastic syringes, the inks were transferred to Optimum® 3cc special printing syringe barrels (Nordson EFD, Bedfordshire, England). The printing syringes were closed with caps and left for one hour in ambient temperature in order to stabilize the inks.

Material assembly was achieved with a 3Dn-Tabletop (nScrypt Inc., Orlando, Florida, USA) and the instrument was controlled with Machine Tool 3.0 system software. Printing head movement only occurred in z-direction and x-y movements were gained by having a printing table that moved in a planar fashion. Inks were deposited from printing syringes through plastic Nordson EFD Optimum® SmoothFlow™ tapered dispensing tips with inner diameters of 0.58 mm. Deposition was done on acrylic Colour Laser Printer & Copier OHP Film sheets (Folex AG, Seewen, Switzerland) and material feed was achieved by applying 12.5–14.0 psi pressure to the printing syringe in order to gain constant flow that matched the speed of x-y movements. Layer patterns were designed to be approximately spherical in order to gain cylindrical scaffolds, as more layers would be deposited along z-axis. Movements in the x-y plane were conducted with 4 mm/s table speed and the spacing between the filaments was 1.18 mm. Layer design is illustrated in Fig. 9. After each layer, the nozzle was elevated in z-direction by 0.45 mm and the pattern of the previous layer was rotated 90°, but otherwise similar pattern was deposited onto the previous one. This allowed constant material deposition and eliminated the need for complex material feed control.
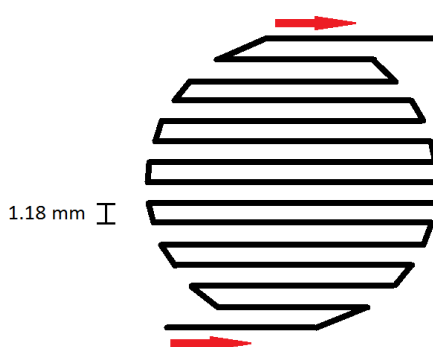
Figure 9. Schematic of the nozzle path during robocasting.

15 layers were deposited in total, after which the green bodies were dried in ambient atmosphere overnight. After drying, the excess ink strands in the corners were removed with a scalpel. Then the green bodies were sintered in Nabertherm L 3/11 electric muffle

furnace using the same parameters as for the scaffolds produced via porogen burn-off method.

3.2.3 Supercritical carbon dioxide processing

Polymer used in the composite scaffold production was PURASORB® PLC 7015, a medical grade poly(L-lactide-co-ε-caprolactone) (PLCL) with 70/30 comonomer ratios (Corbion-Purac Biochem BV, The Netherlands). Before scCO$_2$ processing, studied < 38 μm sized glass powders had to be mixed with the polymer. Polymer granulates and base glass B12.5 were weighed to have 30 wt-% glass content, which corresponded to 15.95 vol-%. Other glass powders were added to PLCL to yield similar glass volume percentages. To gain homogenous mixtures, acetone (VWR Chemicals, CAS No. 67-64-1) was added to the mixtures in a beaker to induce dissolution of the PLCL. The suspensions were mixed with magnetic stirrers overnight in a fume hood at RT, to obtain a homogeneous paste-like mixture after partial evaporation of the acetone. Overtime, a polymeric film formed over the paste lowering the solvent evaporation rates.

The films were manually redissolved into the pastes and the mixtures were transferred to petri dishes in order to increase the rate of acetone evaporation. After the mixtures had become highly viscous, they were manually rolled to rods that would fit into a metallic processing mold with cylindrical holes of 10 mm in diameter. Mold was partially filled with the mixtures before scCO$_2$ processing.

Material processing was conducted with a Supercritical Fluid Extraction (SFE) system (Thar Instruments, Inc., Pittsburg, Pennsylvania, USA) composed of an automated back pressure regulator, temperature controller, CO$_2$ pump, and a heat exchanger. Composite material was saturated at 300 bar pressure and 90 °C temperature for 1 h, after which a steady and continuous depressurization was conducted during 4 hours. The final 50 bars were decreased at a higher rate by manually operating the instrument. After complete depressurization, the mold filled with composite foam was taken from the processing unit and cooled down with pressurized air. The composite rods were extracted from the mold and cut with a scalpel to cylindrical scaffolds with approximately 5 mm height and 10 mm diameter.

Uniform glass distribution was controlled by thermogravimetric analysis (TGA). TGA samples were taken at both ends of the foamed rods. The analysis was done with TGA Q500 (TA Instruments, Delaware, Philadelphia, USA) at 10 °C/min from RT to 700 °C, followed by 1 min hold. Since the polymeric content would decompose during heating, inorganic glass would be left as a residue.

3.3 Scaffold analysis

Scaffolds were analyzed in order to gain information about their morphology, strength, degradation and bioactivity. Whereas the morphological and mechanical characteristics are affected by the processing conditions and sintering ability of the material, bioactivity and degradation are strongly related also to the elemental compositions of the studied glasses.

3.3.1 Physical and structural properties

Scaffold porosity was analyzed by following a previously presented method (Chen *et al.* 2006). Briefly, scaffold densities $\rho_{scaffold}$ were calculated from the masses and physical dimensions of 5 parallel samples and porosities p were obtained with an equation

$$p = \left(1 - \frac{\rho_{scaffold}}{\rho_{solid}}\right) \cdot 100\ \% \ , \tag{3}$$

where ρ_{solid} is the density of the bulk material. PLCL density (1.17 g/cm^3) used to calculate the bulk densities of composite materials was obtained from the literature (Nakielski *et al.*2015). The average porosity values are presented along with their standard deviations.

Micro-computed tomography (μCT) was utilized to gain information about the scaffold 3D structures. Measurements were conducted with MicroXCT-400 (Carl Zeiss X-ray Microscopy, Inc., Pleasanton, California, USA) by having 80 kV tube voltage and 0.4x objective. The resulting pixel size was 16.7 μm. Scaffold structures were constructed from the obtained data with ImageJ software combined with 3D Viewer plugin.

Sintered glass scaffolds were ground to fine powder and analyzed with FTIR spectroscopy by following the same protocol that had been used previously. XRD measurements were again conducted to scaffolds prepared via porogen burn-off method or robocasting in order to evaluate whether the chosen sintering parameters were suitable in avoiding any crystallization.

3.3.2 Mechanical properties

It was observed that the scaffolds produced via porogen burn-off method had shrunk inhomogeneously during sintering. Thus, their top and bottom surfaces were ground flat with grit P800 SiC paper in Ethanol (96 %, VWR Chemicals, CAS No. 64-17-5). Ground samples were dried overnight in a type B 8133 drying oven (Termaks, Bergen, Norway) at 37 °C.

At this point it should be noted that the final dimensions of the obtained scaffolds were dependent on the processing method and glass composition. All scaffolds had heights of

approximately 5–6 mm. Diameters were 11–14 mm, 10–13 mm and 10 mm for scaffolds produced via porogen burn-off method, robocasting and scCO2, respectively. Dimensions were measured with a caliper.

Compression testing was conducted with Instron 4411 mechanical tester (Instron, Massachusetts, USA) by using a 0.5 mm/min deformation speed. 5 kN load cell was used for glass scaffolds and 500 N load cell was used for composite scaffolds. Three parallel samples for each scaffold type and glass composition were used in the measurements. Highest compression values were taken from individual measurements to describe the compressive strength of glass scaffolds. Since the composite scaffolds did not break during testing, the compressive value was recorded after 10 % deformation, as suggested by SFS-EN ISO 844 standard (Finnish Standards Association 2014). Average values and standard deviations were calculated from the obtained results.

3.3.3 *In vitro* testing

In vitro dissolution testing of the fabricated scaffolds, was conducted in SBF to assess their bioactivity, degradation rate and the effect of degradation on scaffold structure and mechanical properties. Analysis was conducted at 8, 24, 72, 168 and 336 h.

SBF buffer solution was produced by following the protocol proposed by Kokubo (Kokubo & Takadama 2006). Analytical grades of NaCl (CAS No. 7647-14-5), $NaHCO_3$ (CAS No. 144-55-8), KCl (CAS No. 7447-40-7), $K_2HPO4 \cdot 3(H_2O)$ (CAS No. 16788-57-1), $MgCl_2 \cdot 6(H_2O)$ (CAS No. 7791-18-6), 1M HCl (CAS No. 7647-01-0), $CaCl_2 \cdot 2(H_2O)$ (CAS No. 10035-05-8), Na_2SO_4 (CAS No. 7757-82-6) and $(CH_2OH)_3CNH_2$ (Trizma[®] base, CAS No. 77-86-1) were used in the preparation of the solution. NaCl was obtained from Merck KGaA, Trizma[®] base from Sigma-Aldrich and other reagents from VWR Chemicals. More information about SBF preparation, including the amount of weighed reagents and the resulting ionic concentrations of SBF, is presented in Appendix A.

For the dissolution study, scaffolds were placed in 120 ml polypropylene (PP) pots (Sarstedt AG & Co, Nümbrecht, Germany) and immersed in SBF. The SBF volume to scaffold mass was adjusted to 100 ml of SBF for 150 mg scaffold material. Scaffolds were cut to smaller pieces with a diamond saw in order to keep the required SBF volumes in reasonable quantity. Three parallel samples of each scaffold type and glass composition were used and in addition to that, three parallel blank SBF samples were used as controls. Pots were placed in an Multitron AJ 188g (Infors, Bottmingen, Switzerland) shaking incubator at 37 °C and 100 RPM. After corresponding test times, the pH of the solutions were measured with S47-K SevenMulti[TM] pH-meter (Mettler-Toledo LLC, Ohio, USA) at 37.0 ± 0.2 °C. To evaluate the ionic release of the scaffold materials, 1 ml of solution was extracted at each time point and replaced with 1 ml of stock SBF. The extracted 1 ml of solution was diluted to 9 ml of 1 M HNO_3 and the ionic concentrations of B, Ca, Mg,

Si, Sr and P were measured with inductively coupled plasma optical emission spectroscopy ICP-OES 5110 (Agilent Technologies, California, USA). The wavelengths used in the ions analysis are collected in Table 6. It should be noted that Na concentration was not analyzed due to the high initial Na content in SBF. Average concentration values and standard deviations were obtained from the three parallel samples at each time point.

Table 6. *Elements and wavelengths used in the concentration analysis.*

Element	B	Ca	Mg	Si	Sr	P
Wavelength (nm)	249.678	422.673	279.553	250.690	216.596	253.561

To assess the bioactivity and HA layer formation, 1 to 3 specimens of each scaffold type and glass composition were immersed in SBF for up to 336 h. At each immersion time point, the specimens were extracted from the solution and rinsed with ethanol in order to stop the glass dissolution and dried. One sample produced via porogen burn-off method and robocasting were ground to fine powder in a mortar and a pestle. The powders were analyzed with FTIR spectroscopy. Samples immersed for 336 h were analyzed with a scanning electron microscope (SEM) combined with energy dispersive X-ray spectroscopy (EDX). For SEM analysis, the scaffold pieces were mounted in epoxy resin and polished with Struers Tegramin-30 automatic polishing machine up to 1 μm diamond suspension. Samples were carbon coated prior to analysis. Imaging was conducted at Åbo Akademi University. 15 kV acceleration voltage and backscattered electrons were used in imaging and magnifications between 30x and 1000x were used. Elemental compositions of unreacted glasses and formed surface layers were analyzed. Thicknesses of the surface layers were obtained via image analysis with ImageJ from 10 different spots. Average values and standard deviations were calculated.

Material degradation and its effect on mechanical properties were evaluated for the scaffolds produced via porogen burn-off method by immersing intact scaffolds to SBF. The SBF volume to scaffold mass was adjusted to 100 ml of SBF to 1 g of scaffold mass. Same incubation and drying conditions were used as with other *in vitro* samples and three parallel samples were used for each time point. The mass of dried samples was measured and mass loss was calculated as follow

$$Mass\ loss = \frac{\Delta W}{W_0} = \frac{W_0 - W_t}{W_0} \cdot 100\ \%\ , \tag{3}$$

Where W_0 is the initial weight and W_t is the weight after a certain immersion time. After mass loss measurements, the samples were subjected to a similar mechanical compression test as was utilized in the characterization of initial scaffolds. Average values were taken and standard deviations were calculated.

4. RESULTS AND DISCUSSION

This chapter presents the results that were obtained during the experimental part of this thesis. The meaning of the results is also discussed.

Previous works have demonstrated that the Ca in bioactive glass can be substituted for Mg and Sr (Hupa *et al.* 2016). Whereas Mg has traditionally been used to decrease the tendency for crystallization, Sr has been used in bioactive glasses due to its ability to promote bone healing (Hoppe *et al.* 2011; Ylänen 2011, p. 8). In the thesis by Jenna Tainio (Tainio 2016) it was found that substitution of Ca with Mg/Sr yield materials that have enhanced viscous flow at the sintering temperature.

The aim of this work was to assess the sintering characteristics of the glasses and to fabricate scaffolds via various production methods without crystallization. Glass scaffolds were produced via porogen burn-off and robocasting. For comparison, composite scaffolds with polymeric matrixes were also produced via supercritical CO_2 method.

4.1 Glass analysis

Material properties have considerable effects on suitable processing conditions and eventually the properties of the resulting scaffold (Jones 2013, Massera & Hupa 2014). Therefore, it was essential to gain information about physical and thermal properties of the studied glasses prior to scaffold fabrication.

4.1.1 Physical properties

Density and molar volume can give information about the network structure of a glass. Tailoring of the elemental composition of a glass can affect its molar volume and thus analysis of the molar volume changes may give indications about the effects of e.g. substituted elements. (Chanshetti *et al.* 2011). Compositional differences in the glasses studied in this thesis were caused by changing the glass network modifier contents (Ca, Mg and Sr) by substituting Mg and Sr for Ca in the base composition.

The densities of the studied glasses were measured using bulk glass pieces with an Archimedean method (equation 1). As the glass compositions were known, molar volumes could be calculated with equation 2. Obtained densities (ρ) and molar volumes (V_m) are presented in Fig. 10.

a)

b)
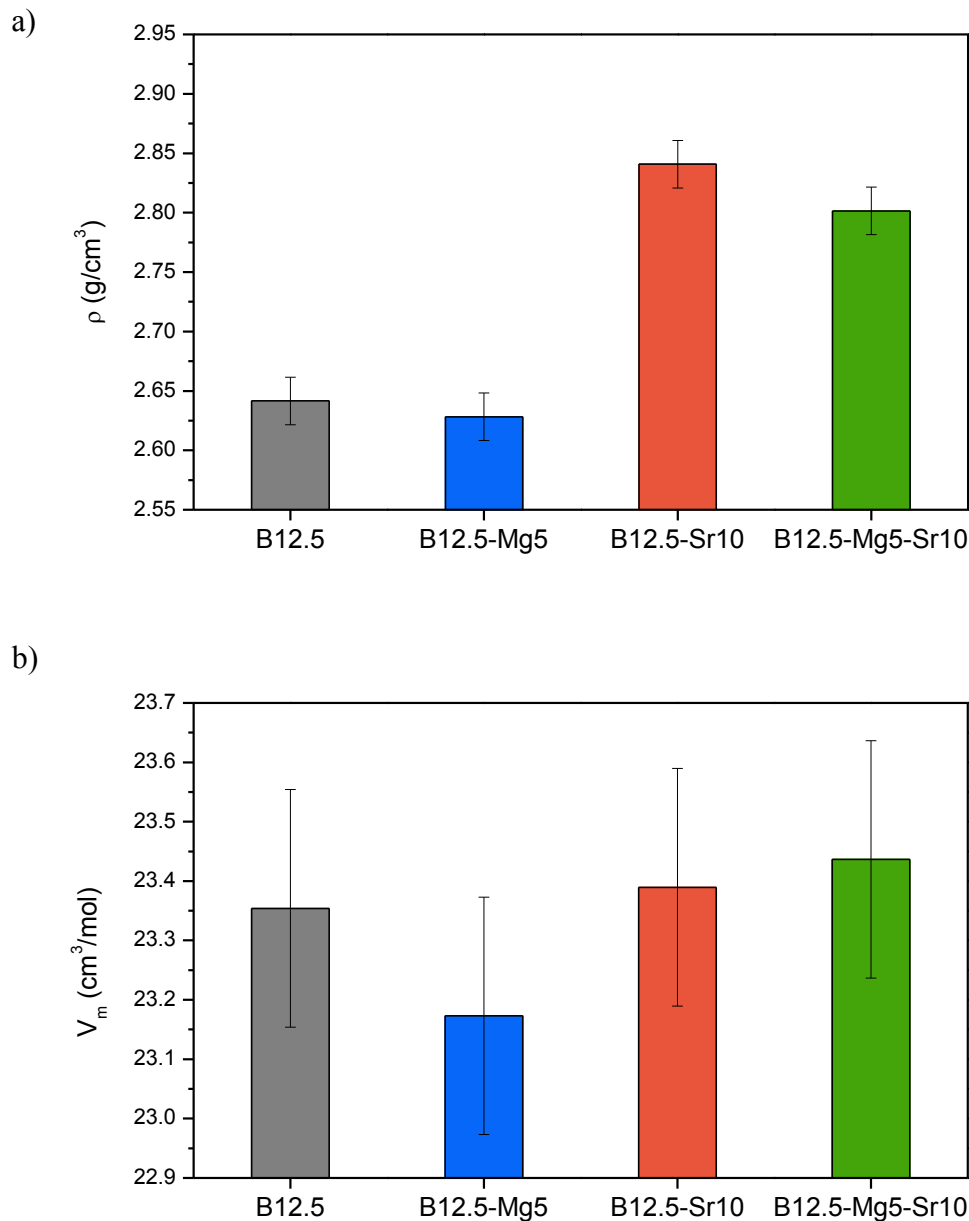
Figure 10. *Average a) densities (ρ ± 0.02) and b) molar volumes (V_m ± 0.2) of the studied glasses. The presented systematic errors are related to the testing methods.*

The density and molar volume of the base glass B12.5 were 2.64 g/cm^3 and 23.4 cm^3/mol, respectively. From Fig. 10 it can be seen that Ca substitution with Mg decreased both density and molar volume. The decrease in V_m, when Mg is substituted for Ca, was further confirmed in (Tainio 2016), with higher Mg substitution. This is in agreement with previous studies (Watts *et al*. 2010). Ca substitution with Sr caused a significant increase in the density but only a minor increase in the molar volume, which was negligible when the margins of error are considered. By substituting both Mg and Sr for Ca, the density increased but not as much as with pure Sr substitution. The change in the molar volume was again negligible when both Mg and Sr are substituted for Ca.

Change in the molar volume gives indications about the compactness of the glass network. Mg as an element has a lower molar mass and smaller ionic radius than Ca and thus substitution of Mg for Ca decreases both density and molar volume. This indicates a compaction of the glass network with Mg substitution. When compared to Ca, Sr has a higher molar mass and is greater in size. This causes an increase in density, as also observed in earlier studies (Fredholm *et al.* 2010, Massera & Hupa 2014). However, it should be noted that within the studied glasses the increase in molar volume was negligible, within the error of the measurement. This was unexpected. One may think that i) the borosilicate glasses are partly phase separated and ii) Ca, Mg and Sr have a preferential tendency to be inserted in the silicate- or the borate-rich phase.

Substituting both Mg and Sr for Ca, led to a glass with slightly lower density than the glass B12.5-Sr10. This was expected as Mg was already found to decrease the density. However, while the Mg led to a slight decrease in the molar volume when substituted to B12.5, the B12.5-Mg5-Sr10 shows similar molar volume than B12.5-Sr10. This indicates that the network compactness is governed by the strontium ion rather than the Mg or Ca. The effects of Mg and Sr to the glass network were expected to affect the thermal properties and dissolution rate, which will be discussed later.

4.1.2 Structural properties

Glasses were analyzed with Raman and FTIR spectroscopy. The assessment of glass structures is essential since e.g. the dissolution characteristics are strongly affected by the molecular structures (Fu *et al.* 2011a). The baseline corrected and normalized Raman spectra are presented in Fig. 11.
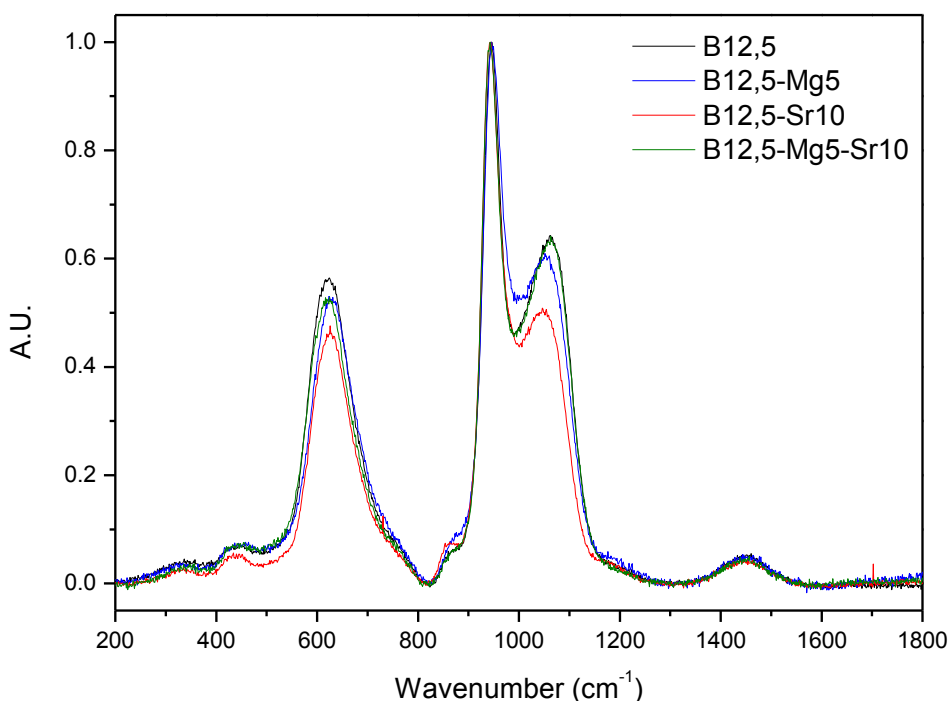
Figure 11. *Raman spectra of the analyzed glasses.*

From Fig. 11 it can be seen that all investigated glasses had similar spectra in terms of shape and presence of peaks. In the 300–500 cm^{-1} wavenumber region, the low intensity bands are caused by Si-O-Si stretching and bending modes. The second region with high intensity bands can be observed between 550 and 800 cm^{-1}. The bands in this region are characteristic to ring breathing modes of borate, borosilicate and metaborate rings. Vibration bands of metaborate rings are present in 610–630 cm^{-1} region, which corresponds to the highest intensities within the discussed region (Koroleva *et al.* 2011). The breathing modes of borosilicate rings have also been linked to peaks around 630 cm^{-1}. However, the possibility to have isolated danburite (CaO·B$_2$O$_3$·SiO$_2$) rings in the glass structures have also been discussed in previous publications, since it has a characteristic peak at 614 cm^{-1}. Generally this region can be attributed to vibrations of Si-O-Si, Si-O-B and B-O-B. (Osipov *et al.* 2013; Manara *et al.* 2009)

Characteristic bands of silica network can be observed within the 850–1250 cm^{-1} region. Stretching modes of Si-O$^-$ (Q^1) units have low intensity bands around 900-920 cm^{-1}. The high intensity band centered around 945 cm^{-1} can be attributed to stretching modes of Si Q^2 units. However, borate tetrahedrons have also been linked to weak and broad bands in the 850–1000 cm^{-1} region (Osipov *et al.* 2013). The band between 1000 and 1100 cm^{-1} is caused by stretching vibrations of Si Q^3 units whereas a fully polymerized silica network composed of Q^4 units can be attributed to the shoulder around 1150 cm^{-1}. (Koroleva *et al.* 2011; Parkinson *et al.*2008; Manara *et al.* 2009).

The band in the 1300–1600 cm^{-1} region is caused by vibrations of borate network. Peaks around 1410 cm^{-1} and 1480 cm^{-1} are caused by BO$_3$ units bonding to BO$_4$ or BO$_3$ units, respectively (Koroleva *et al.* 2011; Osipov *et al.* 2013). BO$_3$ species with "loose" structures have also been assigned to have contribution in the 1320 cm^{-1} region whereas BO$_3$ species in boroxol rings are responsible for the band at 1515 cm^{-1}. (Manara *et al.* 2009)

Even though all glasses possessed similar Raman spectra in terms of shape and observed bands, the relative intensities of different bands was affected by the glass composition. The bands within the 550–800 cm^{-1} region show that addition of either Mg or Sr decreased the intensity of borate-assigned peaks and that the change was more pronounced when only Sr is substituted for Ca. In addition to that, B12.5-Sr10 had a band with slightly lower intensity in the 400–550 cm^{-1} region, where the bending mode of Si-O-Si is present. At the same time, Mg or Sr substitution for Ca caused a slight shift of the band peak around 625 cm^{-1} to higher wavenumbers, which may indicate a more stable network. This phenomenon is reasonable when B12.5-Mg5 is considered, since replacing Ca with Mg has been observed to yield a compacted and chemically more durable glass network (Massera *et al.* 2012b).

Effects of Mg or Sr substitution to the silica network can be seen from the bands centered at 945 cm^{-1} and 1045–1065 cm^{-1} as they can be attributed to vibrations of Q^2 and Q^3 units, respectively. Mg or Sr substitution for Ca in the base glass seemed to cause an increase in the Q^2 band intensity at the expense of the Q^3 structural units. At the same time the Q^3 band shifted to lower wavenumbers, which implies that B12.5 had more stable silica network than the substituted glasses. But when both Mg and Sr were substituted for Ca, it can be seen that the silica-associated bands were identical to the base glass. These observed phenomena are complex and somewhat contradictory with the expectations since e.g. Mg substitution was expected to have an opposite effect on the silica network and lower the amount of NBO species. However, magnesium can have a complex effects on the glass network, as showed by Watts *et al.* They observed that instead of acting purely as a network modifier, magnesium can also partly change its structural role to an intermediate in the silica network when the substitution level is increased. Thus the role of magnesium is dependent to the level of substitution and glass network composition. (Watts *et al.* 2010). It should be noted that parallel measurements of the studied glasses possessed some variance, which was thought to give indications about the possibility for phase separation. From the presented spectra it becomes clear that Mg, Sr and Ca have different affinities to different glass network regions, which caused the observed changes in silica and borate network.

Fig. 12 presents the baseline corrected and normalized FTIR spectra of the studied glasses. It can be seen that all glasses possessed similar spectra and that distinct absorption regions can be observed.
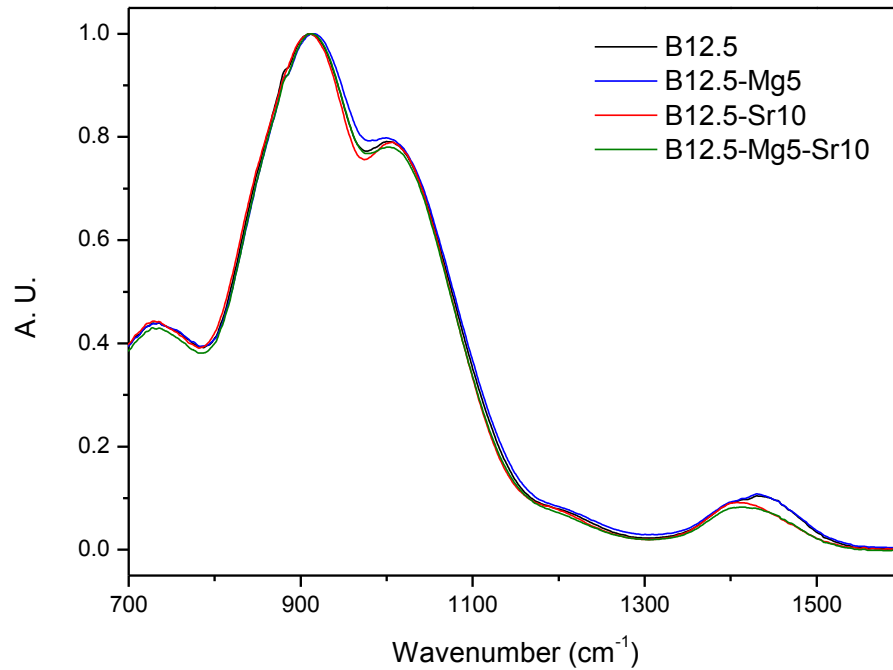
Figure 12. *FTIR spectra of analyzed glass powders.*

The band in the 700–800 cm^{-1} region can be attributed to Si-O-Si symmetric stretching vibrations of the tetrahedra and to Si-O bending. The high intensity band centered at 910 cm^{-1} is caused by Si-O^{-} stretching of non-bridging oxygen atoms, whereas the band centered at 1010 cm^{-1} can be attributed to asymmetric stretching of Si-O-Si bridging oxygen species within the tetrahedra. (Massera *et al.* 2012b; ElBatal *et al.* 2003; Mami *et al.* 2008).

In addition to silica network vibrations, the borate units also have vibration bands within the analyzed wavenumber region. B-O stretching vibrations in [BO$_4$] units are associated to bands between 900 and 1100 cm^{-1}. The shoulder region observed around 1227 cm^{-1} is caused by [BO$_2$O^{-}] vibrations (Fabert *et al.* 2017). B-O stretching vibrations in [BO$_3$] units are also contribute to the band at 1300–1500 cm^{-1}. (Balasubramanian *et al.* 2016).

The overlapping peaks of silica and borate networks leads to challenges in conducting precise analysis from the FTIR spectra. However, similarity in the intensities of the bands in the 800–1200 cm^{-1} region suggests that all investigated glasses had similar ratios of bridging and non-bridging oxygen species in their structures, i.e. that their network connectivity was not affected by Mg or Sr substitution. This indicates that Ca, Mg and Sr had similar roles as network modifiers, which was expected. Watts *et al.* showed that part of Mg tends to take a role as a network former but since only a relatively small amount of Ca was substituted with Mg, it is reasonable that it mainly acts as a network modifier similarly to Ca. (Massera *et al.* 2012b; Watts *et al.* 2010). In addition, the Sr-containing glasses exhibit a band in the 1300–1500 cm^{-1} region that has lower intensities and shift to

lower wavenumber, which could indicate differences in the boron network. As shown in the Raman spectra, this indicates that Sr and/or Mg impact the boron structure, most likely by changing the $[BO_4]$ to $[BO_3]$ ratio.

For precise conclusions about the effects of substitution, further investigation about the structural details is necessary to understand the differences between molecular species and network components. For example, nuclear magnetic resonance (NMR) analysis would be useful to provide complementary data and detailed information about the glass network structures.

4.1.3 Particle size distribution

Glass sintering, processability and tendency for crystallization are directly correlated to particle size. Therefore the particle size distribution and size was evaluated. Reducing the particle size increases the effective surface area and thus enhances sintering but at the same time lowers the resistance for surface crystallization. (Jones 2013). Glass was milled and sieved to obtain powders that had particles with < 38 µm diameters. Particle size distributions were analyzed with laser diffraction measurements and the results are presented in Fig. 13 and 14.
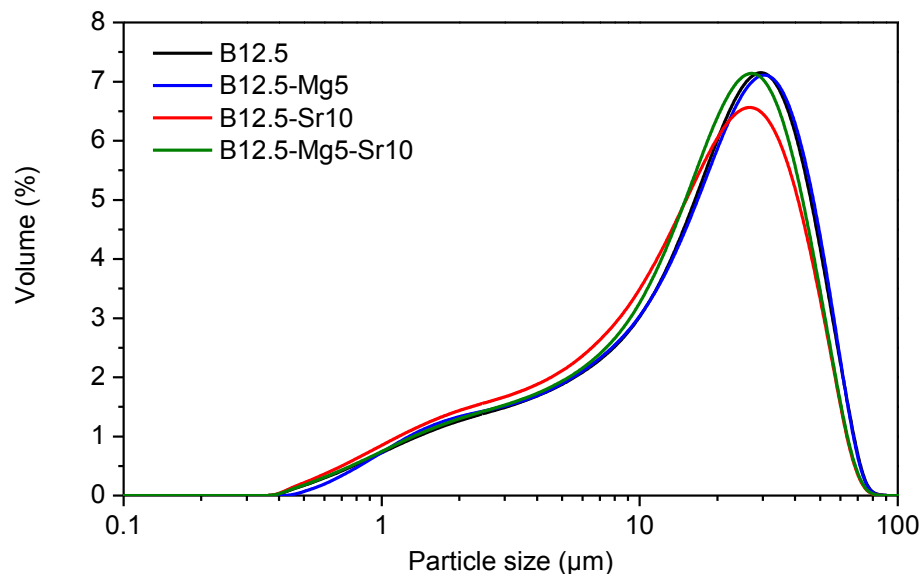
Figure 13. *Particle size distributions of milled and sieved glass powders. Graph shows relative volumes of each particle size presented on a logarithmic scale.*

Fig. 14 shows the D_{10}, D_{50} and D_{90} distribution values. D_{50} represents the median particle size. 10 vol-% of the powder is comprised of particles smaller than D_{10} and 10 vol-% of the powder is comprised of particles greater than D_{90}, respectively.
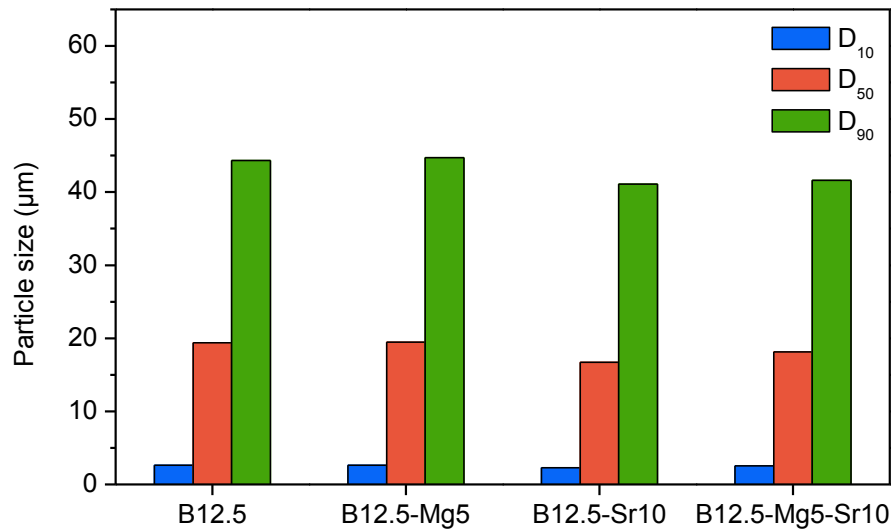
Figure 14. *D_{10}, D_{50} and D_{90} distribution values of the particle diameters ($\pm$ 0.2 μm) in studied glass powders.*

From Fig. 13 and 14 it can be seen that all glass powders possessed similar particle size distributions. D_{10}, D_{50} and D_{90} values for base glass were 2.607 μm, 19.375 μm and 44.326 μm, respectively. The D_{90} value was slightly higher than 38 μm, which could indicate that the particles were not spherical, as would be in an ideal case, but more complex and oblong in shape. This seems to be reasonable when the mechanical milling process is considered. Similar discussion can also be done for powders of other glass compositions. Even though all analyzed glass powders had almost identical particle size distributions, especially the D_i values of B12.5-Sr10 were slightly lower than the values of other powders, as presented in Fig. 14. It can also be seen in Fig. 13 as a lower maximum peak intensity and a slight shift of the curve to smaller particle size region. This could not be linked to any structural differences and was most likely caused by the milling process itself. Variations this small should not affect the thermal properties or significantly the surface area and thus all powders used in scaffold production can be considered to be identical from the particle size point of view. Thus, all differences in thermal properties and *in vitro* behavior can be linked to the glass composition and network structure.

4.1.4 Thermal properties

Glass crystallization and sintering are thermally induced reactions. A wide sintering window is desired in bioactive glass. The sintering window is defined as the gap between T_g and T_x. (Watts *et al.* 2010, Jones 2013). Thus, it was essential to analyze the thermal behavior of glasses used in scaffold processing. In this thesis, the thermal transition values were obtained via DTA by following the methods presented in chapter 3.1.4. It is important to note that thermal analysis is strongly dependent on particle size and heating

rate. Smaller particle size promotes surface crystallization and can even induce it to bulk crystallizing glasses. (Jones 2013). Increase in the heating rate tends to increase the observed T_g and T_p whereas the onset of melting decreases. (Bellucci *et al.* 2010).

Analyzed DTA curves are collected to Appendix B and the obtained characteristic temperature values are shown in Fig. 15 and Table 7, which also presents the sintering temperature windows. It should be noted that B12.5-Mg5-Sr10 possessed two glass transition regions and the higher T_g value was estimated for calculating the sintering window as shown in Fig. 15. This observed phenomenon indicates that there were different phases present within the glass network, which complements the earlier discussion about possible phase separation.
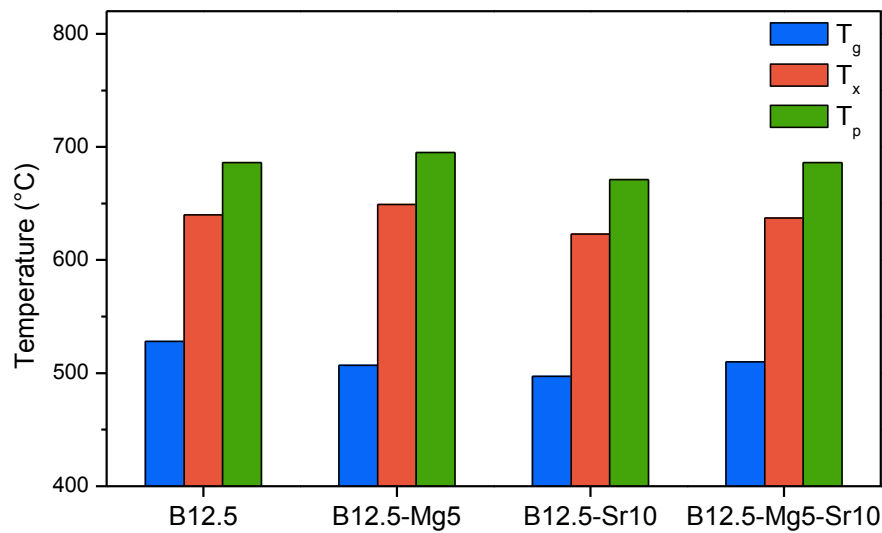
Figure 15.   *Characteristic temperatures of the studied glasses.*

Table 7.   *Thermal transition temperatures (± 3 °C) and sintering windows ($T_x − T_g$) of studied glasses. The errors related to the used instrument.*

Thermal parameter	B12.5	B12.5-Mg5	B12.5-Sr10	B12.5-Mg5-Sr10
T_g (°C)	528	507	497	475/510
T_x (°C)	640	649	623	637
T_p (°C)	686	695	671	686
T_x - T_g (°C)	112	142	126	127

The base glass B12.5 had a T_g of 528 °C, T_x of 640 °C and T_p of 686 °C. The sintering temperature window was determined to be 112 °C. From Table 7 and Fig. 15 it can be seen that Mg substitution for Ca increased both the onset and peak temperature of crystallization (T_x and T_p) but at the same time decreased the T_g. This resulted in a significant 30 °C increase of the sintering window. Magnesium is known to decrease the tendency for crystallization, which is one of the factors driving for its use in bioactive glasses

(Ylänen 2011, p. 8). Souza *et al.* studied 45S5 based glasses that were partially substituted with Mg and they linked the decrease in T_g to a mixed cation effect that decreases the glass viscosity. They also observed an increase in T_x, which was suspected to be caused by magnesium´s ability to form a more stable glass network when compared to Ca. (Souza *et al.* 2013). However, Watts *et al.* linked the decrease of T_g in a different silicate based glass to weakening of the glass network as Mg was substituted for Ca. They observed that Mg might also be present as an intermediate oxide, taking a tetrahedral form in the glass network and weakening the structure by producing Mg-O bonds that are weaker than Si-O. These results also linked the tetrahedral Mg to a simultaneous decrease in the number of NBO species, which results in a higher network connectivity and lower molar volume. (Watts *et al.* 2010). The observed effect of Mg on molar volume was also seen in this study, whereas the discussed Raman spectra suggests that Mg substitution for Ca has an opposite effect on the network connectivity. However, it should be noted that due to the complex nature of the studied glass networks, precise analysis could not be conducted with spectroscopical methods. The observed effects of Mg to thermal transition values in this study are in good agreement with previous publications. (Diba *et al.* 2012).

Strontium substitution for Ca reduced the T_g, T_x and T_p temperatures. The decrease in T_g was around 30 °C, and the decrease in T_x was less than 20 °C, which resulted in a small increase of the sintering window. Massera & Hupa studied different levels of Sr substitution for Ca in S53P4 glass and observed a continuous decrease in T_g with increasing strontium substitution. The effects of Sr on crystallization behavior were more complex as 5 mol-% Sr substitution decreased the main T_p whereas higher than 10 mol-% substitution increased it. (Massera & Hupa 2014). Fredholm *et al.* studied a glass with the composition of 49.46 % SiO_2, 1.07 % P_2O_5, 23.08 % CaO and 26.38 Na_2O % in mol-% and were able to detect a continuous decrease both in T_g and T_p when Ca was gradually replaced with Sr. The decrease in thermal transition values with Sr substitution has been linked to a more disrupted glass network as Sr-O bonds are weaker in nature than Ca-O due to greater size of Sr atoms. Weaker glass network promotes easier molecular motion and thus a decrease in T_g. (Fredholm *et al.* 2010; Salman *et al.* 2012). Results obtained in this thesis were more consistent with the data presented by Fredholm *et al.* even though the glass composition was closer to the one studied by Massera & Hupa. It should be noted, that this body of work is upon borosilicate glasses. Therefore, there are no direct comparisons with current literature.

When both Mg and Sr were substituted for Ca the glass transition behavior became more complex as two partially overlapping glass transition regions could be detected. The lower T_g around 475 °C was the lowest of the studied glasses and thus the effects of both Mg and Sr can be expected to have affected it. The second glass transition region was not clearly visible and the higher T_g had to be estimated to be around 510 °C, which was close to the value of B12.5-Mg5. Interestingly, both T_x and T_p were almost identical to the values of base glass B12.5, which may indicate similar network connectivity, as was also

observed from the discussed Raman spectra. (Fredholm *et al.* 2010, Watts *et al.* 2010). The sintering window of B12.5-Mg5-Sr10 was similar to the value of B12.5-Sr10. However, had a lower T_g value been used in the calculations, the sintering temperature window of B12.5-Mg5-Sr10 would have been the widest observed.

XRD analysis was conducted on compacted glass pellets sintered for 1 h at 550, 575 and 600 °C in order to evaluate suitable sintering temperatures for scaffold processing. The diffraction patterns are presented in Fig. 16.

a)
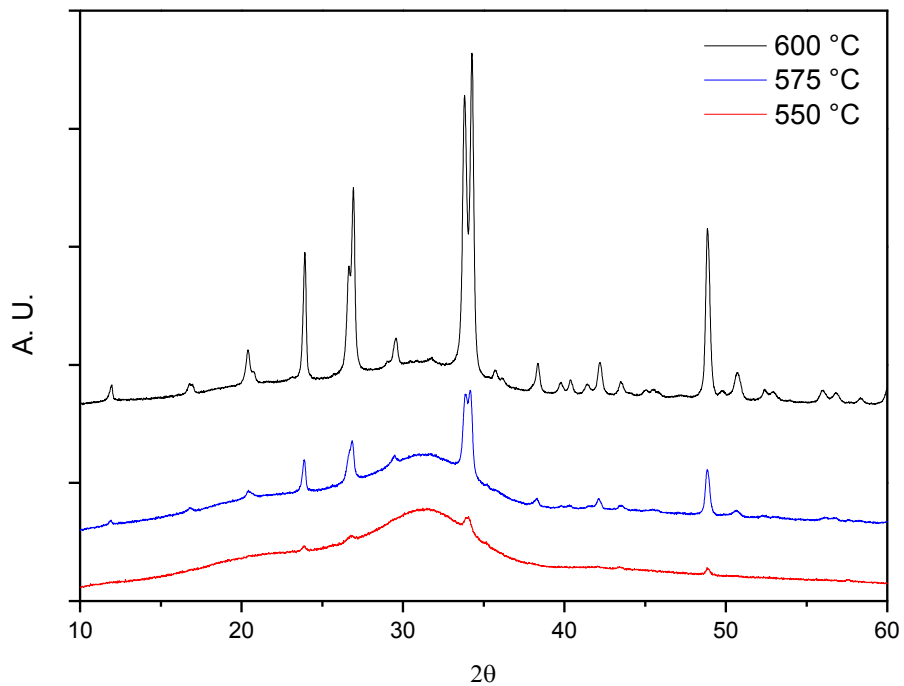
b)
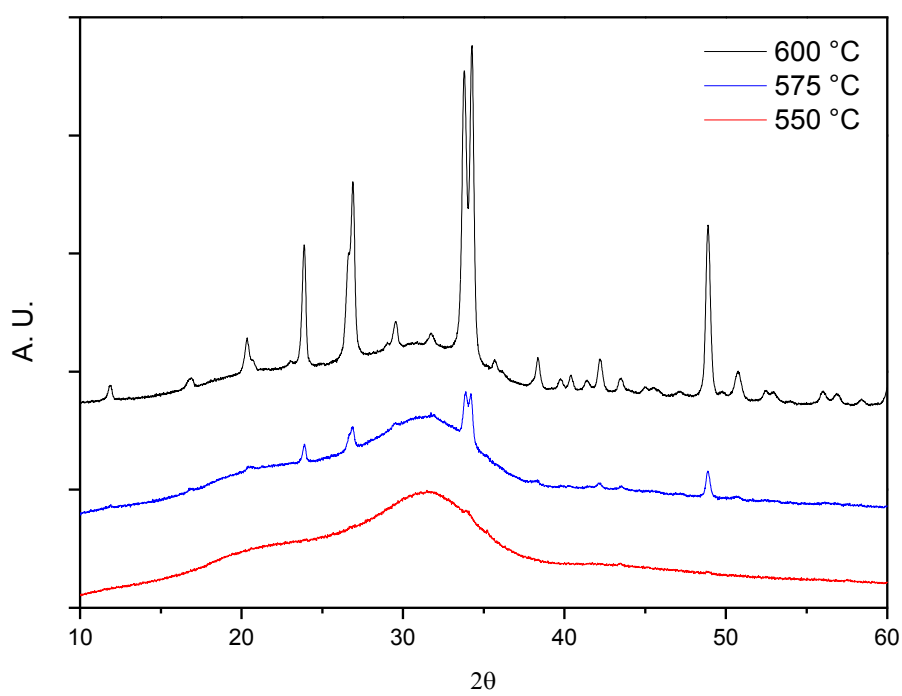
c)
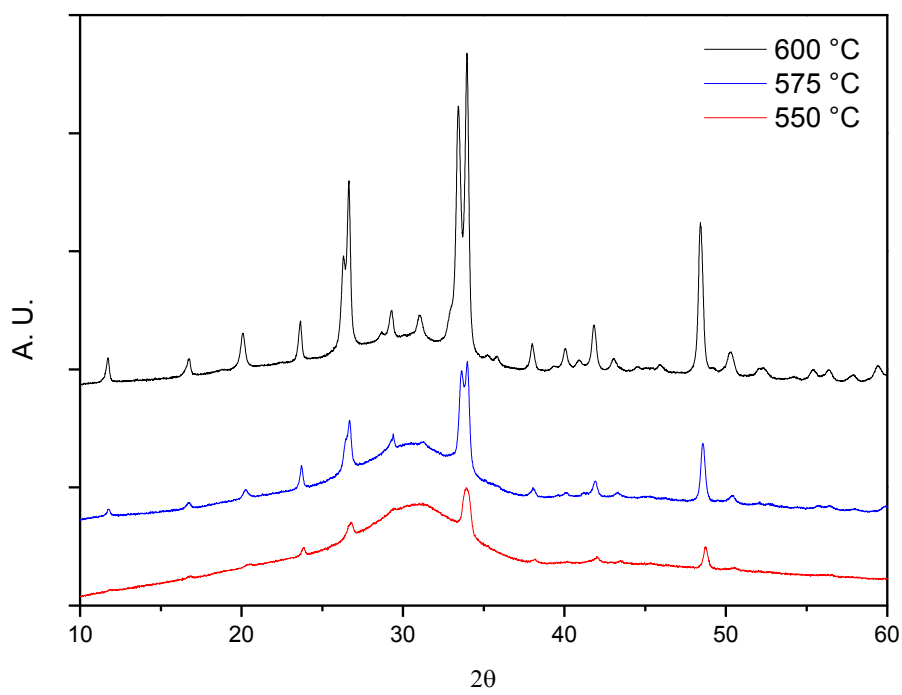
d)
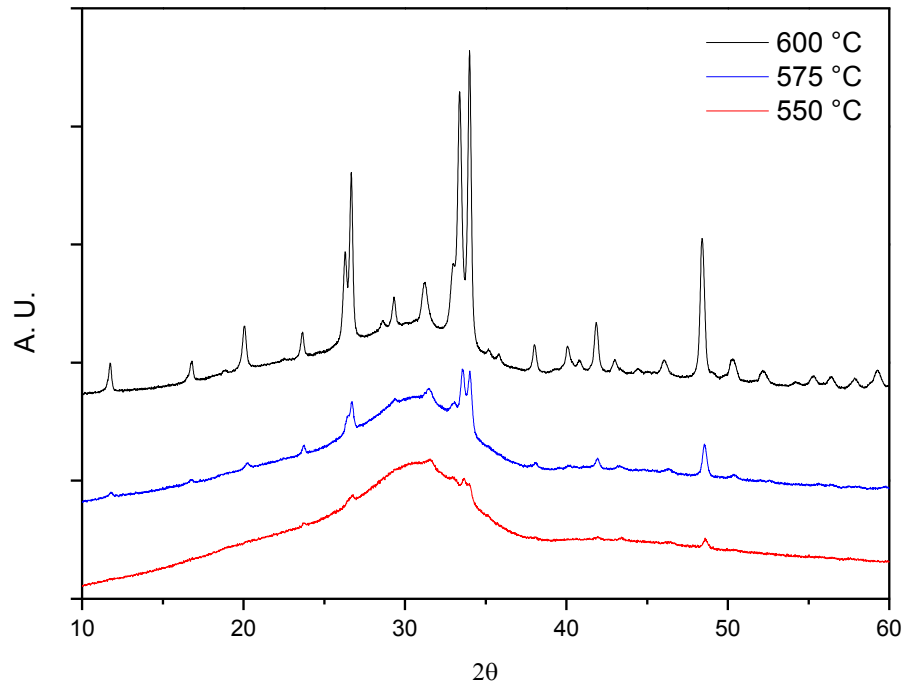
Figure 16. *XRD spectra of compacted glass pellets of a) B12.5, b) B12.5-Mg5, c) B12.5-Sr10 and d) B12.5-Mg5-Sr10*

As expected the results show that with increased temperature the tendency for crystallization increased. Sintering at 600 °C induced severe crystallization to the glasses, as shown by sharp peaks with high intensities in the diffraction patterns. Peak locations were compared to literature values for B12.5 and closest fit was found with sodium calcium silicate, Na_2O-CaO-SiO_2 (ICDD Powder Diffraction File 01-077-2189). Similar primary crystal phase has also been detected with S53P4 and 45S5 (Fagerlund *et al.* 2012). By decreasing the temperature, the peak intensities decreased and finally after sintering at 550 °C, the diffraction patterns showed almost completely amorphous structures with a typical broad amorphous halo. With only B12.5-Sr10 possessing considerable diffraction peaks. It was observed that Sr substitution for Ca caused a slight shift of the halo and diffraction peaks to lower degrees 2θ whereas the opposite but far less pronounced effect was observed with Mg substitution. The locations of B12.5-Mg5-Sr10 bands and peaks were closer to the ones of B12.5-Sr10 but with a smaller shift. These phenomena complement the molar volume results as the band typically shifts to lower 2θ values when glass network expands. (Fredholm *et al.* 2010).

B12.5-Mg5 showed lower peak intensities when compared to the base glass and no crystallization could be detected after sintering at 550 °C. Sr substituted glass crystallized more easily than B12.5 and had greater peak intensities. The similarity in thermal behavior between the base glass and B12.5-Mg5-Sr10 was also observed in the diffraction patterns. When the patterns were analyzed in detail and compared to thermal transition values, it was seen that T_x − 95 °C (Table 5) of all studied glasses would be close to the

highest possible sintering temperature that did not induce crystallization and thus was chosen for scaffold processing.

4.2 Scaffold characterization

Glass scaffolds were produced via porogen burn-off method and robocasting. In addition, composite scaffolds were also produced via $scCO_2$ foaming. Scaffolds were characterized to gain information about the material properties and their 3D structure. Mechanical strength was evaluated in compression. *In vitro* studies were utilized to assess their bioactivity and material degradation. Scaffolds were produced from all four glass compositions.

4.2.1 Scaffold structure and porosity

Scaffolds should have sufficient porosity (> 50 %), pore size (100–500 µm) and interconnectivity in order to allow tissue ingrowth and exchange of nutrients and waste products removal (Sultana 2013, p. 6). However, increased porosity has a negative impact on the mechanical properties and thus it is necessary to study the pore network structure in order to gain deep understanding about the relationship between mechanical and biological performance of scaffolds (Tomlins 2016, p. 39).

Scaffold porosities were calculated by measuring the scaffold densities and comparing the values to bulk material densities (Fig 10). The obtained values are presented in Fig. 17. From the presented results it can be seen that all scaffold types and compositions achieved porosity levels within 49–73 %. Whereas the porosities of sintered glass scaffolds was dependent upon glass composition, the composite scaffolds had comparable porosity levels between 65–68 %. Porosities of sintered B12.5 and B12.5-Sr10 scaffolds had relatively small differences of 72.7 % and 67.0 % for the scaffolds produced via porogen burn-off method and 66.0 % and 63.8 % for robocasted scaffolds, respectively. Mg substitution for Ca decreased the resulting porosities and values around 49–56 % were achieved for sintered B12.5-Mg5 and B12.5-Mg5-Sr10 scaffolds. The observed behavior was expected, since elemental substitution was found to alter the glass sintering behavior and especially Mg substitution for Ca is reported to decrease glass viscosity and lead to enhanced sintering ability (Souza *et al.* 2013; Hupa *et al.* 2016).
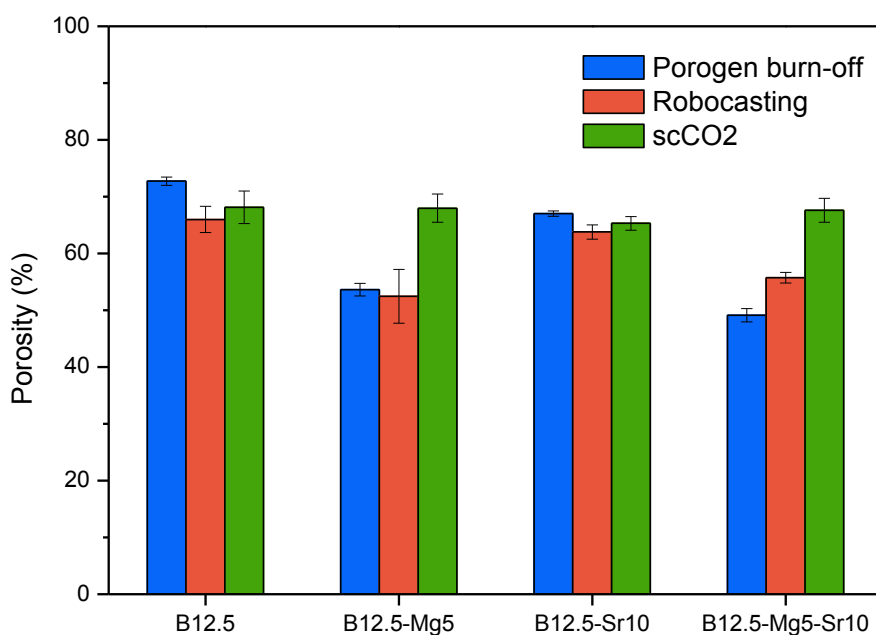
Figure 17. *Scaffold porosities obtained from physical dimensions and masses.*

Generally, scaffolds produced via porogen burn-off method had slightly higher porosities than the robocasted scaffolds, with B12.5-Mg5-Sr10 being the exception. In addition, the standard deviation in the porosity levels was smaller for scaffolds produced via porogen burn-off, which indicates better uniformity between parallel samples and consistency of the processing method. When robocasted scaffolds were fabricated, it was found that even the temperature changes in the vicinity of the printing machine caused some deviations to ink rheology, which made it difficult to maintain a constant quality. Thus the robocasting method could probably be improved by having better temperature control.

The observed porosities and standard deviations of composite scaffolds were comparable to sintered glass scaffolds. In addition, it was seen that the composite scaffold porosity was not greatly affected by the glass composition. This phenomenon was expected, since the processing method was affecting only the polymeric content. Thus, composite fabrication might be an interesting way to utilize different glasses without needing to optimize the processing parameters for each composition.

Typically, at least 50 % interconnected porosity and over 100 μm pore size are said to be required for bone tissue engineering applications (Rahaman et al. 2011; Fabert et al. 2017). Whereas the presented results suggest that the produced scaffolds had adequate porosities, the pore interconnectivity and size had to be assessed with other methods.

Scaffold 3D structures were analyzed with μ-CT combined with image analysis. Fig. 18 presents the constructed models of small scaffold fractions. It can be seen that different

scaffold types possessed considerable structural differences. Whereas the scaffolds produced via porogen burn-off and scCO₂ methods had randomly sized and located round pores, the structures of robocasted scaffolds were highly organized and comprised of parallel filaments with constant spacing.
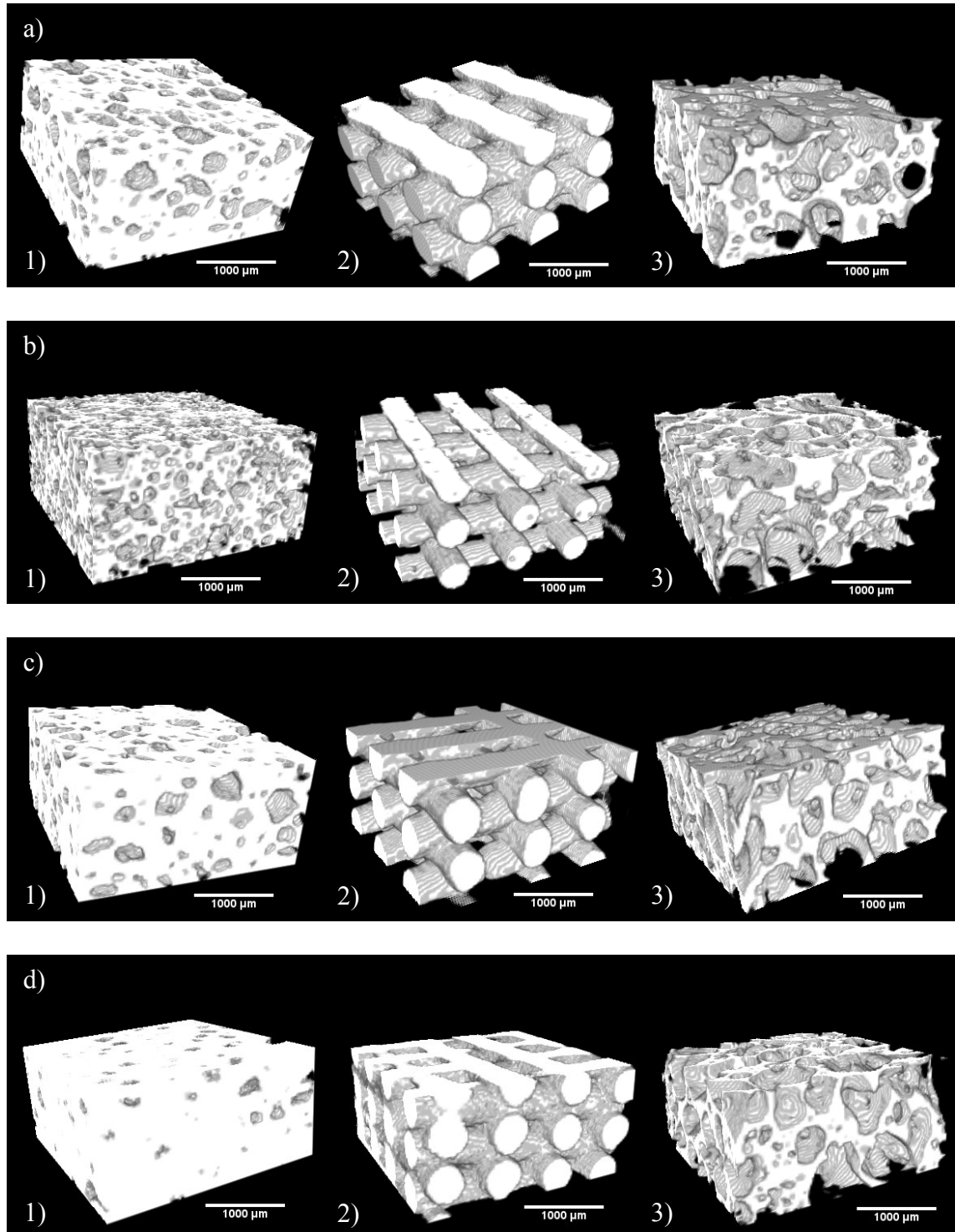
Figure 18. *3D structures of scaffolds produced via 1) porogen burn-off, 2) robocasting and 3) supercritical CO_2 methods of a) B12.5, b) B12.5-Mg5, c) B12.5-Sr10 and d) B12.5-Mg5-Sr10 compositions.*

The presented figures suggest that the composite scaffolds had a more porous structure than B12.5 and B12.5-Sr10 scaffolds produced via porogen burn-off method, whereas Fig. 17 shows the opposite. This could be attributed to limitations of the utilized analysis technique, since the relatively high pixel size used prevented precise detection of microporosity. In addition, the Mg-containing scaffolds produced via porogen burn-off method, which are presented in Fig. 18 b) and d), had almost identical porosities but their reconstructed models had considerable differences. It was seen that the material composition had a strong effect on the image contrast and thus added more variables to the analysis. More inaccuracy was caused by human errors during the image analysis, since especially thresholding the individual image slices was highly dependent on the operator.

When the structures of robocasted scaffolds were analyzed, it was seen that B12.5-Mg5 contained porosity within the individual filaments, which was probably caused by air bubbles trapped within the ink. Other robocasted structures did not show this phenomenon. However, it should be noted that B12.5-Mg5 scaffold produced via porogen burn-off method also seemed to have more detailed structure than the respective structures of other glass compositions. Thus it can be expected that also other robocasted scaffolds contained porosity within the filaments. It was also observed that all robocasted structures contained discontinuities, which were probably caused by larger air bubbles in the inks. This phenomenon could probably be avoided by optimizing the ink preparation process and would be essential in optimizing the strength and reproducibility of the scaffolds.

When the porosities of the presented structures were measured with image analysis, it was seen that the method highly underestimated the porosity for all scaffold types but most considerably for the scaffold produced via porogen burn-off method. This suggests that the scaffolds produced via porogen burn-off method contained higher amounts of small pores below the detection limit with respect to the other scaffold types. However, it can be seen that all scaffold types contained pores with > 100 μm diameters, which indicates suitability for tissue engineering applications (Rahaman et al. 2011). Whereas smaller pores were also present in models 1) and 3), the robocasted scaffold generally contained square-shaped or rectangular pores with uniform sizes in the 100 μm size scale. Good pore interconnectivity could be detected in structures 2) and 3) but not in 1). However, it should be noted that due to the limitations in the analysis, the presented 3D structures cannot be completely trusted and thus further analysis is required to assess the interconnectivity reliably. Nevertheless, the presented figures provide an idea about the structural differences. In the future studies smaller sample size might provide an option for enhancing the resolution. In addition, taking the material differences into account while conducting the measurements may improve the resulting contrast and accuracy.

4.2.2 Material characterization

Glass components in the sintered scaffolds were analyzed to provide further information about the possible changes occurring during processing. XRD analysis was conducted to both the sintered scaffolds produced via porogen burn-off and robocasting methods. The diffraction patterns, which are presented in Fig 19, show only broad bands for all studied scaffold types and glass compositions and a very low intensity peak at 34°. Broad bands are characteristic of amorphous structures and thus it can be concluded that, given the low intensity of the diffraction peak, the chosen sintering temperatures were low enough to avoid any crystallization (Fredholm *et al.* 2010).

a)
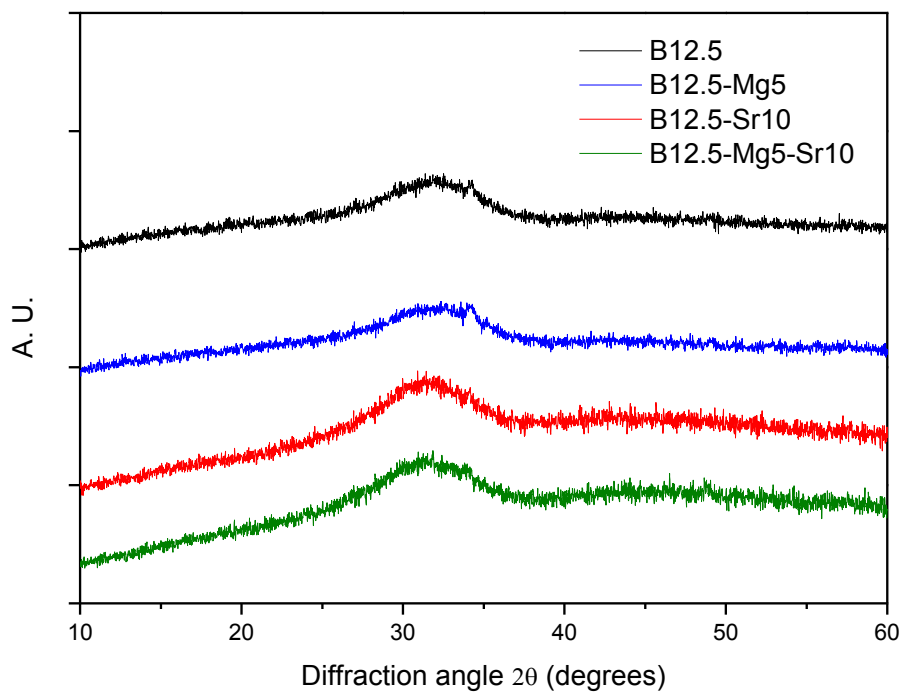
b)
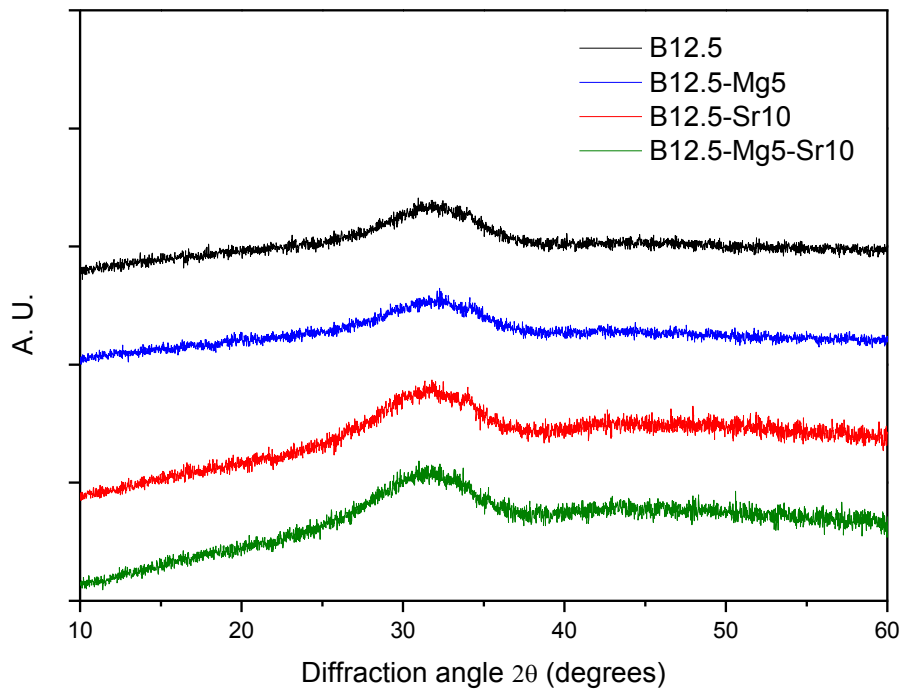
Figure 19. *XRD diffraction patterns of scaffolds produced via a) porogen burn-off and b) robocasting methods.*

TGA curves of the analyzed PLCL-B12.5 composite rod are collected in Appendix C. The analysis was conducted to ensure the homogeneity of the material. The curves show that the polymeric content started decomposing around 200 °C and that after 550 °C only the glass was left. The residual glass accounted for 30.19 and 29.23 mass-% for samples taken from the top and bottom end of the rod, respectively. Since both of these observed values are very close to the initial calculated 30 mass-%, it can be taken as an indication that the glass was uniformly distributed within the polymer matrix and the processing did not affect the glass particles distribution. The curve of the bottom end of the rod shows a slight shift to lower temperature values, but this is probably mostly due to slightly smaller sample size, which resulted in less substantial thermal lag or negligible polymer conformation induced by the $scCO_2$ process.

4.2.3 Mechanical properties

Bone formation and resorption is strongly affected by physical loading. Thus the strength of a scaffold should aim to mimic the body´s tissue. Too high strength may induce harmful bone resorption and too low strength can result in the premature failing of the implant, which should be avoided in order to provide sufficient support during healing. (Sultana, p. 7; Fu *et al.* 2011a).

The mechanical performance of the studied scaffolds was analyzed with compression testing. The highest observed compressive strength value was taken to describe the strength of the glass scaffolds and the compressive strength of the composite scaffolds was taken after 10 % deformation, i.e. at 0.1 strain. Fig. 20 presents the a) typical stress-strain curve of scaffolds produced with B12.5 glass, b) the compressive strength values of each scaffold type for each glass composition and c) the compressive strength at 10 % elongation of the composite (the scale was adjusted compared to Fig. 20 b) for ease of comparison between glass compositions). It should be noted that engineering values were used in the analysis and presentation.

a)
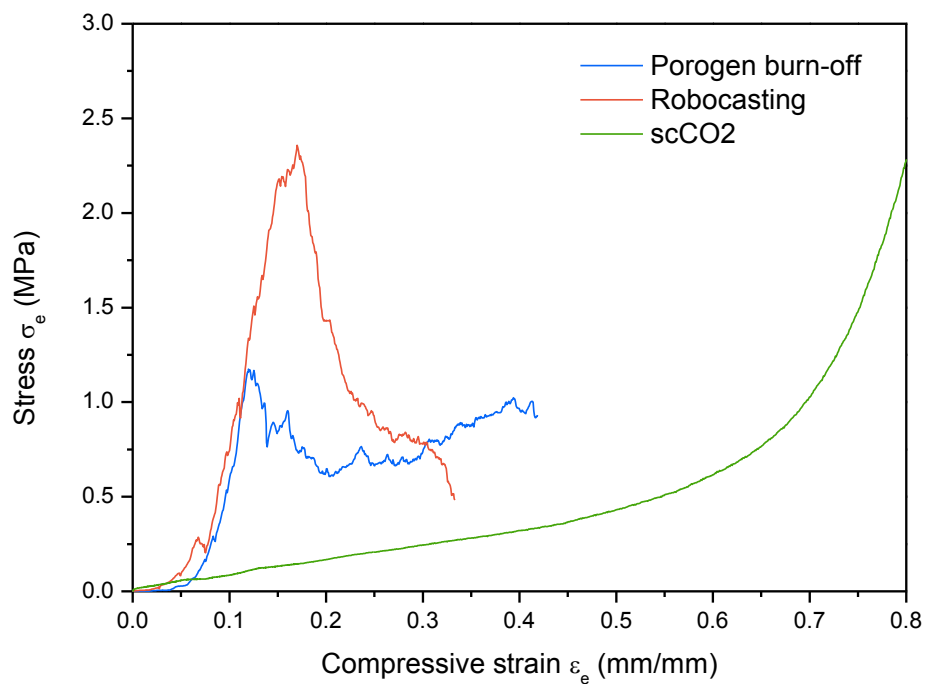
b)
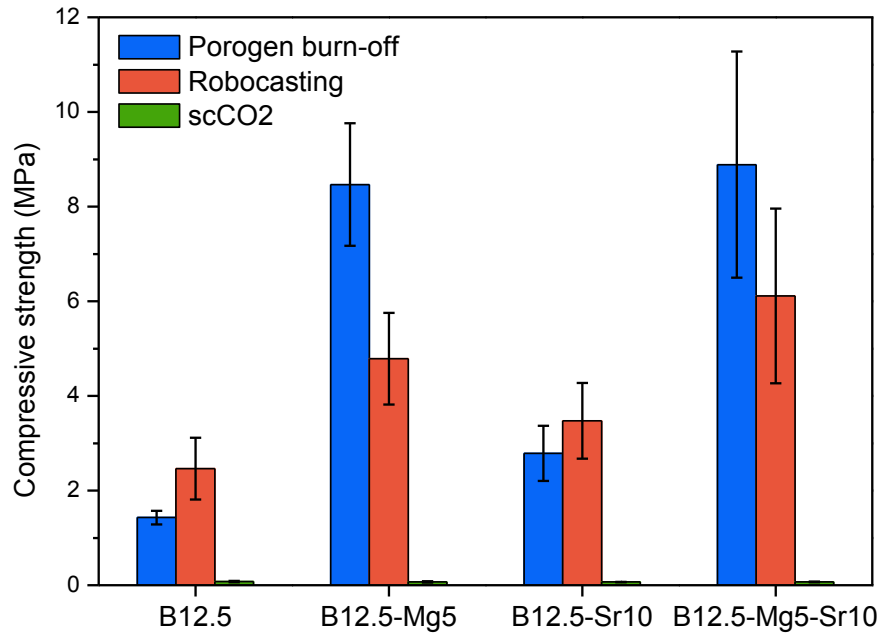
c)
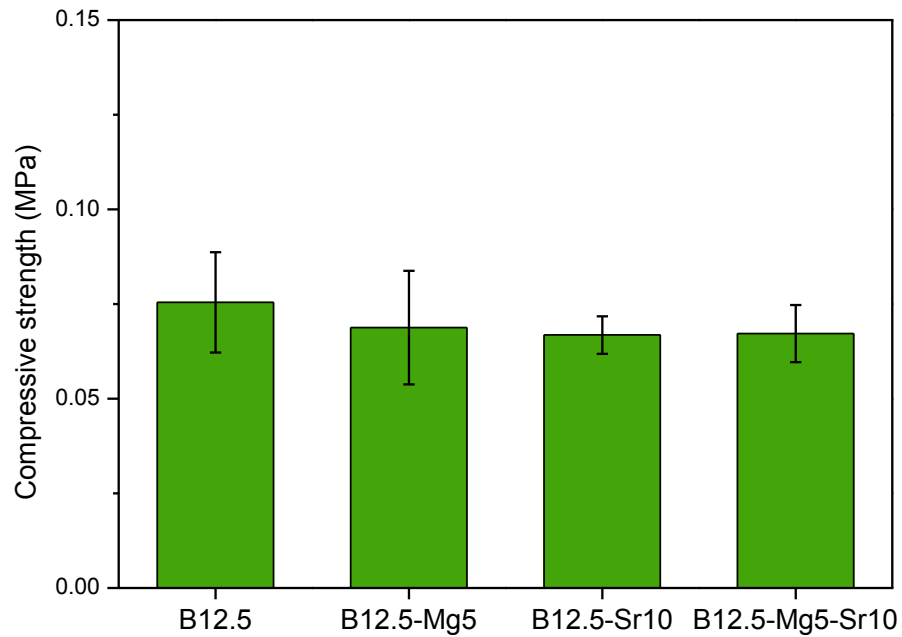
Figure 20. *Compression test results presenting a) typical stress-strain curves for the various scaffolds, b) compression strength values for all scaffolds and compositions and c) compression strength of composite scaffolds.*

Several trends can be observed from the presented figures. In Fig. 20 a) the example curves show that whereas scaffolds produced via either porogen burn-off method or robocasting possessed several peaks and failed before 0.2 strain, the composite scaffold

yielded to great extent even with low stresses and showed no point of failure. It should be pointed that the initial linear domain (from 0 to 45 % strain) correspond to the elastic behavior of the composite whereas the higher stress increase at higher deformation corresponds to compaction of the composites. These observed phenomena can be linked to the material characteristics. Whereas glasses are brittle in nature and possess sharp-edged curves, polymers can yield to great extent before breaking (Fu *et al.* 2011a; Nair & Laurencin 2002). The curves of sintered glass scaffolds also show breaking points before reaching the highest compressive strength value, which has been reported to be caused by progressive failure of individual regions and compaction of the total structural network (Fu *et al.* 2009). The compaction was observed especially with scaffolds produced via porogen burn-off method and can be seen even in the higher strain regions in the stress-strain curve.

In b) the presented compressive strength values show that whereas the strengths of sintered glass scaffolds were within 1.5–10 MPa, the composite scaffolds possessed lower strengths below 0.1 MPa at 10 % deformation. Glass scaffold strength was affected by the composition and processing method. The compressive strengths of B12.5 scaffolds produced via porogen burn-off method and robocasting were 1.5 and 2.5 MPa, respectively. Substitution of either Sr or Mg for Ca in the base glass improved the scaffold strength. However, the effect of Mg was far more pronounced and resulted in almost 500 % increase in the strength of scaffolds produced via porogen burn-off method whereas Sr substitution doubled the strength. Highest values were obtained by substituting both Mg and Sr and again approximately 500 % increase was observed. The effect of glass composition on scaffold strength was not as substantial with robocasted scaffolds and Sr and Mg substitution were able to improve the strength by approximately 40 % and 100 %, respectively. The combined effects of Mg and Sr were able to improve the strength by 150 %. The substantial effect of Mg substitution to scaffold strength can be explained with magnesium´s ability to improve the sintering characteristics by lowering glass viscosity (Souza *et al.* 2013; Diba *et al.* 2012). The effect of Sr substitution can also be explained with the widening of the sintering temperature window, which allowed sintering to be conducted at higher temperature above T_g. The strength is greatly affected by the porosity, as was observed in a previous study by e.g. Fabert *et al.* Thus the increase in strength can also be linked to the lower porosities of especially the Mg-containing glass scaffolds (presented in Fig. 17). (Fabert *et al.* 2017; Tomlins 2016, p. 39).

Magnesium-containing glass scaffolds achieved higher strengths when they were produced via porogen burn-off method, in contrast to other glass compositions. This phenomenon can be explained when the nature of different processing methods are considered. During processing via porogen burn-off method, the glass powders were compacted and thus the contact area between glass particles increased. This most likely promoted the sintering ability of Mg-containing glasses and because of the viscosity decreasing effect of Mg, resulted in greater strength (Souza *et al.* 2013). In robocasting the particles were

relatively loosely packed within the ink and thus the fusing of adjacent particles probably was not as substantial. However, an ordered structure can improve mechanical properties since the material breakage typically starts from the greatest flaw. Whereas the scaffolds produced via porogen burn-off method may contain weak regions with very little glass, the strength of robocasted scaffolds should be uniform throughout the whole structure. These factors are probably the reasons behind the higher strengths when robocasted B12.5 and B12.5-Sr10 scaffolds are considered.

Overall, the strengths of sintered glass scaffolds were mostly within the 2–12 MPa strength of trabecular bone (Fu *et al.* 2011a). It has been reported that hip stems are subjected to 3–11 MPa loading and tibial bones to approximately 4 MPa stresses. (Olah *et al.* 2006; Liu *et al.* 2013). Whereas the base glass B12.5 and B12.5-Sr10 were in the lower region of the reported trabecular bone strengths, Mg-containing glass scaffolds were in the middle region and thus seem to be more suitable for load-bearing applications. Fabert *et al.* produced borosilicate glass scaffolds with over 50% porosities by sintering loosely packed particles and gained 1–3 MPa compressive strengths. Strength values of 1.5–7.0 MPa have been reported for 50–80 % porous scaffolds produced via porogen burn-off method (Wu *et al.* 2014). Values within the same magnitude have been observed with borate and borosilicate glass scaffolds produced with foam-replica method (Fu *et al.* 2009; Fu *et al.* 2010). Additive manufacturing methods have been proven to provide higher strengths than conventional methods and even one order of magnitude higher strengths of 50–150 MPa have been achieved. Several of these studies have utilized robocasting as the production method. (Fu *et al.* 2011b). 45S5 scaffolds with over 70% porosities have been robocasted by Eqtesadi *et al.* They were able to gain 2 MPa compressive strengths without inducing severe crystallization. (Eqtesadi *et al.* 2014). The results obtained in this thesis were more consistent with the values reported by Fabert *et al.* and Eqtesadi *et al.* but substantially lower than the ones reported by Deliormanli & Rahaman. However, as the publication by Deliormanli & Rahaman presented, the resulting strength was highly dependent on glass composition and may be partly responsible for the lower strength observed in this study. In addition, a smaller sample size in the discussed experiments may cause the observed differences as the possibility for critical flaws decreases with decreasing sample size. It should be noted that the relative errors within parallel samples were close to 20 % in this study and similar to the ones observed by Deliormanli & Rahaman and Fabert *et al*. (Deliormanli & Rahaman 2012; Fabert *et al.* 2017). The high relative error can be linked to the minimum amount of parallel samples and to the nature of test materials.

The compressive strengths of composite scaffolds, presented in Fig. 20 c), show that regardless of the glass composition the strength was within 0.065–0.075 MPa. The values were highly similar and can be considered to be identical when the errors of the measurement are taken into account. Since the composite scaffolds were produced by utilizing the processability of the polymer, no sintering had to be conducted and thus the obtained

strengths were similar. This could be an interesting way to utilize glasses that are prone to crystallize during sintering or that have a rapid dissolution rate and therefore cannot be processed using traditional extrusion in bone tissue engineering (Blaker *et al.* 2010). Also, tailoring the glass composition within the composite, could be help in tailoring the biological response without need to optimize the processing parameters for each composition. Previous studies have shown that the volume of the reinforcement within the composite and the shape of the reinforcement have a substantial effect on the strength of the scaffold (Olah *et al.* 2006; Kumar *et al.* 2015). However, since all glasses used in this thesis went through a similar milling process, they had almost identical particle size distributions (Figs. 13 and 14) and similar volume fractions within the composites, it can be expected that all glass compositions had similar effects on the strength of the composite.

The compressive strength values found from existing literature show a range of properties for different polymer and composite scaffolds. PLCL scaffolds (9 mm in diameter and 15 mm in length) with approximately 80 % porosities have been reported to have compressive strengths of 15–40 kPa, measured from the maximum point of the stress-strain curve (Akkouch *et al.* 2011). One order of magnitude higher strengths of 0.5–0.8 MPa (at 10 % elongation) were obtained by Olah *et al.* who added 25 m-% of calcium carbonate in the form of calcite to PCL matrix and produced 7.5 x 7.5 x 10 mm sized composite scaffolds. Similar strength values have been achieved by Zhang *et al.* who produced PLLA/PLGA/HA composites with over 80 % porosities for cranial bone regeneration. They studied cylindrical samples, 10 mm in diameter and 15 mm thick, and measured the strength at 10 % elongation. (Zhang *et al.* 2016). PCL scaffolds (approximately 4.8 mm in diameter and 15.2 mm in length) with HA reinforcements and over 50 % porosities have been reported to achieve ultimate compressive strengths of over 3 MPa, which are considerably higher than the values observed in this thesis (Lu *et al.* 2014). However, it should be noted that due to the differences in materials, sample sizes and processing methods, the direct comparison to existing literature is difficult. The compressive strength values obtained in this thesis were approximately one order of magnitude higher than the strength of pure collagen and similar to that of previously studied chitosan scaffolds (10 mm in diameter and 3 mm thick) with > 80 % porosities (Wu *et al.* 2014; Ji & Shi 2013). The substantial yielding even with low stresses suggests that these scaffolds are not completely suitable for load-bearing applications and more material optimization is required. However, this type of composite structure could be utilized in non-load-bearing applications.

To conclude, it can be stated that it was possible to produce porous structures from the studied bioactive glasses with porosities and mechanical properties well in line with the values reported for trabecular bone. The analyzed composite structures would seem to be suitable to promote release of active components in the medium while favoring the tailoring ability of the material. However, higher strengths could possibly be obtained by optimizing the material choice, glass loading and scaffold processing parameters.

4.3 In vitro testing

In vitro testing was conducted to gain information about the biological activity and behavior of the studied materials and scaffolds. The utilized methods have widely been used to simulate *in vivo* conditions and thus the obtained results may give indications about the *in vivo* behavior (Ylänen 2011, p. 17). Material dissolution and ion release was studied along with surface layer formation. Mass loss and effects of degradation to mechanical response were also analyzed.

4.3.1 Dissolution and bioactivity

During glass dissolution the cations in glass structure are replaced with hydrogen ions from the surrounding solution, which causes the pH of the solution to rise (Jones 2013). Thus studying the pH change can provide information about the dissolution rate (Massera *et al.* 2012b). It should be noted that the constant sample mass to SBF volume ratio used in this study is not ideal. Having constant sample surface area to SBF volume instead would give more accurate information about the effects of compositional tailoring to material reactivity. (Massera & Hupa 2014). However, this being said Macon *et al.* demonstrated in a round robin testing that mass to volume ratio could be used for samples with small compositional change and therefore small variation in surface area (Macon *et al.* 2015). The pH of SBF after different scaffold immersion times are presented in Fig. 21.

a)
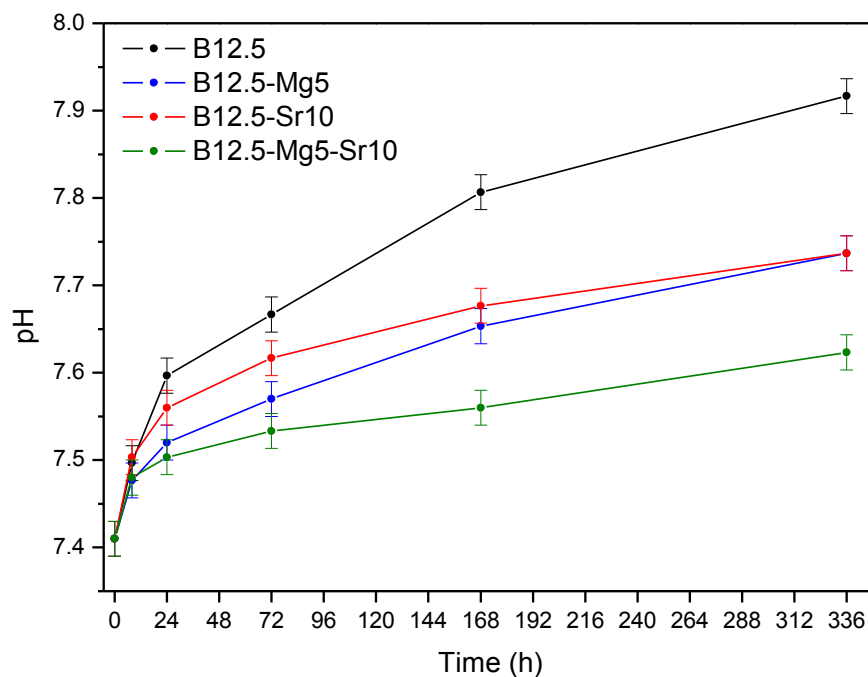
b)
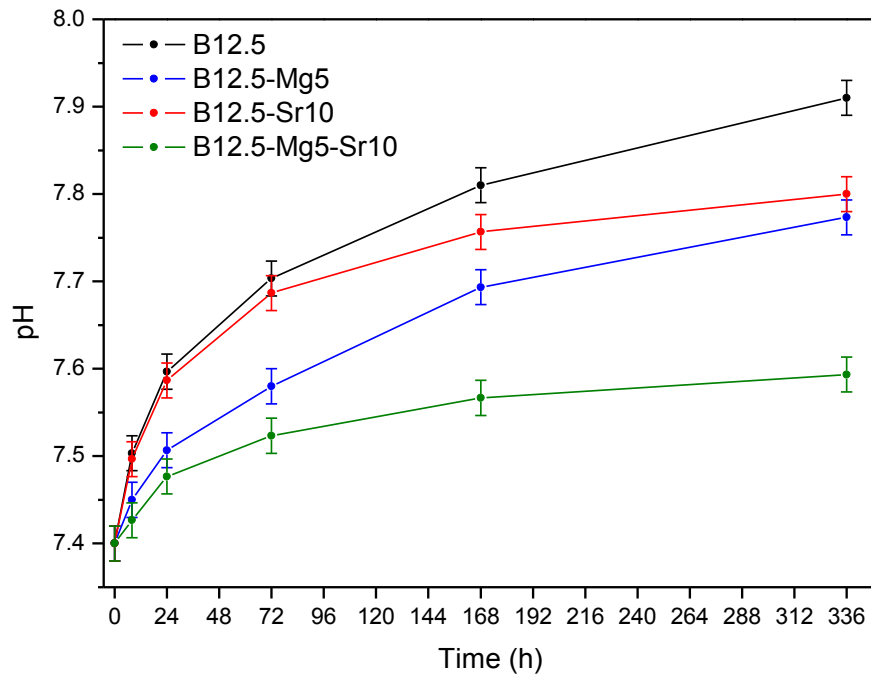
c)
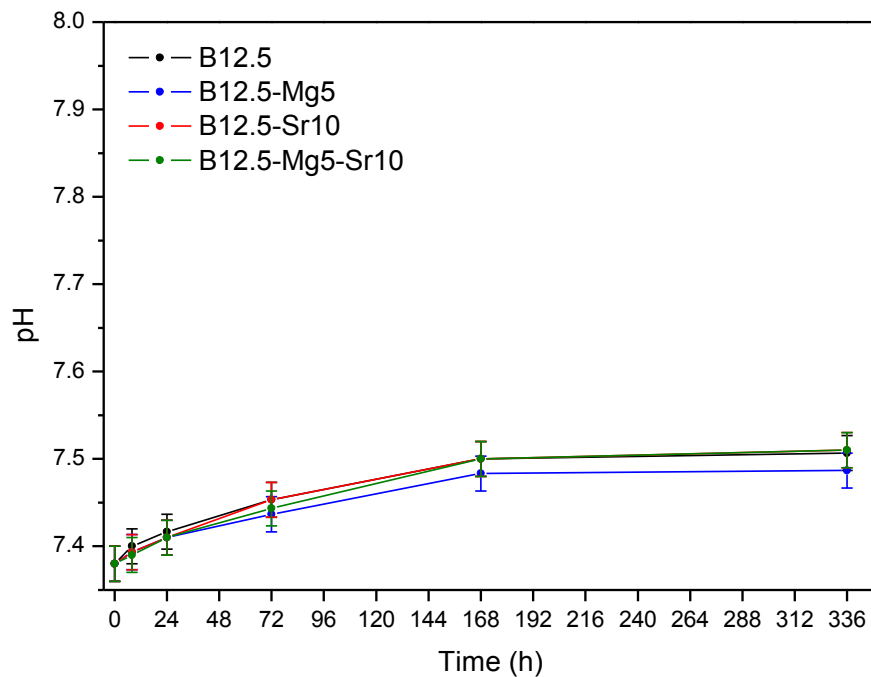
Figure 21. *pH of SBF after immersing scaffolds produced via a) porogen burn-off, b) robocasting and c) supercritical CO_2 methods for different times. Presented errors are related to test method.*

From Fig. 21 it can be seen that all scaffolds caused an increase in the pH of the SBF. At first the pH increased rapidly from the initial 7.40 ± 0.02 and then reached a plateau across longer immersion times. From a) and b) it can be seen that regardless of the processing

method the sintered scaffolds showed similar behavior and relations between different glass compositions. The base glass B12.5 had the highest pH increase and achieved pH of 7.91–7.92 ± 0.02 after 336 h immersion whereas the pH increase was lowered by substitution of either Mg or Sr for Ca in the base glass and values of 7.74–7.80 ± 0.02 were reached. B12.5-Sr10 had a more substantial pH increase than B12.5-Mg5 during the first 168 hours but after 336 hours these glasses seem to have dissolved to approximately to the same extent. B12.5-Mg5-Sr10 had the slowest pH increase and the pH did not rise above 7.62 ± 0.02 even after 336 h immersion, which indicates that both Mg and Sr were again affecting the dissolution rate. There were noticeable differences between the results of different scaffold types of the same glasses. For instance, the pH related to B12.5-Sr10 scaffold produced via porogen burn-off method was 7.68 ± 0.02 after 168 h immersion whereas the robocasted scaffold had caused the pH to increase to 7.76 ± 0.02 in the same time. In general, the robocasted scaffolds seem to have caused a slightly higher pH increase especially during the first 168 hours. This can most likely be attributed to discussed differences in porosities and surface areas (Chapter 4.2.1).

The presented results suggest that the base glass had the fastest dissolution rate and by substituting Mg or Sr the glass become chemically more durable. The effect of Mg substitution for Ca in S53P4 has been studied by Massera *et al.*, who suggested that Mg substitution improved the chemical durability and slowed down the ionic release as the glass network became more compact. (Massera *et al.* 2012b). Similar phenomenon was observed by Hupa *et al.*, who substituted Mg and Sr for Ca in the same glass. In addition to that, they were able to detect a considerable decrease in the chemical durability of the glass when Sr for substituted for Ca. (Hupa *et al.* 2016). However, Goel *et al.* studied different levels of Sr substitution for Ca in a silicate based glass and observed a decrease in ionic release and apatite formation with increasing substitution levels. They attributed this phenomenon to a stronger Sr-O bond strength when compared to Ca-O and also to lower electronegativity of Sr, which reduced the tendency for strontium cations to be exchanged with hydrogen ions from the solution. (Goel *et al.* 2011). The observed effect of Sr in this study is in contradiction with the observations of Hupa *et al.* and more consistent with the results of Goel *et al.* More precise analysis of the effects of Sr substitution for Ca in B12.5 could be done e.g. by studying different substitution levels, as was partly done in (Tainio 2016).

The pH increase caused by the composites, which is presented in Fig. 21 c), shows that the increase was much slower and more stable than with the sintered glass scaffolds. This can be attributed to two different factors. Firstly, the composites contained only 15.95 vol-% of glass, which resulted in 29.89–31.55 mass-%, depending on glass composition. Thus the SBF volume to glass mass ratio in the tests was 100 ml of SBF for 44.84–47.32 mg of glass, which is considerably higher when compared to the 100 ml of SBF for 150 mg of glass ratio with sintered glass scaffolds. This will cause a slower pH increase, even though the surface area of glass may remain relatively high, since no sintering has been

conducted and thus no particles have fused together. However, the polymer matrix surrounding or partly covering the glass particles may have limited ion exchange. Secondly, the polymeric matrix degrades in aqueous solutions too and releases acidic degradation products, which will buffer the pH change. This phenomenon is widely known and considered to be one of the advantages of composites, since high pH change may be harmful for cells. (Boccaccini & Maquet 2003; Rezwan *et al.* 2006). The pH of all samples remained below 7.52 ± 0.02 even after 336 hours of immersion and all samples resulted in a similar increase. All composite scaffolds had similar porosities and glass volumes. Thus the reactive surface areas can be expected to have been similar too, whereas the porosities of sintered scaffolds depended on the composition and thus the samples possessed different surface areas. This might partly explain the highly similar pH increase observed with composite scaffolds. The pH increase of B12.5-Mg5 was slightly lower than the ones of other samples after 168 hours and the difference remained even after 336 hours. This phenomenon was not present in a) or b), which indicated a lower dissolution rate for B12.5-Mg5-Sr10 instead.

Ion release of the scaffolds was further evaluated with ICP-OES. The aim was to gain information about the effects of scaffold structure and composition to the rate of dissolution. Fig. 22 presents a) Si, b) B, c) Ca, d) P, e) Mg and f) Sr ion concentrations post immersion of the scaffolds obtained via porogen burn-off method, taken as examples. Results of all glass compositions and scaffold types are collected to Appendix D.

a)
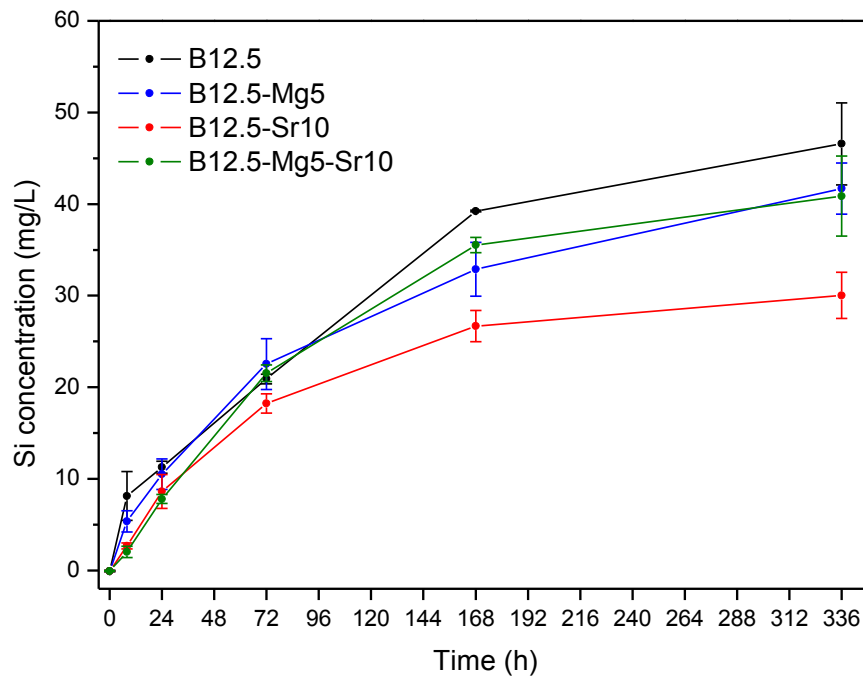
b)
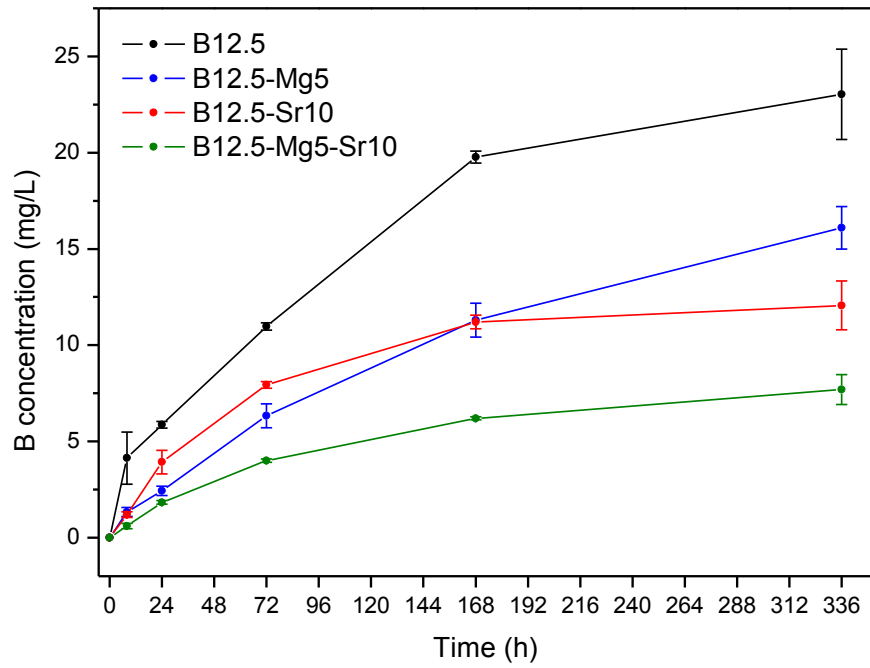
c)
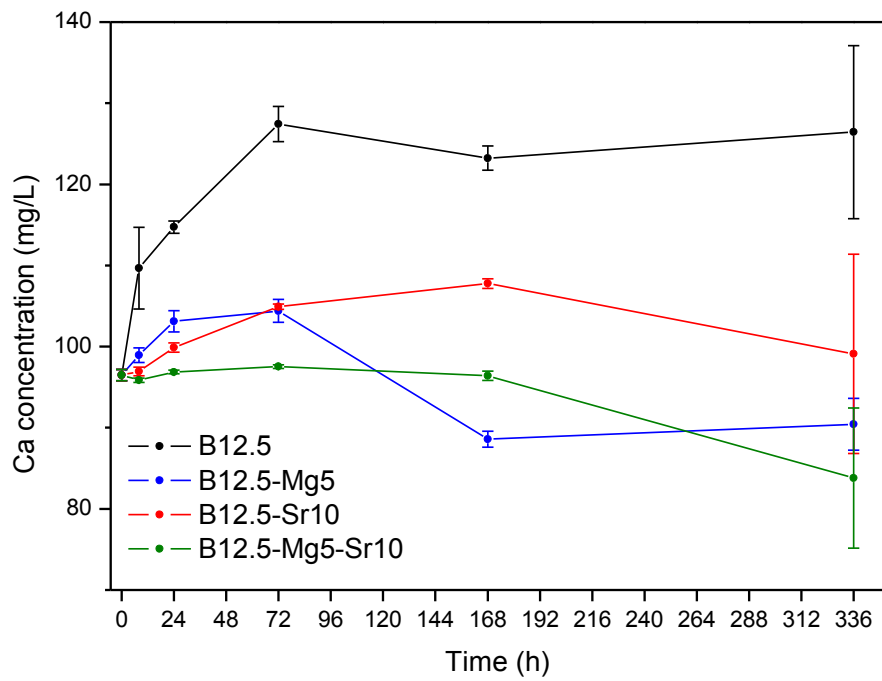
d)
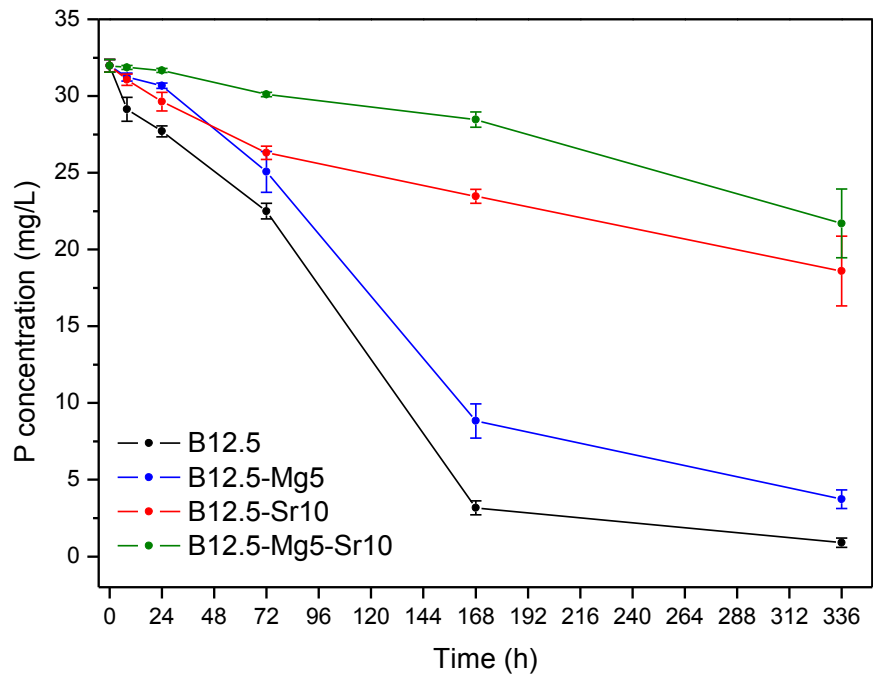
e)
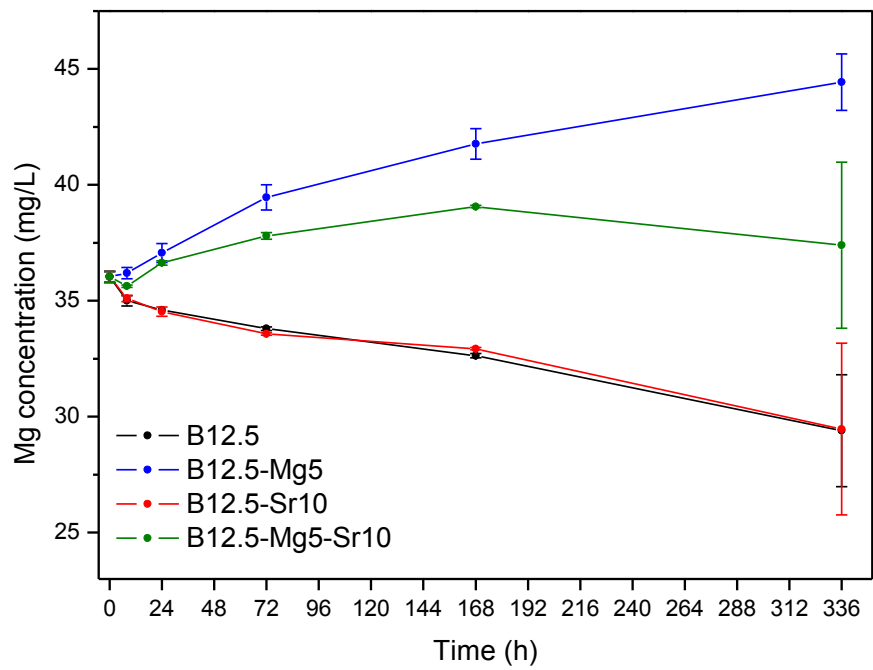
f)
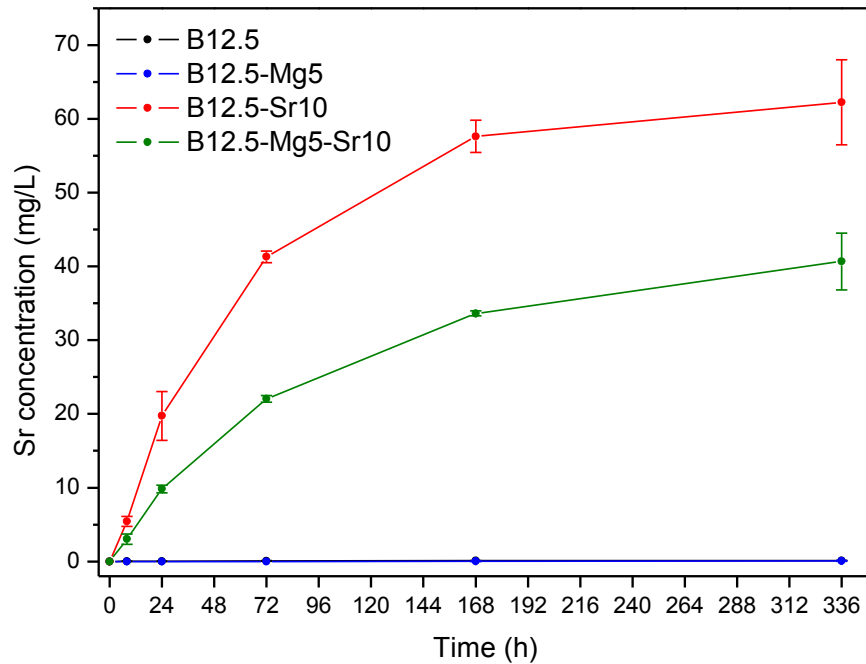
Figure 22. *Ionic concentrations (mg/L) of a) Si, b) B, c) Ca, d) P, e) Mg and f) Sr in SBF as a function of scaffold immersion time. Results are related to scaffolds produced via porogen burn-off method.*

Fig 22 a) and b) present the change in glass forming ions (Si and B) concentrations in the SBF. Si and B are the backbone of the glass structure. As expected form previous research on borosilicate, the Si and B ions are released in the solution, showing breakage of the glass network. However it is important to point out that, while, up to 72 h of immersion no real differences in the Si release can be seen as a function of glass composition. The Mg- and/or Sr-containing glasses exhibit a much lower B release than the base glass. This indicates that Mg and Sr mainly have effects on the stabilization of the borate network. The decrease in boron release could be a desired effect since high amounts of these ions has been shown to be harmful for cell proliferation (Fu et al. 2009).

The Ca concentration first increases for all glass compositions and then either stabilizes after 168 h of immersion or starts decreasing between 72 and 168h. The higher Ca ion concentration of the solution containing the B12.5 glass is consistent with the larger glass former release in solution and with the higher Ca concentration in the glass composition.

The P ion concentration was found to decrease with time. The base glass shows faster P decrease than the substituted glasses. Typically, a phosphate consumption is related to the precipitation of a calcium phosphate reactive layer. The slower P consumption may indicate a slower precipitation of a reactive layer, as has been reported previously. (Massera & Hupa 2014).

The Mg ions concentration was found to decrease in all glasses which did not contain Mg in their structure. One can therefore think that, given the similarity between the Ca and the Mg ions part of the Mg in the solution is consumed due to the precipitation of a Mg-substituted calcium phosphate. All glasses containing Mg show an increase in the Mg concentration which could be beneficial for new bone formation.

Finally the Sr ion concentration was found to increase in the solution for all glasses containing Sr. As expected from the lower dissolution of the B12.5-Mg5-Sr10 glass backbone, compared to the B12.5-Sr10 the amount Sr in the solution containing the former was lower. However, the presence of Sr in the solution may also indicate that part of the Sr, which is also similar than Ca, enters the calcium phosphate reactive layer. Also the presence of Sr in the solution was found to be beneficial for the activity of human gingival fibroblast (Massera *et al.* 2015).

The results obtained for robocasted scaffolds showed similar trends in terms of ion concentration changes. However, the results were not completely identical. When Si release is considered, the difference between B12.5 and B12.5-Mg5/B12.5-Sr10 was more substantial for the scaffolds produced via porogen burn-off method. Indeed robocasted scaffolds exhibit a Si release almost identical for all glass compositions during the first 168 hours (29–33 mg/L), whereas differences could be seen after 72 hours with scaffolds produced via porogen burn-off method. At 168 hours, the average Si concentrations related to scaffolds produced via porogen burn-off method were approximately 39, 36, 33 and 27 mg/L for B12.5, B12.5-Mg5-Sr10, B12.5-Mg5 and B12.5-Sr10, respectively. One may assume that the high pressure used in compaction of scaffolds prepared via porogen burn-off method and the successive sintering may have altered to some extent the silicate structure of the glasses.

Overall, greatest differences were observed with B12.5-Sr10, which possessed lower Si release and P consumption than B12.5-Mg5 when the scaffolds produced via porogen burn-off method were considered. No great differences between these two compositions could be detected with robocasted scaffolds. In addition, the robocasted B12.5-Sr10 had higher Sr release than the scaffold produced via porogen burn-off method and average concentrations of approximately 97 and 62 mg/L were reached after 336 hours, respectively.

When the Mg or Sr release is studied, the results seem to suggest that both B12.5-Mg5 and B12.5-Sr10 dissolved faster than B12.5-Mg5-Sr10. The Mg concentrations of B12.5-Mg5 samples reached approximately 45 mg/L after 336 hours whereas B12.5-Mg5-Sr10 samples reached a maximum of 37–39 mg/L at 168 hours, after which a slight decrease could be detected. The Sr concentrations related to B12.5-Mg5-Sr10 scaffolds produced via robocasting and porogen burn-off method were approximately 48 and 40 mg/L after 336 hours, respectively. These values are approximately 50 % and 65 % of the values of B12.5-Sr10 samples. These results are again possibly due to the combined effects of Mg

and Sr to glass network and complementary to earlier discussions. Similar observation can also be seen with B and Ca release and P consumption rate. These observations are in line with the discussed pH changes and effects of Mg and Sr to glass dissolution and apatite formation rates. (Diba *et al.* 2012; Massera *et al.* 2012b; Goel *et al.* 2011; Massera & Hupa 2014). The results are also in line with the dissolution study performed on glass particles within these compositions (Tainio 2016). Since both sintered scaffold types went through similar thermal processing cycles, the differences between the different scaffolds of the same composition can be expected to be due to the differences in scaffold structures (presented in Fig. 18), e.g. the differences in the amount of open porosity and pore size affecting total surface area. In addition, the ion release behavior was generally more linear and consistent for the robocasted scaffolds. The benefit of robocasting is that scaffolds can be designed to have reproducible uniform structures with comparable surface areas. Whereas the scaffolds produced via porogen burn-off method are affected by porogen structure, loading and distribution, thus causing differences in surface areas between samples.

The ionic release from composite scaffolds produced via $scCO_2$ was considerably lower than from the glass scaffolds, which can be explained with the lower amount of glass in the composite structure. In addition, some of the observed trends were not identical to the ones of sintered glass scaffolds. Whereas the results of glass scaffolds indicated that all glasses had relatively similar Si release, the Si release from composite scaffolds suggests that both Sr-containing glasses have faster degradation rate than other glass compositions as their Si release was higher (approximately 16 and 12 ppm after 336 h for Sr-containing glass and other compositions, respectively). This observation is in line with the earlier discussed results of Hupa *et al.* but in contradiction with the discussed results of glass scaffolds (Hupa *et al.* 2016). The boron release from B12.5-Sr10 was also higher than from the other glass compositions, even though being only slightly higher than the release from B12.5. Both Mg-containing glasses seemed to dissolve to a lower extent. When the Si release was considered, with B12.5-Mg5-Sr10 fell in between of B12.5-Sr10 and B12.5-Mg5, which could be caused by the combined effects of Mg and Sr to glass network.

The Ca concentration change related to composite scaffolds showed that first all glasses caused an increase in the Ca concentration in the solution. However, the values started decreasing after the first 24 hours of immersion. This decrease was coupled with P consumption from the solution, again indicating formation of calcium phosphate layer (Massera & Hupa 2014). The Sr-containing glasses seemed to have higher initial Ca release rate than other glasses and reached approximately 106 mg/L concentration, whereas the other glasses reached 101-102 mg/L maximum at 8–24 hours. However, the P consumption of B12.5 was the highest and the concentration dropped to approximately 13 mg/L after 336 hours, which suggests that it may have had a higher rate of layer formation. The P concentrations of B12.5-Mg5, B12.5-Sr10 and B12.5-Mg5 were approximately 16, 17 and

22 mg/L after the same time. Thus the change in Ca concentration is complex to interpret, as both release and consumption reactions are present. The highest reaction rate of B12.5 is in line with the results of the glass scaffolds. In addition, B12.5-Mg5-Sr10 again showed indications of the slowest rate of layer formation and dissolution, which could be due to increased chemical durability caused by Mg and Sr substitution.

The solutions containing the composite scaffolds with Mg-free glass seemed to exhibit a minute decrease in Mg concentration, whereas all composite scaffolds with Mg-containing glasses clearly leached out Mg into the solution during the first 168 h. For longer immersion times the concentration of Mg remained constant. Whereas the results of both glass scaffold types showed higher Sr release rate for B12.5-Sr10 than for B12.5-Mg5-Sr10, the composite scaffolds of these two compositions had almost identical Sr release during the whole studied period and 18–19 mg/L concentrations were reached. Overall, the B12.5-Mg5-Sr10 composites seemed to have dissolved relatively more rapidly than the glass scaffolds of the same composition. This could also been seen in the pH change, which indicated relatively similar overall reactivity for all compositions.

These observed differences are possibly due to the dissimilar scaffold structures. The reactive surface areas of glass scaffolds were affected by the sintering process and fabrication method. In contrast, the composite scaffolds contained similar volumes of glass particles that had not fused together and thus the surface areas should have been comparable regardless of the glass composition. Another point to take into account is that the ion migration from the scaffold to the medium might be affected by the ability of the ion (due to e.g. electronegativity and size) to diffuse through the polymeric matrix. Also, while the glass degrades it should be pointed out that the polymer too degrades, leading to a buffering of the solution. This in turn will lead to slower glass degradation.

Scaffolds were analyzed via FTIR spectroscopy in order to gain information about changes in the surface of the glass due to the immersion in SBF. Spectra were background corrected and normalized to the peak with highest intensity. Fig. 23 presents the spectra of sintered B12.5 scaffolds produced via porogen burn-off method a) and robocasting b) at various immersion times. Fig. 24 shows the spectra of all sintered glass scaffolds produced via porogen burn-off method a) robocasting b) after 336 h of immersion. The spectra of all glass compositions and scaffold types after different immersion times are collected in Appendix E.
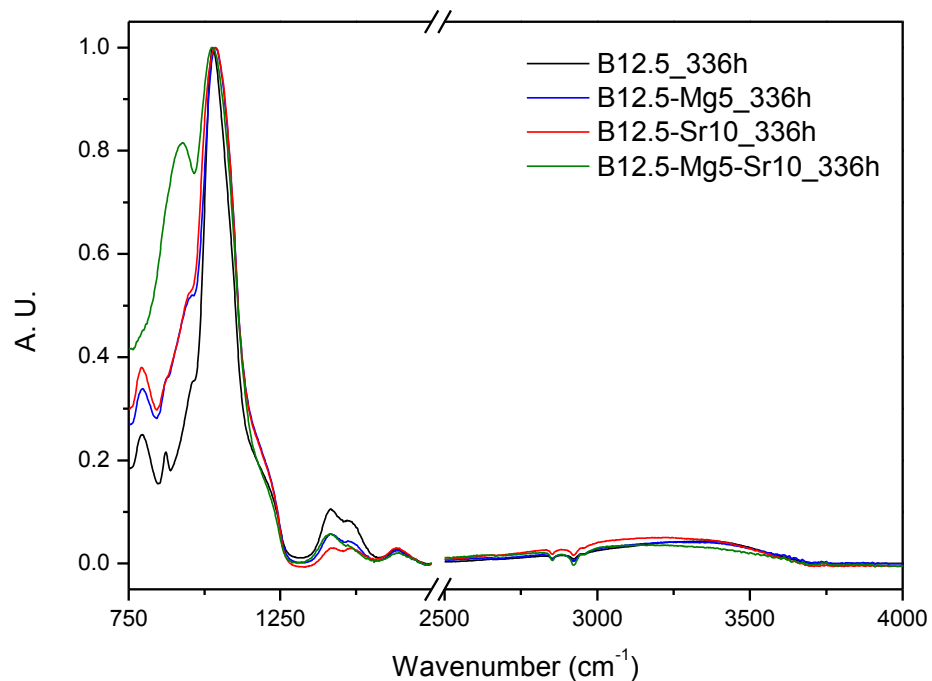
a)
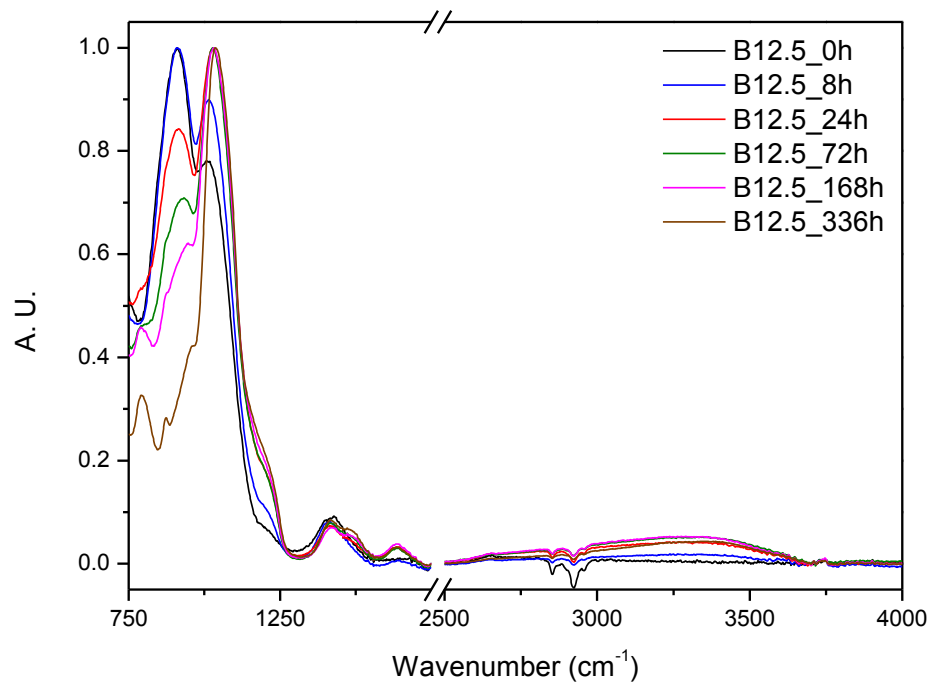
b)
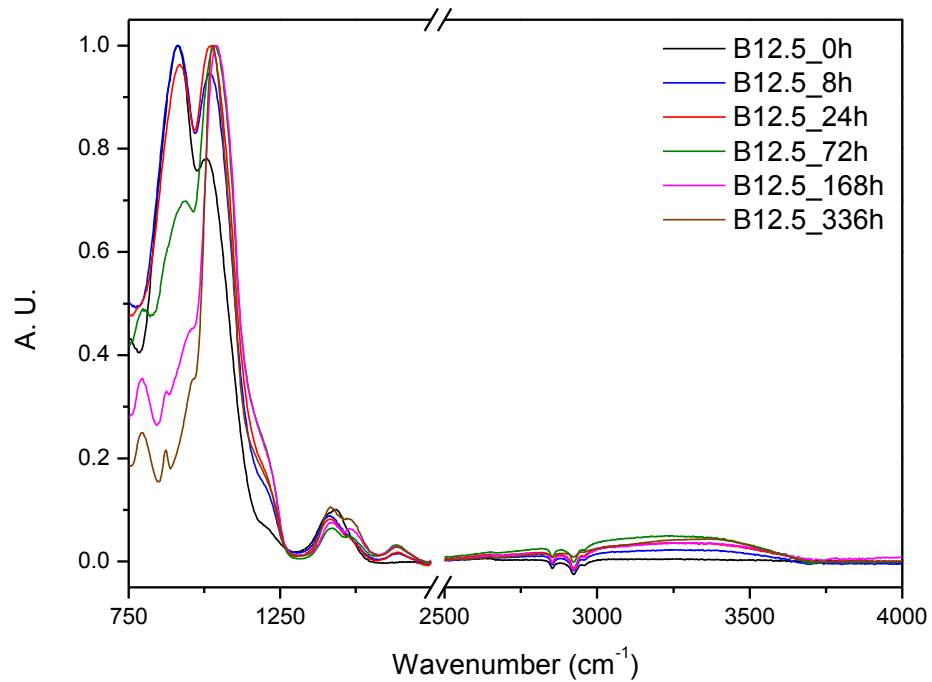
Figure 23. *FTIR spectra of B12.5 scaffolds produced via a) porogen burn-off method and b) robocasting after different SBF immersion times. 2800–2950 cm^{-1} region is susceptible for artefacts related to the instrument in use.*

a)
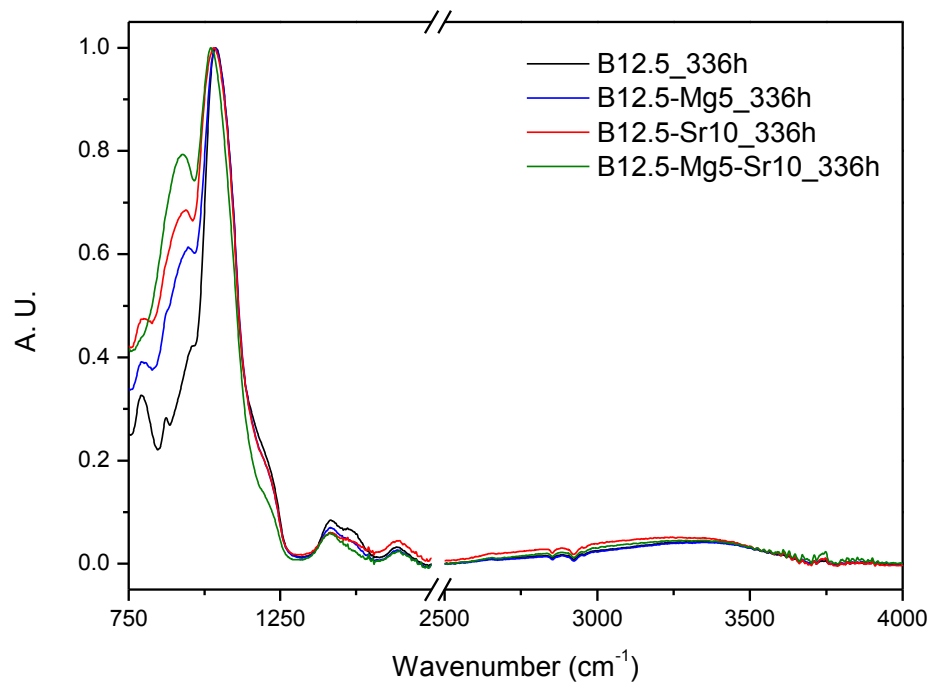
b)

Figure 24. *FTIR spectra of scaffolds produced via a) porogen burn-off method and b) robocasting after 336 h immersion to SBF.*

The spectra presented in Fig. 23 reveal the changes occurring to B12.5 scaffolds taken as an example. From Fig. 23 it can be seen that the earlier discussed silicate and borate related bands (Chapter 4.1.2) decreased during increasing immersion time and new bands centered at 1030 cm^{-1}, 1670 cm^{-1} and in the 2800–3600 cm^{-1} region rose. In addition,

shoulders around 960 cm^{-1} and 1200 cm^{-1} appeared and the band in the 1300–1500 cm^{-1} transformed to a doublet. A small intensity peak at 870 cm^{-1} appeared too. The peak at 870 cm^{-1} has been linked to carbonate vibrations and the shoulder around 960 cm^{-1} can be attributed to both carbonate and P-O-P vibrations. The high intensity band centered at 1030 cm^{-1} can be attributed to P-O stretching vibrations whereas P=O stretching is contributing to the shoulder around 1200 cm^{-1}. In addition, Si Q^4 units have a characteristic peak around 1212 cm^{-1} and thus the appearance of the shoulder may also be caused by a silica rich surface layer, typical in silicate bioactive glasses, that has been exposed during measurements (Massera *et al.* 2012b). The doublet in the 1300–1500 cm^{-1} region is caused by carbonate vibrations, which together with the phosphate related peaks can be indicative of the formation of a carbonated HA layer. (Fabert *et al.* 2017). The weak band centered at 1670 cm^{-1} can be attributed to molecular water and the broad band in the 2800–3600 cm^{-1} region to hydroxyl or silanol groups. (ElBatal *et al.* 2003).

The impact of the glass composition on the structural changes are reported in Fig. 24. With addition of Mg or Sr one can see that even at 336 h the peaks related to the phosphate vibration are broader and the carbonate band lower in intensity. This could be attributed to a reactive layer not fully formed at the surface of the scaffolds. When both Mg and Sr, are substituting Ca, one can see that the band at 922 cm^{-1} is still very intense and the band in the 1300-1500 as not yet changed into a doublet. This could be interpreted by a slower rate of the reactive layer deposition induced by this glass composition (Massera *et al.* 2012b; Fabert *et al.* 2017).

These results indicate that the base glass B12.5 had the fastest rate of change and either Mg or Sr substitution for Ca slowed down the rate of reaction. B12.5-Mg5-Sr10 again, was affected by both Mg and Sr substitution and showed even lower rate of reactive layer precipitation. The presented results complement the discussed ionic release behaviors as B12.5 had the fastest ionic release and B12.5-Mg5-Sr10 the slowest. Both B12.5-Mg5 and B12.5-Sr10 ionic release fell between these two compositions, as was also witnessed in the discussed FTIR spectra. It should be noted that B12.5-Mg5 seemed to have a higher reaction rate than B12.5-Sr10 in Fig. 24 a), whereas both compositions have reacted approximately to same extent in b). This phenomenon was also observed with the discussed ionic release behavior, which showed comparable release rate between these two compositions when the scaffolds were produced with robocasting.

Overall, the robocasted scaffolds seem to have reacted to a slightly greater extent than the scaffolds produced via porogen burn-off method, especially after longer immersion times. This might be explained with differences in the pore network. Scaffold structures presented in Fig. 18 showed that robocasted scaffolds had highly open pore network composed of pores in the 100 μm scale, which facilitates fluid penetration and exchange. In contrast, scaffolds produced via porogen burn-off method possibly had lower pore interconnectivity than the robocasted scaffolds and thus their reactive surface area was smaller. It is also possible that since the scaffolds produced via porogen burn-off method

contained microporosity, the reaction rate may have been decreased if the pores became closed by accumulating degradation debris or due to the precipitating surface layer, as has been discussed in (Fabert *et al.* 2017). It is worth noting that Mg or Sr substitution for Ca seemed to cause a slight shift to the band centered at 1030 cm^{-1}. This shift is clearly visible in the case of the scaffolds produced via porogen burn-off method. Typically such shift indicates the introduction of Sr within the calcium phosphate layer. Overall, both Mg and Sr have been reported to decrease dissolution and apatite formation rate, which is also indicated by the discussed results. In addition, Mg ion addition to the amorphous surface layer has been reported to retard the precipitated layer´s crystallization. (Massera & Hupa 2014; Goel *et al.* 2011; Diba *et al.* 2012).

SEM/EDX imaging was used to analyze scaffolds after 336 hours of immersion in SBF. Representative images of B12.5 scaffolds are shown in Fig. 25 at 30x and 250x magnifications. Similar images of all glass compositions and scaffold types are collected to Appendix F and the following discussion also applies to them.

From Fig. 25 a), c) and e) it can be seen that all scaffolds contained pores over 100 µm in diameter, as was suggested by the µ-CT results. In addition, the porosity levels in SEM images seemed to match the measured porosities, whereas the structures presented in Fig. 18 seemed to underestimate them. The scaffolds produced via porogen burn-off method and robocasting also contained internalized pores with < 10 µm diameters, whereas the composite scaffolds mostly contained larger pores. The sintered scaffolds had high levels of internal microporosity as shown in Fig. 25 b) and d) showing loose particles suggesting insufficient sintering. Similar observations were also done with B12.5-Sr10 glass scaffolds and to a less extent with magnesium-containing glass scaffolds. This complements earlier discussion about the ability of magnesium to promote sintering, which also resulted in greater compressive strengths (Chapter 4.2.3). However, robocasted B12.5-Mg5 and B12.5-Mg5-Sr10 seemed to have sintered to a lesser extent than the scaffolds produced via porogen burn-off method. This observation validates the earlier discussion about the benefits of powder compaction prior to sintering. In addition, all robocasted samples seemed to have greater pores within the filaments, which may have been caused by residual air bubbles within the ink during printing. When comparing the sintering behavior of the glasses within this study, it can be concluded that it is necessary to further optimize the processing parameters and glass compositions to obtain optimum sintering protocols.

Fig. 25 b), d) and f) show a bright layer at the surface of the glass particles. The thickest layers were observed on the outer surfaces of the samples, which indicates that the fluid penetration and ionic exchange in the inner regions was partly restricted.
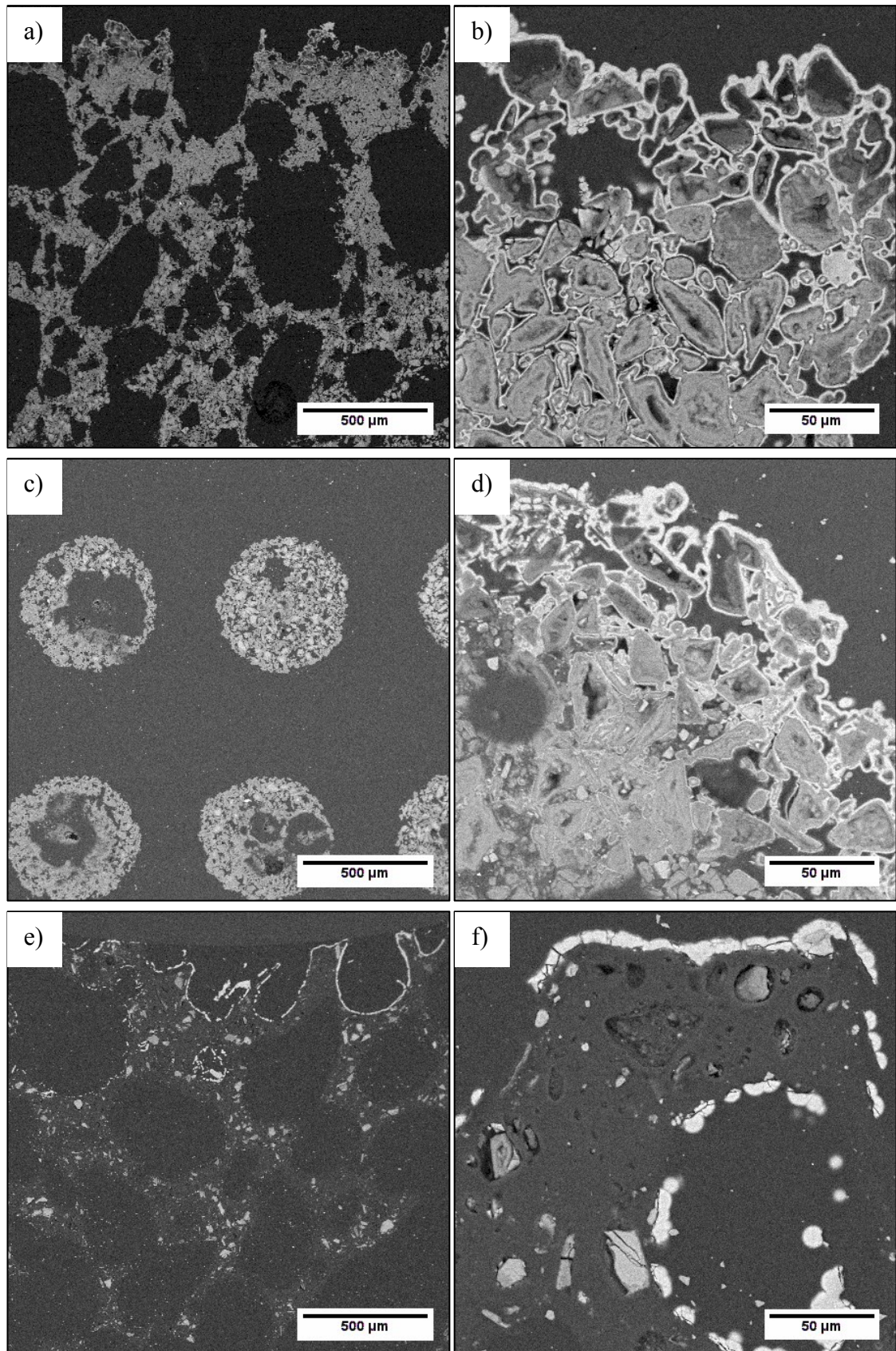
Figure 25.   *SEM images of B12.5 scaffolds produced via porogen burn-off (a, b), robocasting (c, d) and scCO$_2$ (e, f) methods.*

It was also observed that the surface layer thicknesses had considerable variation along the glasses´ surfaces. Thicknesses between 2 and 45 μm were observed but due to the considerable variation from place to place (in a single scaffold), no conclusive analysis between scaffolds could be conducted. Possible differences in the layer thicknesses between the studied glass compositions and scaffolds could have been caused by different glass reactivities as well as different scaffold morphologies. No surface layer could be detected on B12.5-Sr10 glass scaffolds, which was thought to be due to the limited contrast as Sr incorporation darkens the formed layer. However, the surface layer was clearly visible on the B12.5-Sr10 composite scaffold and thus it is probable that the glass scaffolds were also able to precipitate a surface layer.

Elemental compositions of unreacted glass and formed surface layers were analyzed. Table 8 presents the presence of some chosen elements in the unreacted glasses in atom-%. It should be noted that the exact values were highly dependent on the analyzed spot, the high levels of variation might indicate phase separation within the glasses, as was suspected by the presented Raman spectra (Chapter 4.1.2). It can be seen that all glasses had over 13 atom-% of Na and 20 atom-% of Si present. In addition, substituted elements (Mg and Sr) were present in the corresponding glasses. The (Ca + Mg + Sr)/P ratios had considerable differences, which could indicate that the analyzed spot had reacted to some extent as the ratios should be identical.

Table 8. *Atom-% of some elements present in unreacted glasses.*

Element	B12.5	B12.5-Mg5	B12.5-Sr10	B12.5-Mg5-Sr10
Na	13.84 ± 0.14	12.85 ± 0.16	16.05 ± 0.15	13.7 ± 0.15
Si	20.28 ± 0.13	21.3 ± 0.13	20.66 ± 0.15	20.55 ± 0.15
Mg	0.00	1.08 ± 0.08	0.00	1.33 ± 0.08
Sr	0.00	0.00	1.89 ± 0.11	2.61 ± 0.11
P	1.06 ± 0.08	0.96 ± 0.09	1.27 ± 0.12	1.35 ± 0.07
Ca	7.34 ± 0.10	5.64 ± 0.10	2.87 ± 0.05	2.59 ± 0.05
(Ca + Mg + Sr)/P	6.92	7.00	3.75	4.84

Tables 9–11 present the elemental compositions of the analyzed surface layers for scaffolds produced via porogen burn-off, robocasting and scCO$_2$ methods, respectively. Again it should be noted that the elemental compositions had some variance across the surface layers. The presented values reveal that the initially high amounts of Na and Si in the unreacted glasses were no longer present in the formed surface layers. Robocasted B12.5-Sr10 sample seems to be an exception but this was most likely caused by detachment of the surface layer during sample preparation, which exposed the base glasses, or an inadequate analyzed spot. However, the SEM images of B12.5-Sr10 glass scaffolds showed great compositional variance within the analyzed area, which makes further analysis necessary.

Table 9. *Atom-% of some elements present in the surface layers of scaffolds produced via porogen burn-off method.*

Element	B12.5	B12.5-Mg5	B12.5-Sr10	B12.5-Mg5-Sr10
Na	0.60 ± 0.07	0.59 ± 0.07	0.92 ± 0.07	0.95 ± 0.14
Si	0.63 ± 0.08	0.00	0.00	0.00
Mg	0.38 ± 0.07	0.95 ± 0.07	1.95 ± 0.07	2.34 ± 0.09
Sr	0.00	0.00	2.88 ± 0.08	2.71 ± 0.09
P	13.74 ± 0.14	14.63 ± 0.12	15.41 ± 0.17	15.77 ± 0.18
Ca	23.95 ± 0.19	22.92 ± 0.18	17.06 ± 0.16	16.18 ± 0.17
(Ca + Mg + Sr)/P	1.77	1.63	1.42	1.35

Table 10. *Atom-% of some elements present in the surface layers of scaffolds produced via robocasting.*

Element	B12.5	B12.5-Mg5	B12.5-Sr10	B12.5-Mg5-Sr10
Na	0.70 ± 0.07	0.61 ± 0.06	16.19 ± 0.15	0.34 ± 0.05
Si	0.00	0.2 ± 0.03	19.97 ± 0.15	0.00
Mg	0.48 ± 0.07	0.9 ± 0.06	0.00	0.84 ± 0.05
Sr	0.00	0.00	2.23 ± 0.11	1.07 ± 0.05
P	14.09 ± 0.12	14.53 ± 0.12	1.31 ± 0.12	8.27 ± 0.11
Ca	24.21 ± 0.19	22.91 ± 0.17	3.39 ± 0.09	9.68 ± 0.11
(Ca + Mg + Sr)/P	1.75	1.64	4.29	1.40

Table 11. *Atom-% of some elements present in the surface layers of scaffolds produced via scCO2 method.*

Element	B12.5	B12.5-Mg5	B12.5-Sr10	B12.5-Mg5-Sr10
Na	0.86 ± 0.06	0.61 ± 0.07	0.85 ± 0.07	1.01 ± 0.08
Si	0.00	0.00	0.00	0.53 ± 0.04
Mg	0.81 ± 0.03	0.97 ± 0.07	1.00 ± 0.06	1.47 ± 0.08
Sr	0.00	0.00	0.55 ± 0.07	0.99 ± 0.04
P	15.39 ± 0.11	15.01 ± 0.03	15.34 ± 0.14	14.55 ± 0.16
Ca	21.56 ± 0.16	22.24 ± 0.17	20.88 ± 0.16	20.01 ± 0.18
(Ca + Mg + Sr)/P	1.45	1.55	1.46	1.54

It can be seen that all surface layers (except the one of the already discussed robocasted B12.5-Sr10) contained Mg, which indicates incorporation of this element. This observation can be done also with those glasses that did not contain any magnesium, which can be explained with consumption of Mg ions from SBF, as witnessed from ICP-OES results. Interestingly some Sr-containing glasses seemed to incorporate more Mg into the surface layer than B12.5-Mg5. Similarly to magnesium, the Sr incorporation into the layer could be seen in the results of B12.5-Sr10 and B12.5-Mg5-Sr10.

The (Ca + Mg + Sr)/P ratios of the surface layers of B12.5 glass scaffolds were 1.75–1.77, which are close to the 1.67 ratio of hydroxyapatite (Ralston 2013). This suggests that the precipitated calcium phosphate layer is highly similar to HA. It can also be seen that with increasing substitution levels the ratio decreases, with the robocasted B12.5-Sr10 scaffold being an exception. This decrease in the ratio could be caused by different tendencies of the substituted elements to be incorporated into the surface layer. However, the (Ca + Mg + Sr)/P ratios of all composite scaffolds were within 1.45–1.55 and thus lower than the typical 1.67. It would be of interest to assess if the lower (Ca + Mg + Sr)/P ratio is due to incomplete precipitation of Sr and Mg substituted HA, as seen in the FTIR spectra, or if the calcium phosphate formed is indeed HA.

To conclude, it can be stated that all glass compositions within all scaffold types under investigation were able to precipitate calcium phosphate close to HA, which can be taken as an indication of bioactivity (Ylänen 2011, p. 17). In addition, the incorporation of the substituted elements into the surface layers could be detected. However, further analysis of the precipitation rates and effects of substituted elements are necessary in the following studies.

4.3.2 Material degradation

Scaffolds for tissues repair are designed so that they degrade, however, they should maintain their strength for long enough to provide support for the healing tissue (Hutmacher 2000). Material degradation and its effects were analyzed with scaffolds produced using the porogen burn-off method. Scaffolds were immersed to SBF for varying times, after which they were dried and their mass loss was measured. Effect of degradation on scaffold strength was evaluated using compression testing. Mass loss is presented in Fig. 26.

From Fig. 26 it can be seen that measurable mass loss occurred to all scaffold compositions, although the loss was relatively small and between 3 to 7 percent after 336 hours of immersion. The rate of mass loss was higher during the first 72 hours and decreased during time, which could be due to the deposition of HA layer. Mass losses of B12.5 and B12.5-Sr10 samples were substantially higher than the mass losses of Mg-containing glasses during the first 168 hours, which further proves that the glass network becomes chemically more durable when Mg is substituted for Ca (Massera *et al.* 2012b). However, the mass loss of B12.5-Sr10 and B12.5-Mg5 were comparable after 336 hours. Similar comparisons could be seen with the pH change, which indicated that during longer times these glasses have similar ionic release. After 336 hours of immersion all glasses except B12.5-Mg5-Sr10 have lost 6.0–6.5 % of their mass. The difference between the mass losses of B12.5-Mg5 and B12.5-Mg5-Sr10 was negligible during the first 72 hours but after that the mass loss became substantially lower for B12.5-Mg5-Sr10, which only lost approximately 3.5 % of the mass at 336 hours of immersion. This observed phenomenon complements the results of ICP-OES and FTIR measurements since especially during longer times B12.5-Mg5-Sr10 had lower ionic release and less substantial structural

change induced by the dissolution. Presented pH and ionic concentrations indicated higher dissolution rate for B12.5 than for B12.5-Sr10, which was not observed in the mass loss. These contradictory results can be explained with faster surface layer formation for B12.5, which means that more HA is deposited to the material´s surface and thus the observed mass loss is not as substantial. This is supported by the discussed ICP-OES results. However, the discussed SEM images could not prove this statement reliably due to the limited analyzed area.
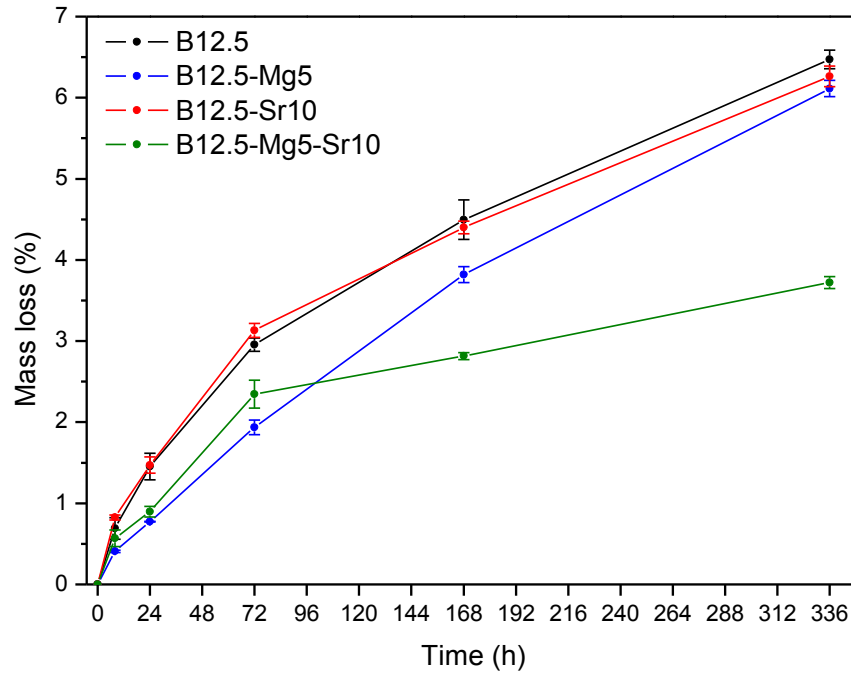
Figure 26. *Mass loss of scaffolds produced via porogen burn-off method.*

The average compressive strength after different immersion times are presented in Fig. 27. The results show that no great loss in mechanical properties occurred when the standard deviations are considered. Also the relative errors between different glass compositions were comparable. Whereas B12.5 showed no change in the properties, a slight drop could be observed with B12.5-Sr10. However, this drop falls within the error margins. Mg-containing glasses maintained their higher strength even after 336 h immersion, but again, still showed high variance between parallel samples. Between 8–168 h test points the B12.5-Mg5-Sr10 seemed to have higher strength than B12.5-Mg5. Since only three parallel samples were tested and sample preparation was affected by human errors, the obtained values possessed great relative errors. And since the observed mass losses were relatively small, high drop in the mechanical properties could not be expected.
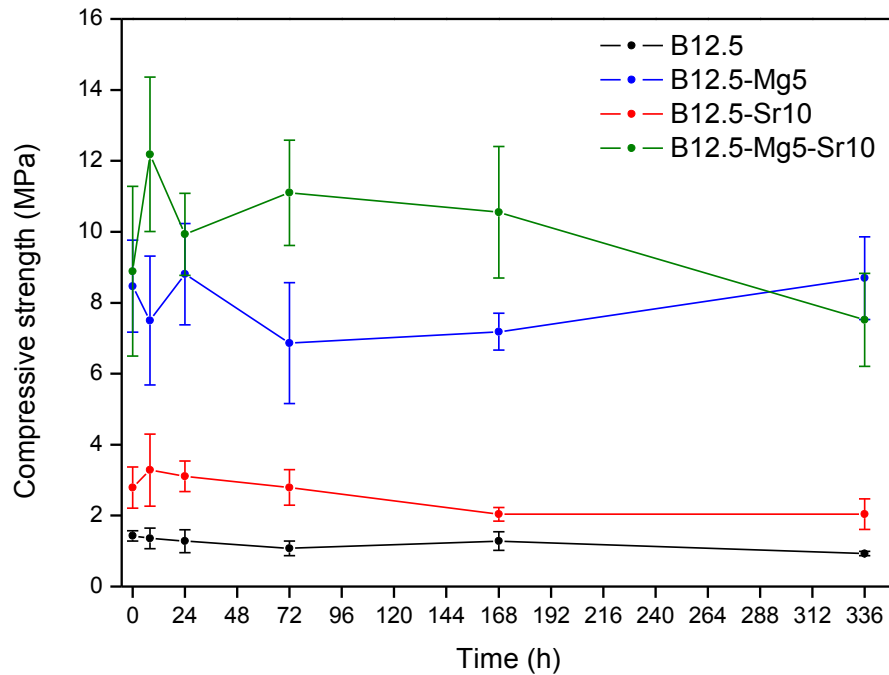
Figure 27. *Average strength of scaffolds produced via porogen burn-off method after different immersion times.*

Fabert *et al.* studied S53P4 based glasses with different boron substitution levels. One of their glasses, named B25, was highly similar to the base glass used in this study with the exception of having 2-fold borate substitution. They produced cylindrical scaffolds with approximately 6 mm diameters and 8 mm heights by sintering loosely packed particles and were able to achieve 50 % overall porosities. They observed a strength loss from over 3 MPa to around 1 MPa after one week of SFB immersion. (Fabert *et al.* 2017). Fu *et al.* studied borate based glass scaffolds produced with polymer foam replication method. Their scaffolds were cylindrical with diameters and heights of 7.5 mm, and had 72 ± 3 % porosities. The scaffolds had a significant drop in the mechanical properties: from approximately 6 MPa to 2 MPa during two weeks of immersion when the measured mass loss was around 8 % (Fu *et al.* 2009). Liu *et al.* used robocasting to produce 47 % porous scaffolds (6 mm x 6 mm x 6mm in size) made of silicate based 13-93 glass. They conducted dissolution studies with the same scaffold mass to SBF volume ratios as was used in this thesis. Their scaffolds had initial compressive strengths of over 80 MPa and after 2 week SBF immersion the strength had dropped to below 60 MPa. (Liu *et al.* 2013). However, they did not study the mass loss and conducted mechanical testing to wet samples straight after immersion.

Similar observations regarding strength loss were not evident in this study even though the porosities of the studied scaffolds were somewhat similar to the ones in the discussed experiments. However, it should be noted that the sample size in this study was much bigger and that the production method and glass compositions were also different. These

factors may cause differences to degradation behavior and strength loss. To conclude, it can be stated that the studied scaffolds maintained their strength for at least two weeks and seem to be promising for longer term treatments. For more precise analysis, higher amount of parallel samples and longer immersion times are required.

5. CONCLUSIONS

In this study, four different borosilicate glasses based on commercially available S53P4 were produced. The composition was tailored by substituting Mg and/or Sr for Ca in the base glass with the aim being to improve the processability and reactivity. Glasses were utilized in scaffold production via different methods and scaffold performance was tested *in vitro*.

The glass network were analyzed and suitable sintering conditions were evaluated prior to scaffold production. Sintered glass scaffolds were produced via porogen burn-off method and robocasting. In addition, composite scaffolds containing glass particles in PLCL matrix were produced via supercritical CO_2 foaming method. Preliminary analysis revealed that all glasses could be sintered at $T_x - 95$ °C regardless of processing method without inducing crystallization. Porosities within 49–73 % were obtained for all scaffold types, and featured pores over 100 μm in diameter, which indicated suitability for bone tissue engineering applications. Compressive strengths of glass scaffolds were between 1.5–10.0 MPa, comparable to human trabecular bone, whereas composite scaffolds possessed strengths below 0.1 MPa but were highly ductile. Thus the composite scaffolds seem to be more suitable for non-load bearing applications. It was seen that especially the incorporation of Mg into the glass led to considerable widening of the sintering window, resulting in a reduction in porosity but enhancing the mechanical strength. Sr substitution had similar but less substantial effect.

Scaffold degradation behavior and bioactivity was assessed via *in vitro* testing in SBF. All glass compositions within all scaffold types showed indications of bioactivity within 336 hours of immersion. In addition, elemental analysis proved incorporation of the substituted elements into the surface layer. Based on the results it was concluded that both Mg and Sr substitution decreased the glasses´ bioactivity but did not prevent HA formation. It was seen that by substituting both Mg and Sr the effects of these individual elements were combined. However, the results presented here are the findings of preliminary studies of this system. A more comprehensive analysis of the effects of the substituted elements could be conducted to gain further understanding.

To conclude, sufficiently porous and strong scaffolds were able to be fabricated without inducing crystallization or loss of bioactive properties from glasses under investigation. Mg and Sr substitution seems to be an effective way to enhance both glass processability and biological performance. However, despite the promising results obtained within this study, cell compatibility tests of the studied glasses and scaffolds produced are essential to fully understand their potential.

REFERENCES

Akkouch, A., Zhang, Z., Rouabhia, M. (2011). A novel collagen/hydroxyapatite/poly(lac-tide-co-ϵ-caprolactone) biodegradable and bioactive 3D porous scaffold for bone regeneration. Journal of Biomedical Material Research. Part A, pp. 693–704

Amini, A. R., Laurencin, C. T., Nukavarapu, S. P. (2012). Bone Tissue Engineering: Recent Advances and Challenges. Journal of Critical Reviews in Biomedical Engineering. Vol. 45, Iss. 5, pp. 363–408

Balasubramanian, P., Grünewald, A., Detsch, R., Hupa, L., Jokic, B., Tallia, F., Solanki, A. K., Jones, J. R., Boccaccini, A. R. (2016). Ion Release, Hydroxyapatite Conversion, and Cytotoxicity of Boron-Containing Bioactive Glass Scaffolds. International Journal of Applied Glass Science. Vol. 7, Iss. 2, pp. 206–215

Barone, D. T.-J., Raquez, J.-M., Ph Dubois. (2010). Bone-guided regeneration: from inert biomaterials to bioactive polymer(nano)composites. Polymers for Advanced Technologies. Vol. 22, Iss. 5, pp. 463–475

Bastioli, C. (2005). Handbook of Biodegradable Polymers. Rapra Technology Limited, Shawbury, UK, 534 p.

Bellucci, D., Cannillo, V., Sola, A. (2010). An Overview of The Effects of Thermal Processing on Bioactive Glasses. Science of Sintering. Vol. 42, pp. 307–320

Bhamidipati, M., Scurto, A. M., Detamore, M. S. (2013). The Future of Carbon Dioxide for Polymer Processing in Tissue Engineering. Tissue Engineering, part B. Vol. 19, No. 3, pp. 221–232

Blaker, J. J., Bismarck, A., Boccaccini, A. R., Young, A. M., Nazhat, S. N. (2010). Premature degradation of poly(α-hydroxyesters) during thermal processing of Bioglass®-containing composites. Acta Biomaterialia. Vol. 6, pp. 756–762

Boccaccini, A. R., Brauer, D. S., Hupa, L. (2016). Bioactive Glasses: Fundamentals, Technology and Applications. The Royal Society of Chemistry, Cambridge, UK, 530 p.

Boccaccini, A. R., Maquet, V. (2003). Bioresorbable and bioactive polymer/Bioglass® composites withtailored pore structure for tissue engineering applications

Bose, S., Vahabzadeh, S., Bandyopadhyah, A. (2013). Bone tissue engineering using 3D printing. Materials Today. Vol. 16, pp. 496–504

Brauer, D. S. Al-Noaman, A., Hill, R. G., Doweidar, H. (2011). Density-structure correlations in fluoride-containing bioactive phospho-silicate glasses. Materials Chemistry and Physics. Vol. 130, pp. 121–125

Brovarone, C. V., Verné, E., Appendino, P. (2006). Macroporous bioactive glass-ceramic scaffolds for tissue engineering. Journal of Materials Science: Materials in Medicine. Vol. 17, pp. 1069–1078

Burg, K. J. L., Porter, S., Kellam, J. F. (2000). Biomaterial developments for bone tissue engineering. Biomaterials. Vol. 21, pp. 2347–2359

Chanshetti, U. B., Shelke, V. A., Jadhav, S. M., Shankarwar, S. G., Chondhekar, T. K., Shankarwar, A. G., Sudarsan, V., Jogad, M. S. (2011). Density and Molar Volume studies of Phosphate Glasses. Physics, Chemistry nad Technology. Vol. 9, No. 1, pp. 29–36

Chen, Q. Z., Thompson, I. D., Boccannici, A. R. 45S5 Bioglass®-derived glass–ceramic scaffolds for bone tissue engineering. Biomaterials, Vol. 27, pp. 2414–2425

Chevalier, E., Chulia, D., Pouget, C., Viana, M. (2008). Fabrication of Porous Substrates: A Review of Processes Using Pore Forming Agents in the Biomaterial Field. Journal of Pharmaceutical Sciences. Vol. 97, No. 3, pp. 1135–1154

Davies, O. R., Lewis, A. L., Whitaker, M. J., Tai, H., Shakesheff K. M, Howdle, S. M. (2008). Applications of supercritical CO_2 in the fabrication of polymer systems for drug delivery and tissue engineering. Advanced Drug Delivery Reviews. Vol. 60, pp. 373–387

Deliormanlı, A. M., Rahaman, M. N. (2012). Direct-write assembly of silicate and borate bioactive glass scaffolds for bone repair. Journal of the European Ceramic Society. Vol. 32, pp. 3637–3646

Diba, M., Tapia, F., Boccaccini, A. R. (2012). Magnesium-Containing Bioactive Glasses for Biomedical Applications. International Journal of Applied Glass Science. Vol. 3, Iss. 3, pp. 221–253

Domb, A. J., Kumar, N., Ezra, A. (2011). Biodegradable Polymers in Clinical Use and Clinical Development. John Wiley & Sons, Inc., New Jersey, USA, 752 p.

Dressler, M., Reinsch, S., Schadrack, R., Benemann, S. (2009). Burnout behavior of ceramic coated open cell polyurethane (PU) sponges. Journal of European Ceramic Society. Vol. 29, pp. 3333–3339

ElBatal, H. A., Azooz, M. A., Khalil, E. M. A., Monem, A. C., Hamdy, Y. M. (2003). Characterization of some bioglass-ceramics. Materials Chemistry and Physics. Vol. 80, pp. 599–609

Ertuğ, B. (2013). Sintering Applications. InTech Open, Rijeka, Croatia, 342 p.

Eqtesadi, S., Motealleh, A., Miranda, P., Pajares, A., Lemos, A., Ferreira, J. M. F. (2014). Robocasting of 45S5 bioactive glass scaffolds for bone tissue engineering. Journal of European Ceramic Society. Vol. 34, pp. 107–118.

Fabert, M., Ojha, N., Erasmus, E., Hannula, M., Hokka, M., Hyttinen, J., Rocherullé, J., Sigalas, I., Massera, J. (2017). Journal of Materials Chemistry B. Vol. 5, pp. 4514–4525

Fagerlund, S., Massera, J., Moritz, N., Hupa, L., Hupa, M. (2012). Phase composition and in vitro bioactivity of porous implants made of bioactive glass S53P4. Acta Biomaterialia. Vol. 8, pp. 2331–2339

Fernández, J., Larrañaga, A., Etxeberría, A., Sarasua, J. R. (2013). Effects of chain microstructures and derived crystallization capability on hydrolytic degradation of poly(L-lactide/ε-caprolactone) copolymers. Polymer Degradation and Stability. Vol. 98, pp. 481–489

Filho, O. P., LaTorre, G. P., Hench, L. L. (1996). Effect of crystallization on apatite-layer formation of bioactive glass 45S5. Journal of Biomedical Materials Research. Vol. 30, pp. 509–514

Finnish Standards Association. (2014) SFS-EN ISO 844 "Rigid cellular plastics - Determination of compression properties". Helsinki. 10 p.

Florencio-Silva, R., da Silva Sasso, G. R., Sasso-Cerri, E., Simões, M. J., Cerri, P. S. (2015). Biology of Bone Tissue: Structure, Function, and Factors That Influence Bone Cells. BioMed Research International. Vol. 2015, pp. 1–17

Fredholm, Y. C., Karpukhina, N., Law, R. V., Hill, G. R. (2010). Strontium containing bioactive glasses: Glass structure and physical properties. Journal of Non-Crystalline Solids. Vol. 356, pp. 2546–2551

Fu, H., Fu, Q., Zhou, N., Huang, W., Rahaman, M. N., Wang, D., Liu, X. (2009). In vitro evaluation of borate-based bioactive glass scaffolds prepared by a polymer foam replication method. Materials Science and Engineering. Vol. C 29, pp. 2275–2281

Fu, Q., Saiz, E., Rahaman, M. N., Tomsia, A. P. (2011a). Bioactive glass scaffolds for bone tissue engineering: state of the art and future perspectives. Materials Science and Engineering. Vol. 31(C), pp. 1245–1256

Fu, Q., Saiz, E., Tomsia, A. P. (2011b). Direct Ink Writing of Highly Porous and Strong Glass Scaffolds for Load-bearing Bone Defects Repair and Regeneration. Acta Biomateria. Vol. 7, Iss. 10, pp. 3547–3554.

Fu, Q., Rahaman, M. N., Fu, H., Liu, X. (2010). Silicate, borosilicate, and borate bioactive glass scaffolds with controllable degradation rate for bone tissue engineering applications. I. Preparation and in vitro degradation. Journal of Biomedical Materials Research A. Vol. 95A, Iss. 1, p. 164–171

Gerhardt, L.-Z., Boccaccini, A. R. (2010). Bioactive Glass and Glass-Ceramic Scaffolds for Bone Tissue Engineering. Materials. Vol. 3, pp. 3867–3910

Goel, A., Rajagopal, R. R., Ferreira, J. M. F. (2011). Influence of strontium on structure, sintering and biodegradation behavior of $CaO–MgO–SrO–SiO_2–P_2O_5–CaF_2$ glasses. Acta Biomaterialia. Vol 7, pp. 4071–4080

Hollinger, J. O., Einhorn, T. A., Doll, B. A., Sfeir, C. (2004). Bone Tissue Engineering. CRC Press, 352 p.

Hoppe, A., Güldal, N. S., Boccaccini, A. R. (2011). A review of the biological response to ionic dissolution products from bioactive glasses and glass-ceramics. Biomaterials. Vol. 32, pp. 2757–2774

Hupa, L., Fagerlund, S., Massera, J., Björkvik, L. (2016). Dissolution behavior of the bioactive glass S53P4 when sodium is replaced by potassium, and calcium with magnesium or strontium. Journal of Non-Crystalline Solids. Vol. 432, pp. 41–46

Hutmacher, D. W. (2000). Scaffolds in tissue engineering bone and cartilage. Biomaterials. Vol. 21, pp. 2529–2543

Ji, C., Shi, J. (2013). Thermal-crosslinked porous chitosan scaffolds for soft tissue engineering applications. Materials Science and Engineering. Vol. 33 C, pp. 3780–3785

Jones, J. R. (2013). Review of bioactive glass: From Hench to hybrids. Acta Biomaterialia. Vol. 9, pp. 4457–4486

Jones, J. R., Ehrenfried, L. M., Hench, L. L. (2006). Optimising bioactive glass scaffolds for bone tissue engineering. Biomaterials. Vol. 27, pp. 964–973

Kasper, C., Witte, F., Pörtner, R. (2012). Tissue Engineering III: Cell–Surface Interactions for Tissue Culture. Springer, Heidelberg, Germany, 339 p.

Kokubo, T., Takadama, H. (2006). How useful is SBF in predicting in vivo bone bioactivity? Biomaterials. Vol. 27, pp. 2907–2915

Koroleva, O. N., Shabunina, L. A, Bykov, V. N. (2011) Structure of Borosilicate Glass According to Raman Spectroscopy Data. Glass and Ceramics. Vol. 67, No. 11–12. pp. 340–342.

Kumar, D. S., Ekanthamoorthy, J., Kumar, S. K. (2015). Study of Development and Applications of Bioactive Materials and Methods In Bone Tissue Engineering. Biomedical research. Vol. 26, Iss. 4, pp. 55–61

Lendlein, A., Sisson, A. (2011). Handbook of Biodegradable Polymers: Synthesis, Characterization and Applications. Wiley-VCH, Weinheim, Germany, 405 p.

Liao, X., Zhang, H., He, T. (2012). Preparation of Porous Biodegradable Polymer and Its Nanocomposites by Supercritical CO2 Foaming for Tissue Engineering. Journal of Nanomaterials. Vol. 2012, pp. 1–12

Lindfors, N., Koski, I., Heikkilä, J. T., Mattila, K., Aho, A. J. (2010). A prospective randomized 14-year follow-up study of bioactive glass and autogenous bone as bone graft substitutes in benign bone tumors. Journal of Biomedical Materials Research Part B: Applied Biomaterials. Vol. 94 B, Iss. 1, pp. 157–164

Liu, X., Rahaman, M. N., Hilmas, G. E., Bal, B. S. (2013). Mechanical properties of bioactive glass (13-93) scaffolds fabricated by robotic deposition for structural bone repair. Acta Biomaterialia. Vol. 9, Iss. 6. pp. 7025–7034

Lu, L., Zhang, Q., Wootton, D. M., Chiou, R., Li, D., Lu, B., Lelkes, P. I., Zhou, J. (2014). Mechanical study of polycaprolactone-hydroxyapatite porous scaffolds created by porogen-based solid freeform fabrication method. Journal of Applied Biomaterials & Functional Materials. Vol. 12, Iss. 3, pp. 145–154

Macon, A. L. B., Kim, T. B., Valliant, E. M., Goetschius, K., Brow, R. K., Day, D. E., Hoppe, A., Boccaccini, A. R., Kim, i. Y., Ohtsuki, C., Kokubo, T., Osaka, A., Vallet-Regí, M., Arcos, D., Fraile, L., Salinar, A. J., Teixeira, A. V., Vueva, Y., Almeida, R. M., Miola, M., Vitale-Brovarone, C., Verné, E. Höland, W., Jones, J. R. (2015). Journal of Materials Science: Materials in Medicine. Vol. 26, Iss. 115

Mami, M., Oudadesse, H., Dorbex-Sridi, R., Capiaux, H., Pellen-Mussi, P., Chauvel-Lebret, D., Chaair, H., Cathelineau, G. (2008). Synthesis and In Vitro Characterization of Melt Derived 47S $CaO–P_2O_5–SiO_2–Na_2O$ Bioactive Glass. (2008). Ceramics – Silikáty. Vol. 52, Iss. 3, pp. 121-129

Manara, D., Grandjean, A., Neuville, D. R. (2009). Advances in understanding the structure of borosilicate glasses: A Raman spectroscopy study. American Mineralogist. Vol. 94, pp. 777–784

Massera, J., Fagerlund, S., Hupa, L., Hupa, M. (2012a). Crystallization Mechanism of the Bioactive Glasses, 45S5 and S53P4. Journal of the American Ceramic Society. Vol. 95, Iss. 2, pp. 607–613

Massera, J., Hupa, L. Hupa, M. (2012b). Influence of the partial substitution of CaO with MgO on the thermal properties and in vitro reactivity of the bioactive glass S53P4. Journal of Non-Crystalline Solids. Vol. 358, pp. 2701–2707

Massera, J., Hupa, L. (2014). Influence of SrO substitution for CaO on the properties of bioactive glass S53P4. Journal of Materials Science: Materials in Medicine. Vol. 25, pp. 657–668

Massera, J., Kokkari, A., Närhi, T., Hupa, L. (2015). The influence of SrO and CaO in silicate and phosphate bioactive glasses on human gingival fibroblasts. Journal of Materials Science: Materials in Medicine. Vol. 26, Iss. 196

Massera, J., Mayran, M., Rocherullé, J., Hupa, L. (2015). Crystallization behavior of phosphate glasses and its impact on the glasses' bioactivity. Journal of Materials Science. Vol 50, pp. 3091–3102

Miguez-Pacheco, V., Büttner, T., Maçon, A. L. B., Jones, J. R., Fey, T., de Ligny, D., Greil, P., Chevalier, J., Malchere, A., Boccaccini, A. R. (2016). Development and characterization of lithium-releasing silicate bioactive glasses and their scaffolds for bone repair. Journal of Non-Crystalline Solids. Vol. 432, pp. 65–72

Nair, L. S., Laurencin, C. T. (2007). Biodegradable polymers as biomaterials. Progress in Polymer Science. Vol. 32, pp. 762–798

Nakielski, P., Kowalczyk, T., Zembrzycki, K., Kowalewski, T. A. (2015). Experimental and numerical evaluation of drug release from nanofiber mats to brain tissue. Journal of Biomedical Materials Research Part B: Applied Biomaterials. Vol. 103, Iss. 2, pp. 282–291

Nampoothiri, K. M., Nair, N. R., John, R. P. (2010). An overview of the recent developments in polylactide (PLA) research. Bioresource Technology. Vol. 101, pp. 8493–8501

Olah, L., Filipczak, K., Jaegermann, Z., Czigany, T., Borbas, L., Sosnowski, S., Ulanski, P., Rosiak, M. J. (2006). Synthesis, structural and mechanical properties of porous polymeric scaffolds for bone tissue regeneration based on neat poly(e-caprolactone) and its composites with calcium carbonate. Polymers for Advanced Technologies. Vol. 17, pp. 889–897

Olszta, M. J., Cheng, X., Jee, S. S., Kumar, R., Kim, Y.-Y., Kaufman, M. J., Douglas, E. P., Gower, L. B. (2007). Bone structure and formation: A new perspective. Materials Science and Engineering, Vol. R 58, pp. 77–116

Osipov, A. A., Osipova, L. M., Eremyashev, V. E. (2013). Structure of Alkali Borosilicate Glasses and Melts according to Raman Spectroscopy Data. Glass Physics and Chemistry. Vol. 39, No. 2, pp. 105–112

Parkinson, B. G., Holland, D., Smith, M. E., Larson, C., Doerr, J., Affatigato, M., Feller, S. A., Howes, A. P., Scales, C. R. (2008). Quantitative measurement of Q^3 species in silicate and borosilicate glasses using Raman spectroscopy. Journal of Non-Crystalline Solids. Vol. 354, pp. 1936–1942

Rahaman, M. N., Day, D. E., Bal, B. S., Fu, Q., Jung, S B., Bonewald, L. F., Tomsia, A. P. (2011). Bioactive glass in tissue engineering. Acta Biomaterialia. Vol. 7, pp. 2355–2373

Ralston, S. H. (2013). Bone structure and metabolism. Medicine. Vol. 41, Iss. 10, pp. 581–585

Ray, C. S., Yang, Q., Huang, W., Day, D. E. (1996). Surface and Internal Crystallization in Glasses as Determined by Differential Thermal Analysis. Journal of the American Ceramic Society. Vol 79, Iss. 12, pp. 3155–3160

Reznikov, N., Shahar, R., Weiner, S. (2014). Bone hierarchical structure in three dimensions. Acta Biomaterialia. Vol. 10, pp. 3815–3826

Rezwan, K., Chen, Q. Z., Blaker, J. J., Boccaccini, A. R. (2006). Biodegradable and bioactive porous polymer/inorganic composite scaffolds for bone tissue engineering. Biomaterials. Vol. 27, pp. 3413–3431

Rich, J., Jaakkola, T., Tirri, T., Närhi, T., Yli-Urpo, A., Seppälä, J. (2002). In vitro evaluation of poly(ε-caprolactone-co-DL-lactide)/bioactive glass composites. Biomaterials. Vol. 23, pp. 2143–2150

Salman, S. M., Salama, S. N., Abo-Mosallam, H. A. (2012). The role of strontium and potassium on crystallization and bioactivity of Na_2O-CaO-P_2O_5-SiO_2 glasses. Ceramics International. Vol. 38, pp. 55-63

Serra, J., González, P., Liste, S., Chiussi, S., León, B., Pérez-Amor, M., Ylänen, H. O., Hupa, M. (2002). Influence of the non-bridging oxygen groups on the bioactivity of silicate glasses. Materials in Medicine. Vol. 13, pp. 1221–1225

Souza, M. T., Crovace, M. C., Schröder, C., Eckert, H., Peitl, O., Zanotto, E. D. (2013). Effect of magnesium ion incorporation on the thermal stability, dissolution behavior and bioactivity in Bioglass-derived glasses. Journal of Non-Crystalline Solids. Vol. 382, pp. 57–65

Sultana, N. (2013). Biodegradable Polymer-Based Scaffolds for Bone Tissue Engineering. Springer, 64 p.

Tainio, J. (2016). Impact of Magnesium and Strontium on Dissolution and Sintering of Bioactive Borosilicate Glasses. Master´s Thesis. Tampere University of Technology. 67 p. Available: https://dspace.cc.tut.fi/dpub/handle/123456789/24379

The Chapman & Hall CRC Polymers: A Properties Database, Taylor & Francis Group, webpage. Available (accessed 5.6.2017): http://poly.chemnetbase.com/dictionary -search.do?method=view&id=12130286&si=POLY

Tomlins, P. (2016). Characterisation and Design of Tissue Scaffolds. Elsevier Ltd., 294 p.

Velasco, M. A., Narváez-Tovar, C. A., Garzón-Alvarado, D. A. (2015). Design, Materials, and Mechanobiology of Biodegradable Scaffolds for Bone Tissue Engineering. Vol. 2015, pp. 1–21

Watts, S. J., Hill, R. G., O'Donnell, M. D., Law, R. V. (2010). Influence of magnesia on the structure and properties of bioactive glasses. Journal of Non-Crystalline Solids. Vol. 356, pp. 517–524

White, L. J., Hutter, V., Tai, H., Howdle, S. M., Shakesheff, K. M. (2012). The effect of processing variables on morphological and mechanical properties of supercritical CO_2 foamed scaffolds for tissue engineering. Acta Biomaterialia. Vol. 8, pp. 61–71

Woodruff, M. A., Hutmacher, D. W. (2010). The return of a forgotten polymer—Polycaprolactone in the 21st century. Progress in Polymer Science. Vol. 35, pp. 1217–1256

Wu, S., Liu, X., Yeung, K. W. K., Liu, C., Yang, X. (2014). Biomimetic porous scaffolds for bone tissue engineering. Materials Science and Engineering. Vol. R 80, pp. 1–36

Xiang, Y., Du, Y. (2011). Effect of Strontium Substitution on the Structure of 45S5 Bioglasses. Chemistry of Materials. Vol. 23, pp. 2703–2717

Ylänen, H. O. (2011). Bioactive glasses, Materials, properties and applications. Woodhead Publishing Limited, 273 p.

Zhang, J., Liu, H., Ding, J.-X., Wu, J., Zhuang, X.-L., Chen, X.-S., Wang, J.-C., Ying, J.-B., Li, Z.-M. (2016). High-Pressure Compression-Molded Porous Resorbable Polymer/Hydroxyapatite Composite Scaffold for Cranial Bone Regeneration. ACS Biomaterials Science & Engineering. Vol. 2, pp. 1471–1482.

Zreiqat, H., Rosen, V., Dunstan, C. R. (2015). A Tissue Regeneration Approach to Bone and Cartilage Repair. Springer, Switzerland, 261 p.

APPENDIX A: SBF REAGENTS AND IONIC CONCENTRATIONS

SBF was produced by dissolving the reagents presented in Table A.1 to distilled water in numerical order. Quantities are for 1 L of SBF. The pH of the solution was adjusted to 7.40 ± 0.2 at the temperature of 37.0 ± 0.2 °C by titration with 1 M HCl.

Table A.1. *Reagents for SBF production.*

Order	Reagent	Amount
1	NaCl	7.996 g
2	$NaHCO_3$	0.350 g
3	KCl	0.224 g
4	$K_2HPO_4 \cdot 3(H_2O)$	0.228 g
5	$MgCl_2 \cdot 6(H_2O)$	0.305 g
6	1M HCl	40 ml
7	$CaCl_2 \cdot 2(H_2O)$	0.368 g
8	Na_2SO_4	0.071 g
9	$(CH_2OH)_3CNH_2$	6.057 g

Ionic concentrations of produced SBF and human blood plasma are shown in Table A.2.

Table A.2. *Ionic concentrations of SBF and human blood plasma (Kokubo & Takadama 2006).*

Ion	SBF concentration (mM)	Blood plasma concentration (mM)
Na^+	142.0	142.0
K^+	5.0	5.0
Mg^{2+}	1.5	1.5
Ca^{2+}	2.5	2.5
Cl^-	148.8	103.0
HCO_3^-	4.2	27.0
HPO_4^{2-}	1.0	1.0
SO_4^{2-}	0.5	0.5

APPENDIX B: DTA CURVES
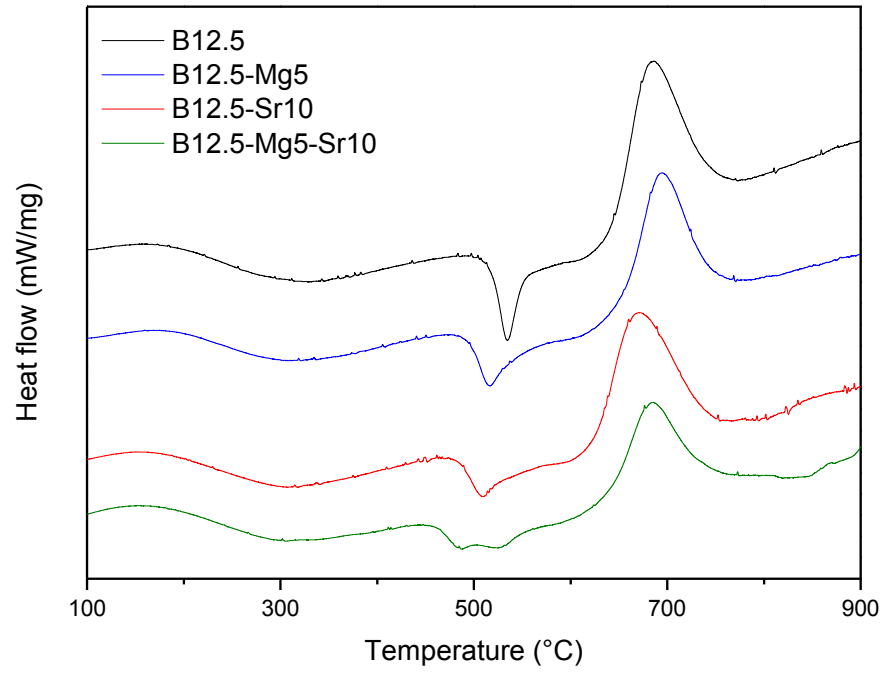
Figure B.1. DTA curves of the studied glasses.

APPENDIX C: TGA CURVES
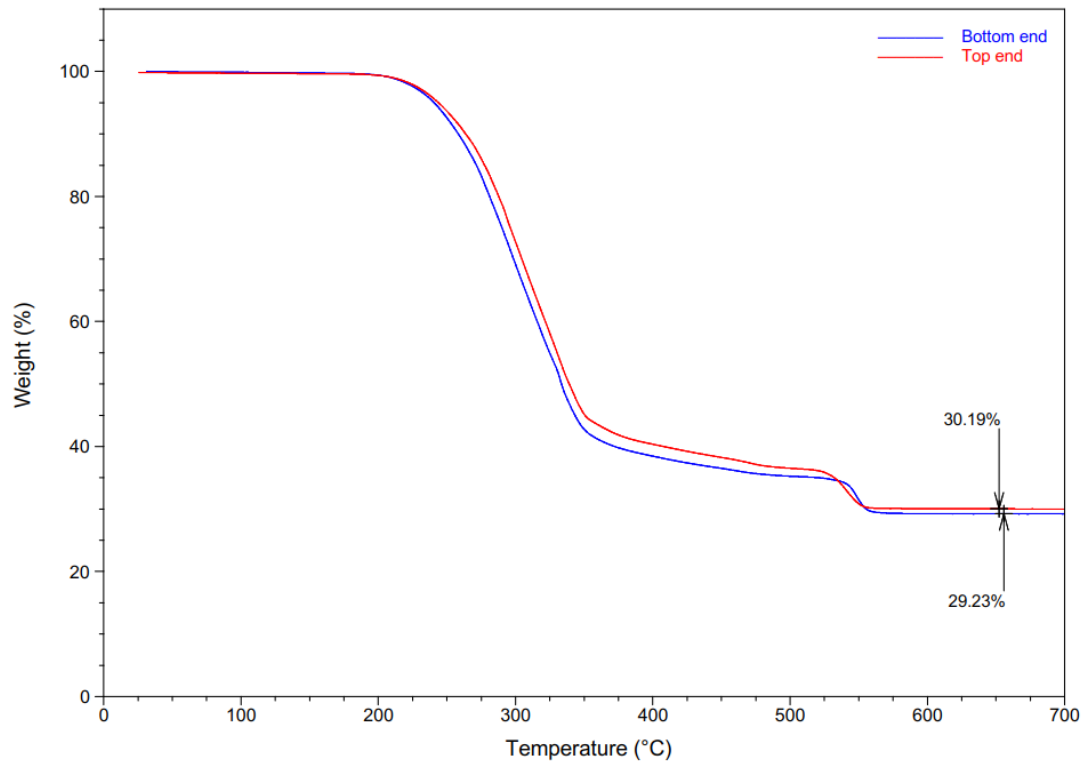
Figure C.1. *TGA curves of PLCL-B12.5 composite rod.*

# APPENDIX D: ICP-OES RESULTS

1)
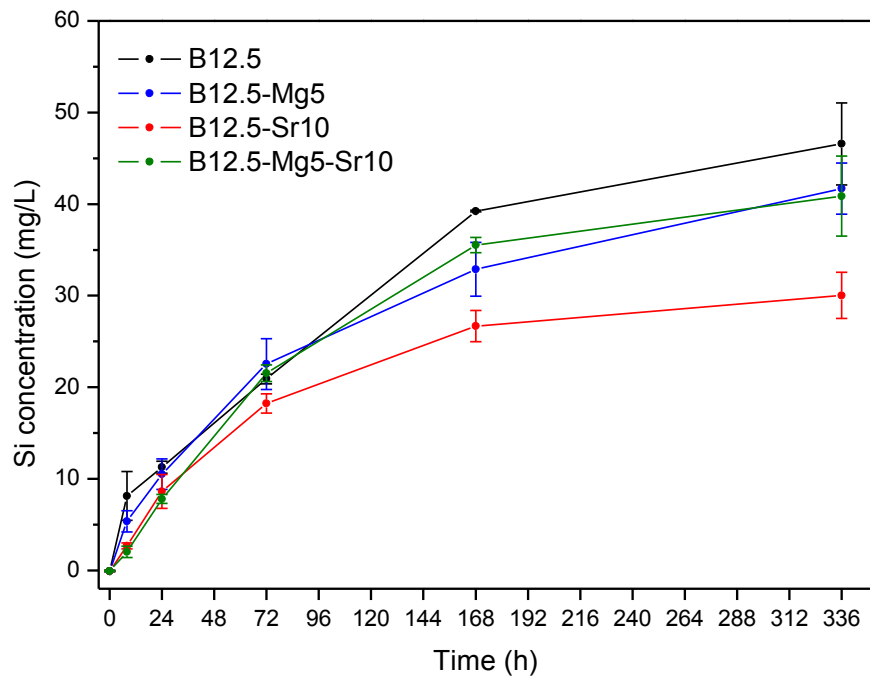
2)
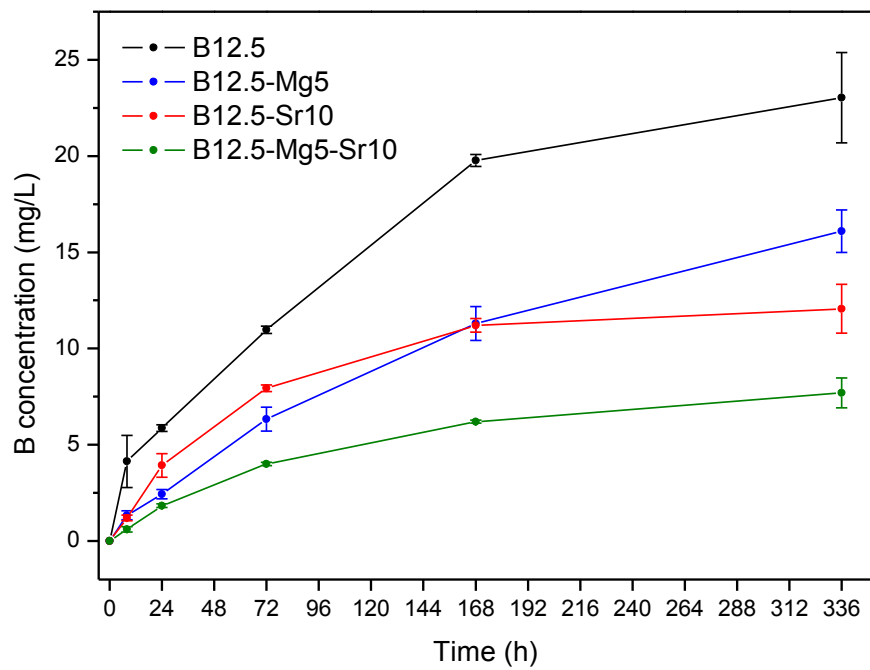
3)
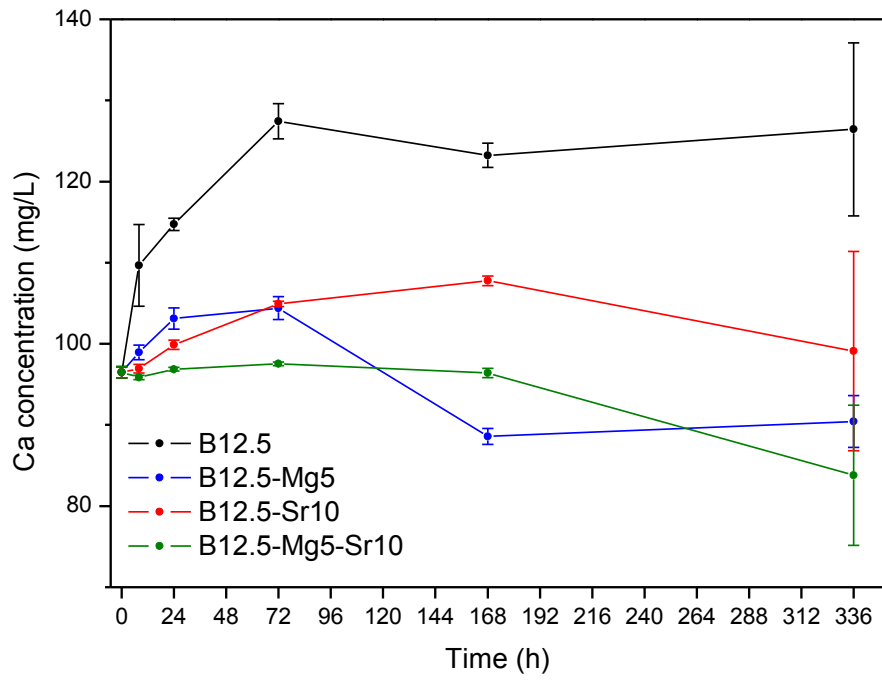
4)
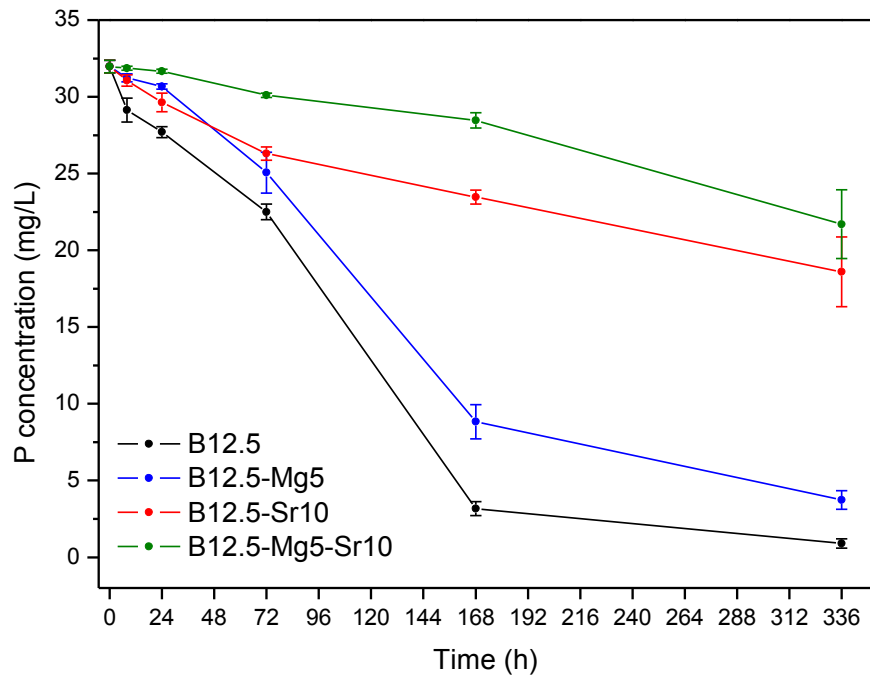
5)
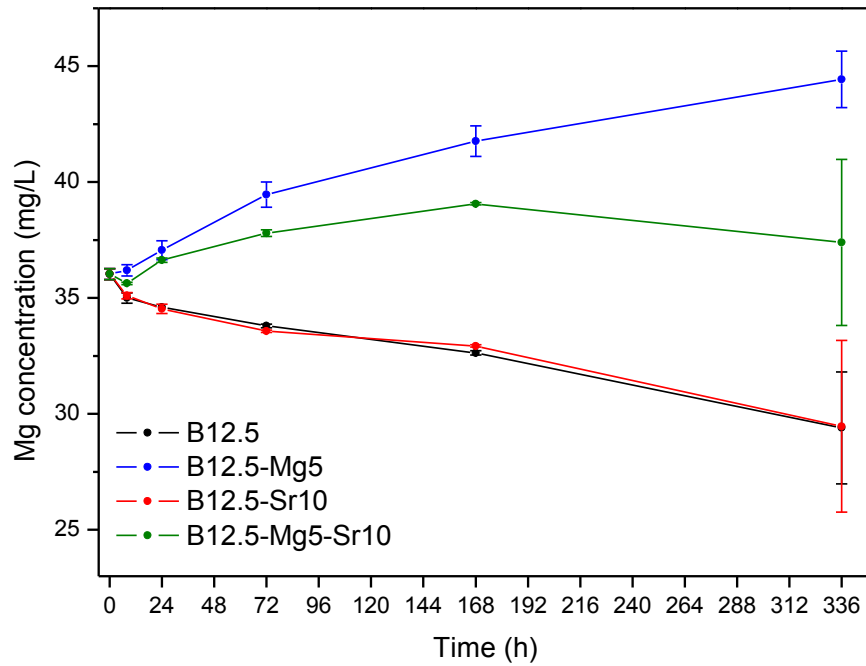
6)
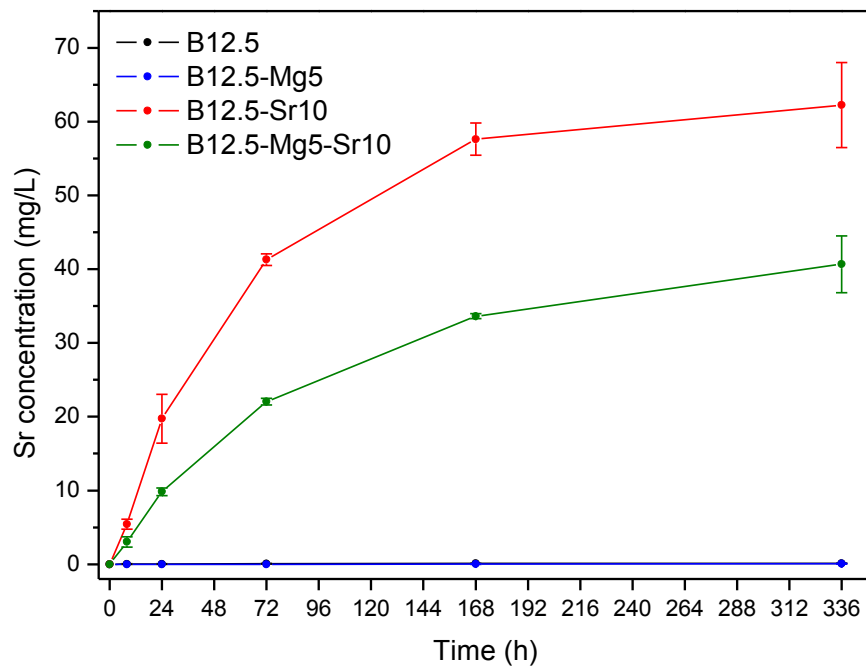
Figure D.1. *Ionic concentrations (mg/L) of 1) Si, 2) B, 3) Ca, 4) P, 5) Mg and 6) Sr in SBF as a function of scaffold immersion time. Results are related to scaffolds produced via porogen burn-off method.*

1)
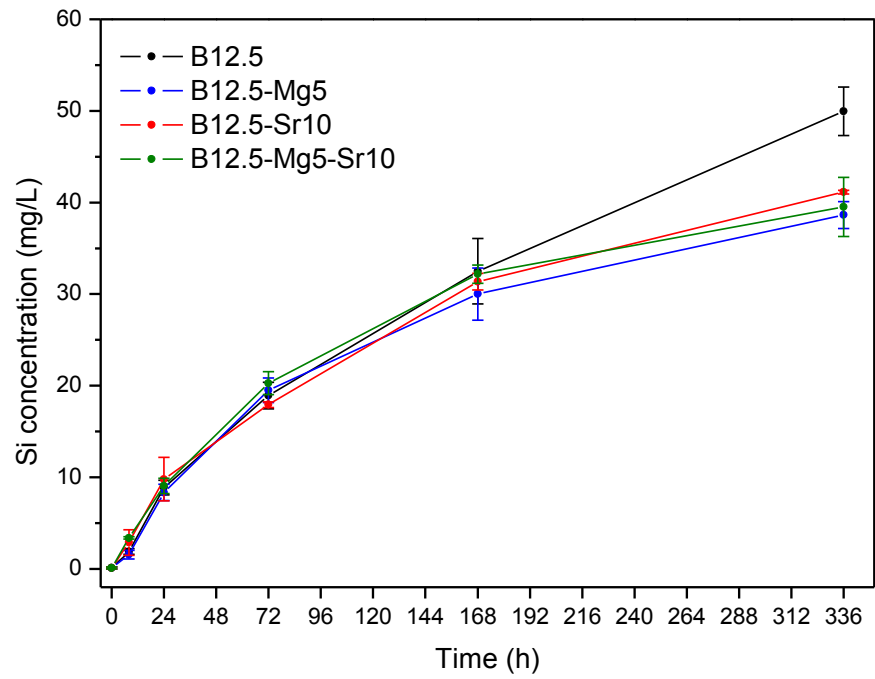
2)
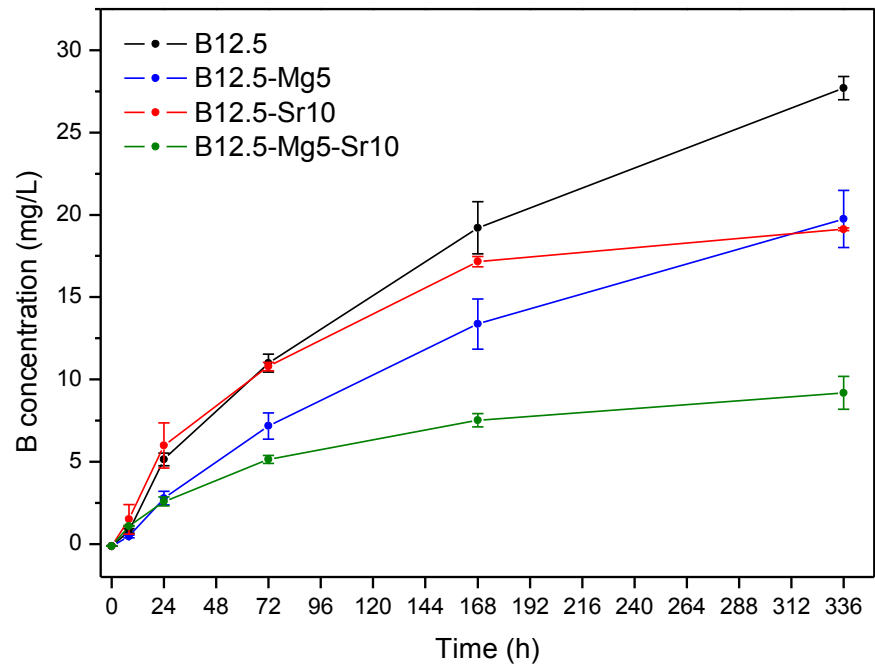
3)
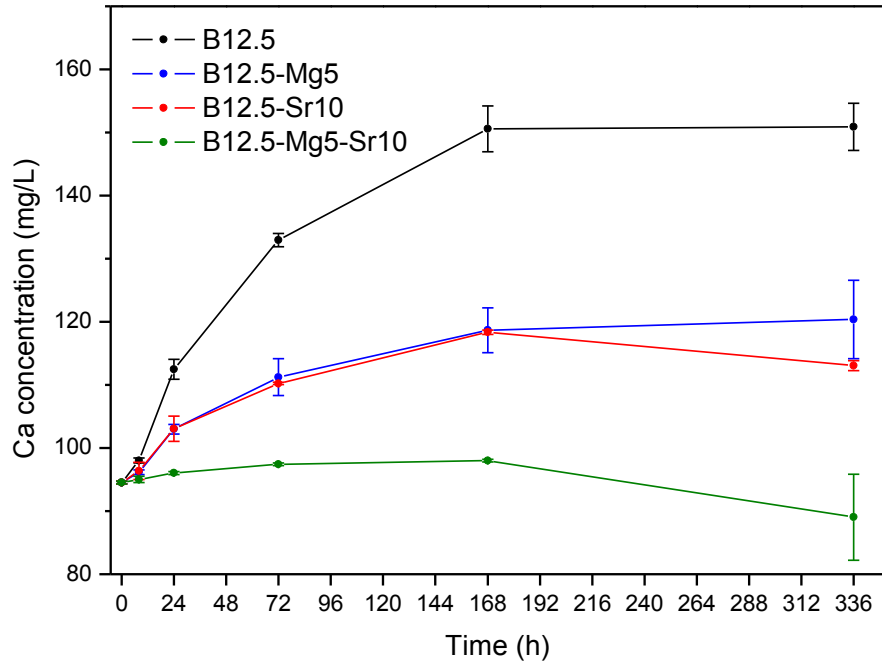
4)
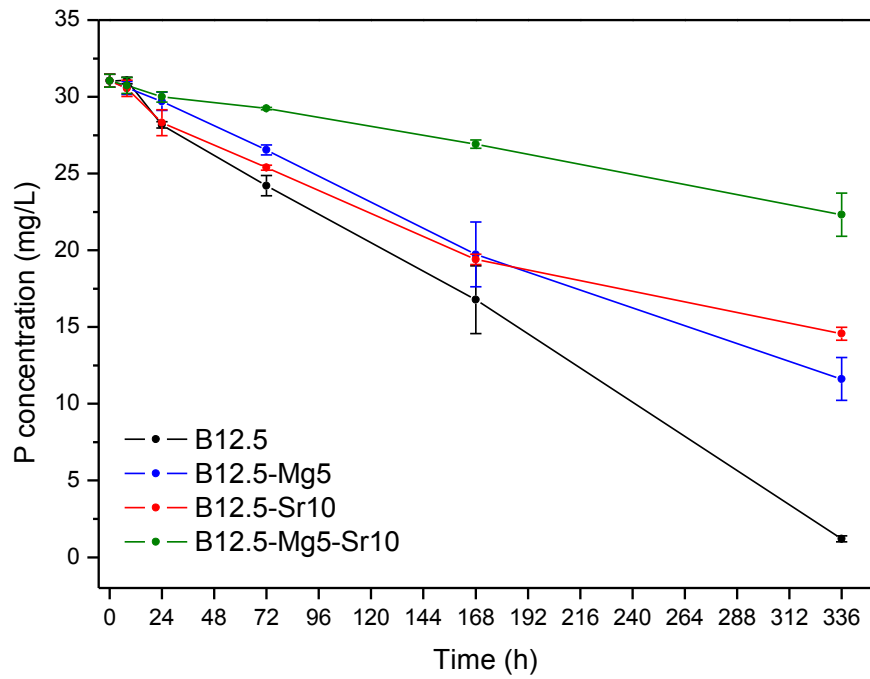
5)
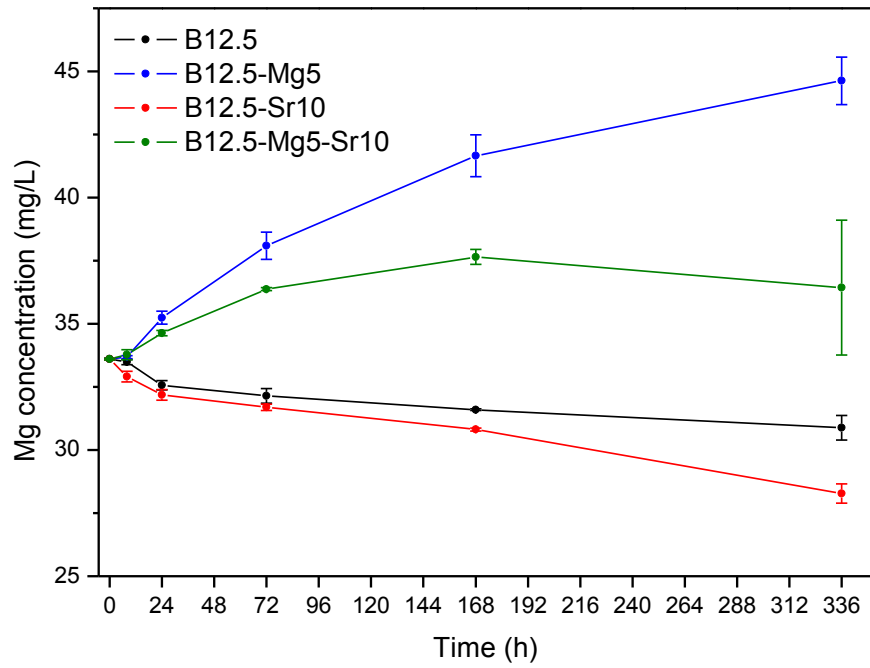
6)
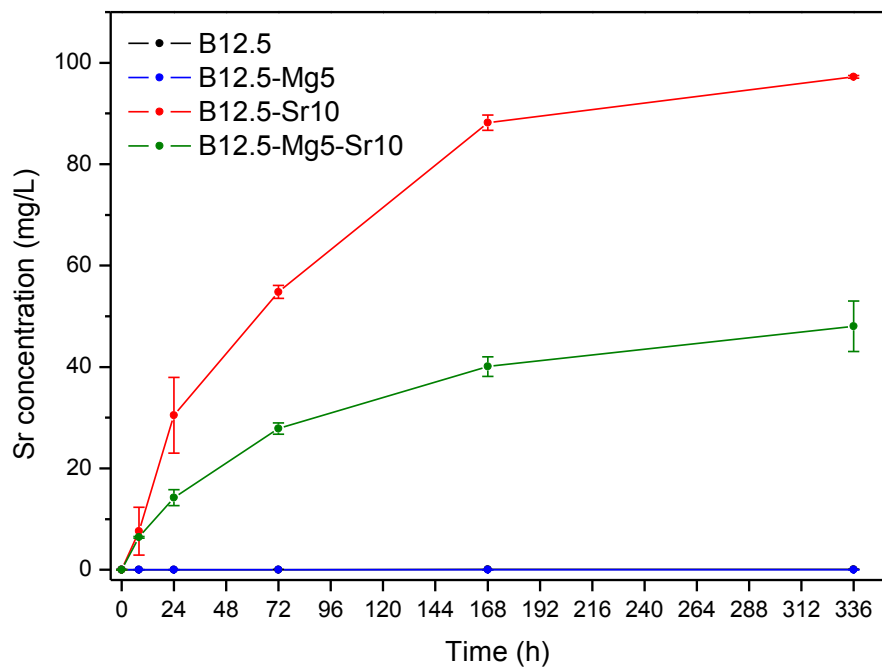
Figure D.2. Ionic concentrations (mg/L) of 1) Si, 2) B, 3) Ca, 4) P, 5) Mg and 6) Sr in SBF as a function of scaffold immersion time. Results are related to robocasted scaffolds.

1)
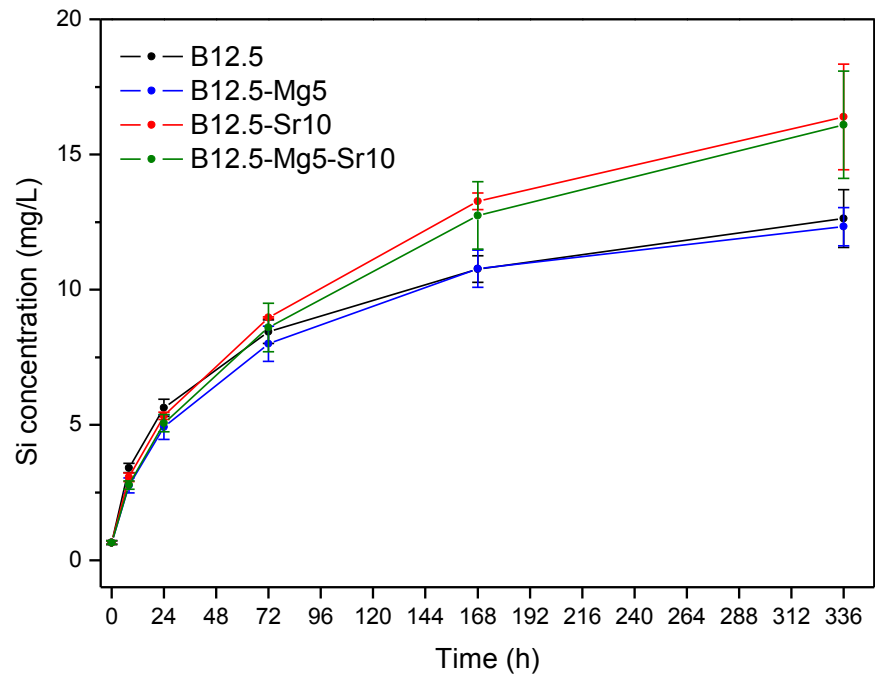
2)
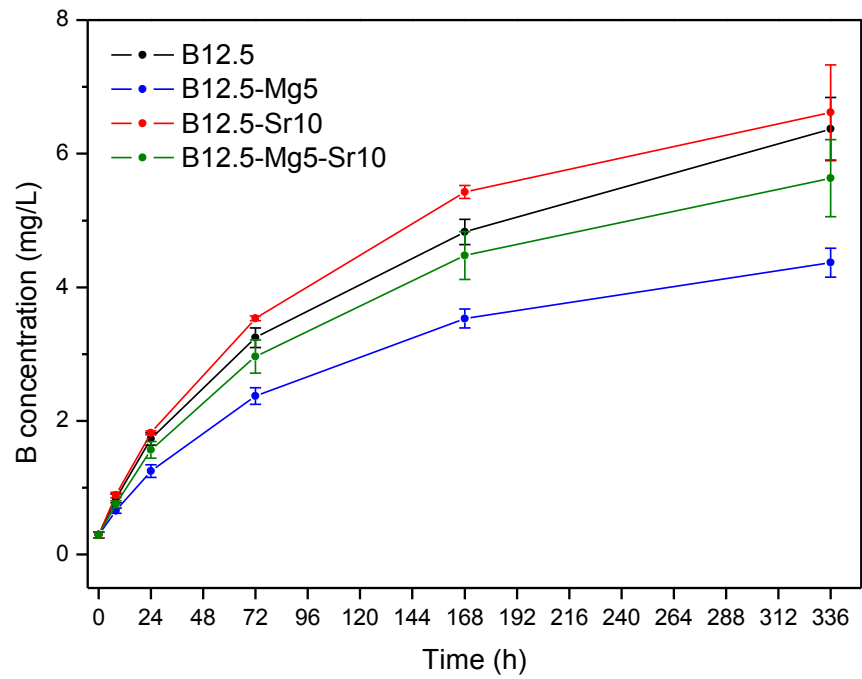
3)
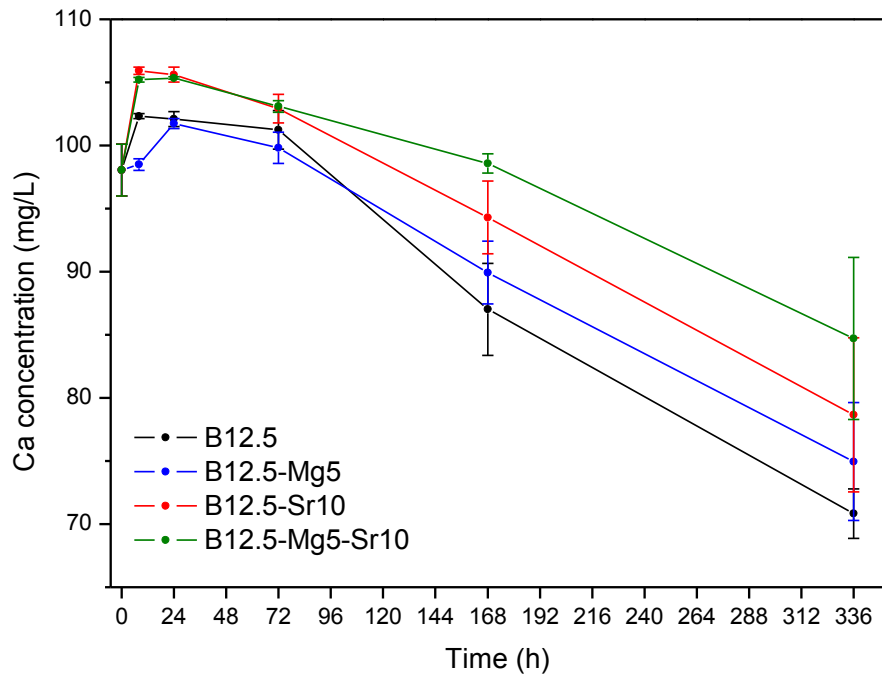
4)
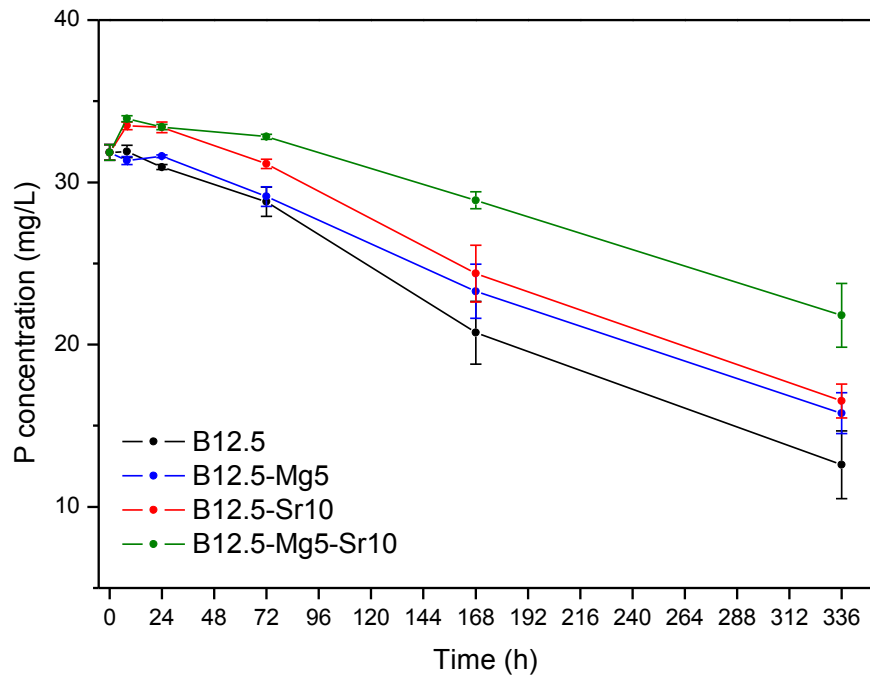
5)
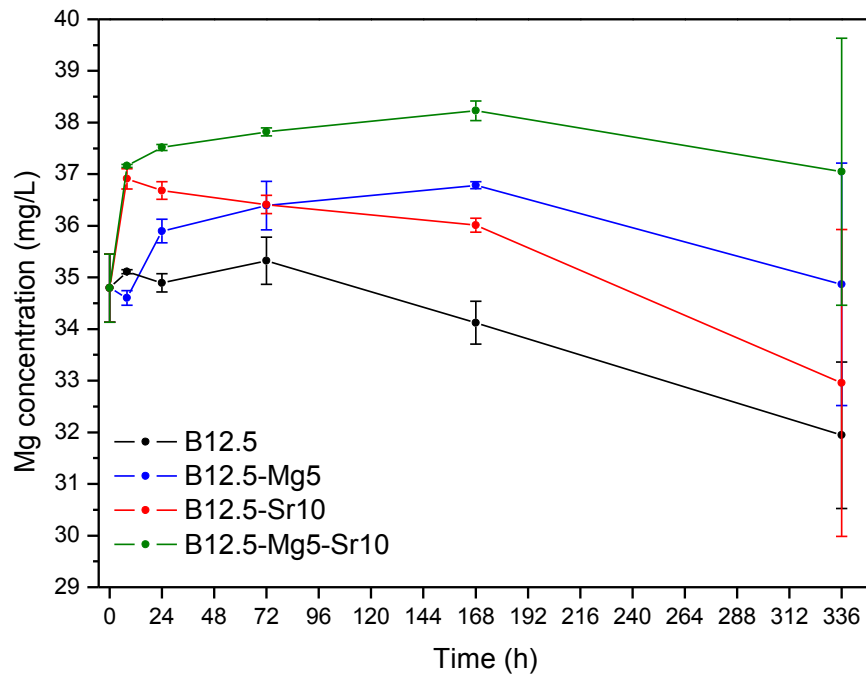
6)
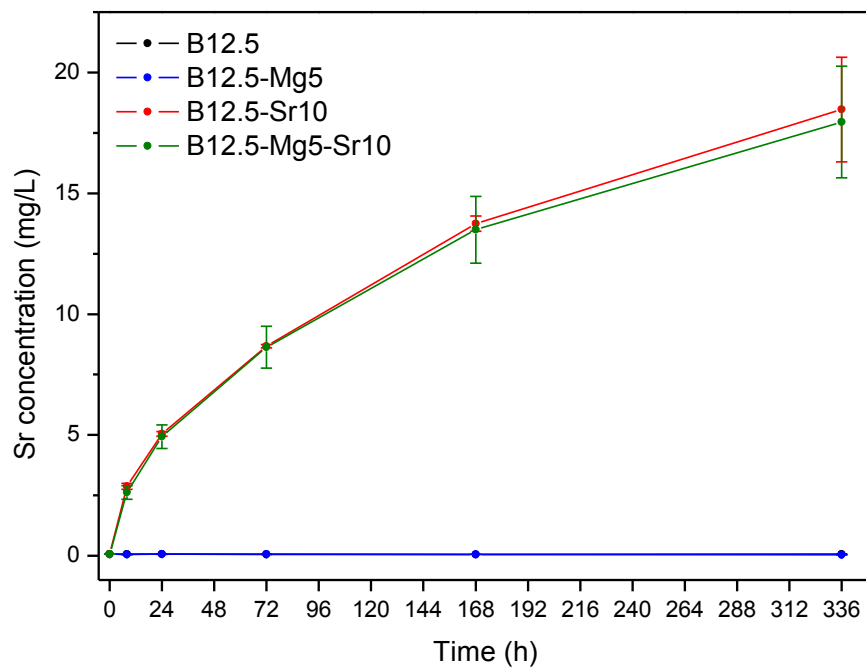
Figure D.3. *Ionic concentrations (mg/L) of 1) Si, 2) B, 3) Ca, 4) P, 5) Mg and 6) Sr in SBF as a function of scaffold immersion time. Results are related to composite scaffolds produced via scCO₂ method.*

APPENDIX E: FTIR SPECTRA

1)
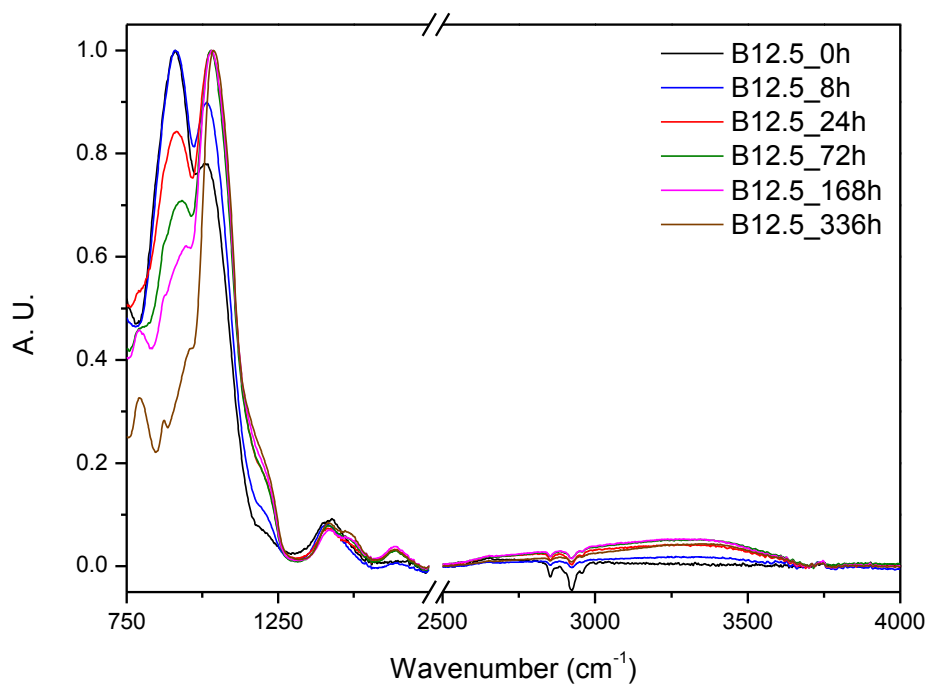
2)
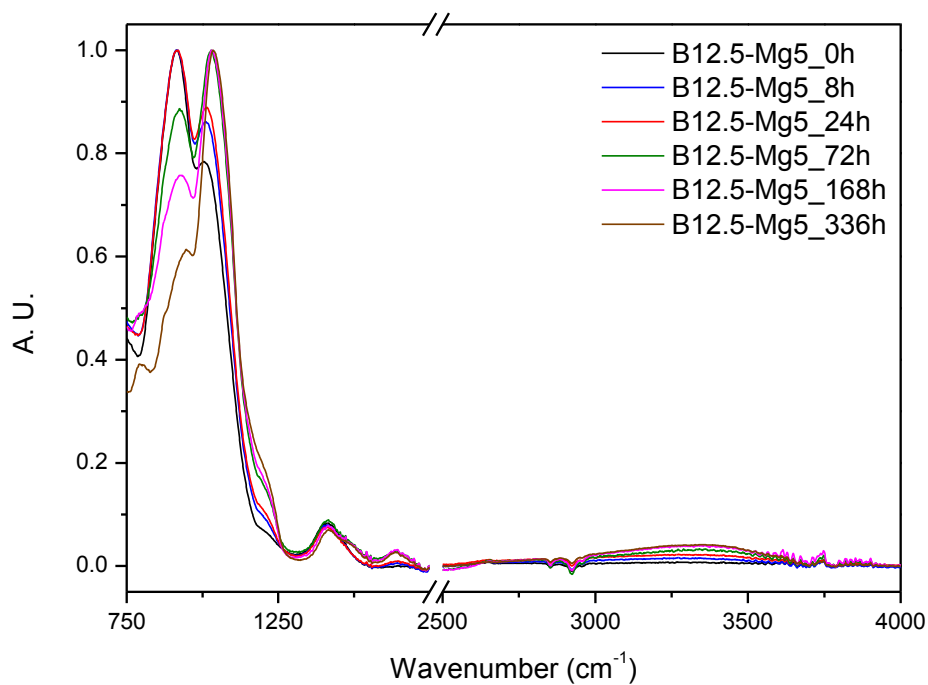
3)
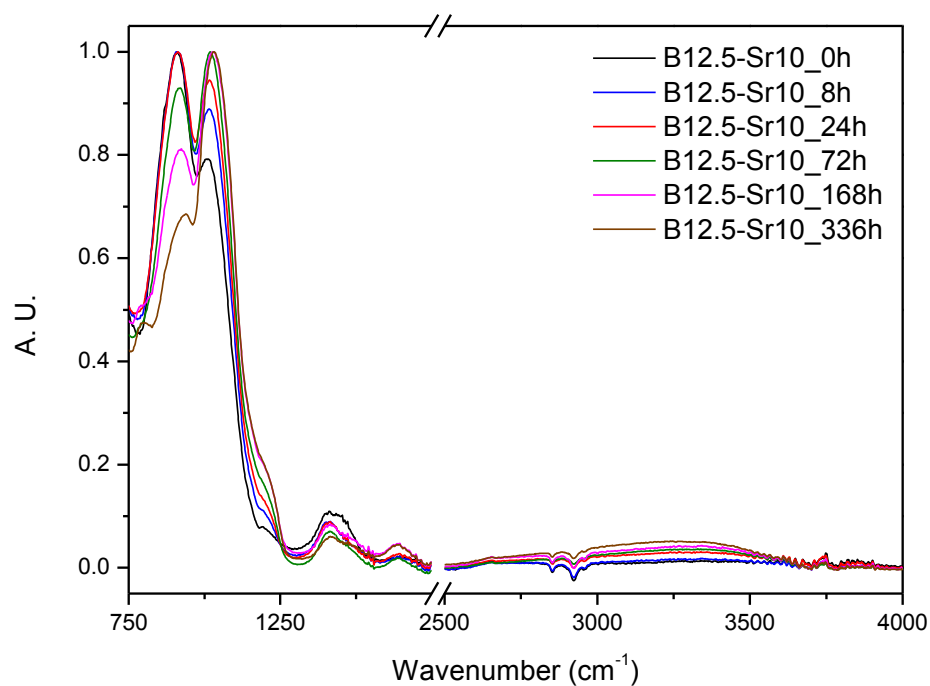
4)
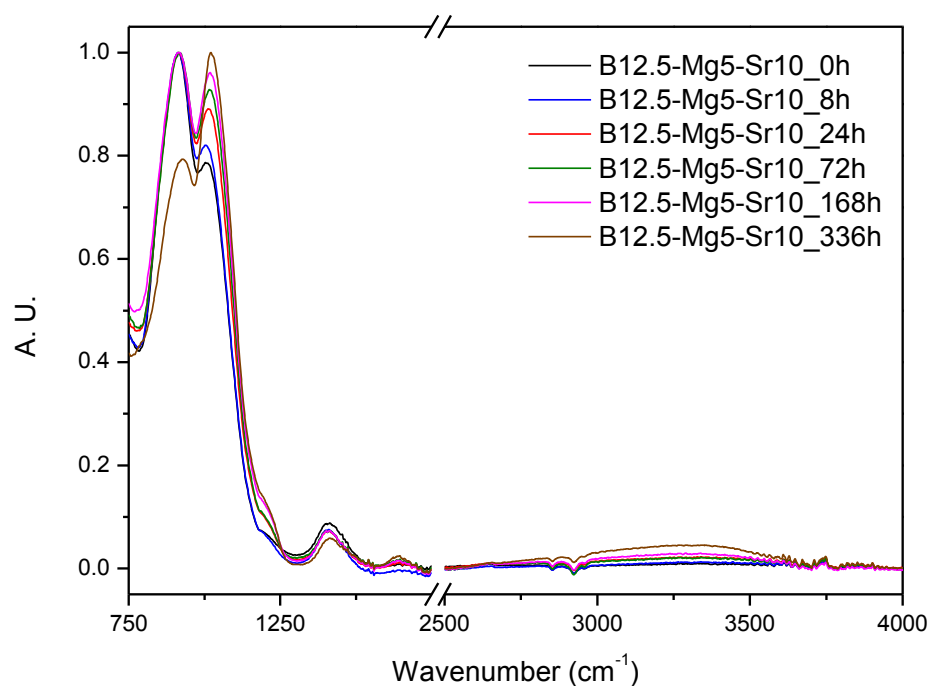
Figure E.1. *FTIR spectra of 1) B12.5, 2) B12.5-Mg5, 3) B12.5-Sr10 and 4) B12.5-Mg5-Sr10 scaffolds produced via porogen burn-off method after different SBF immersion times.*
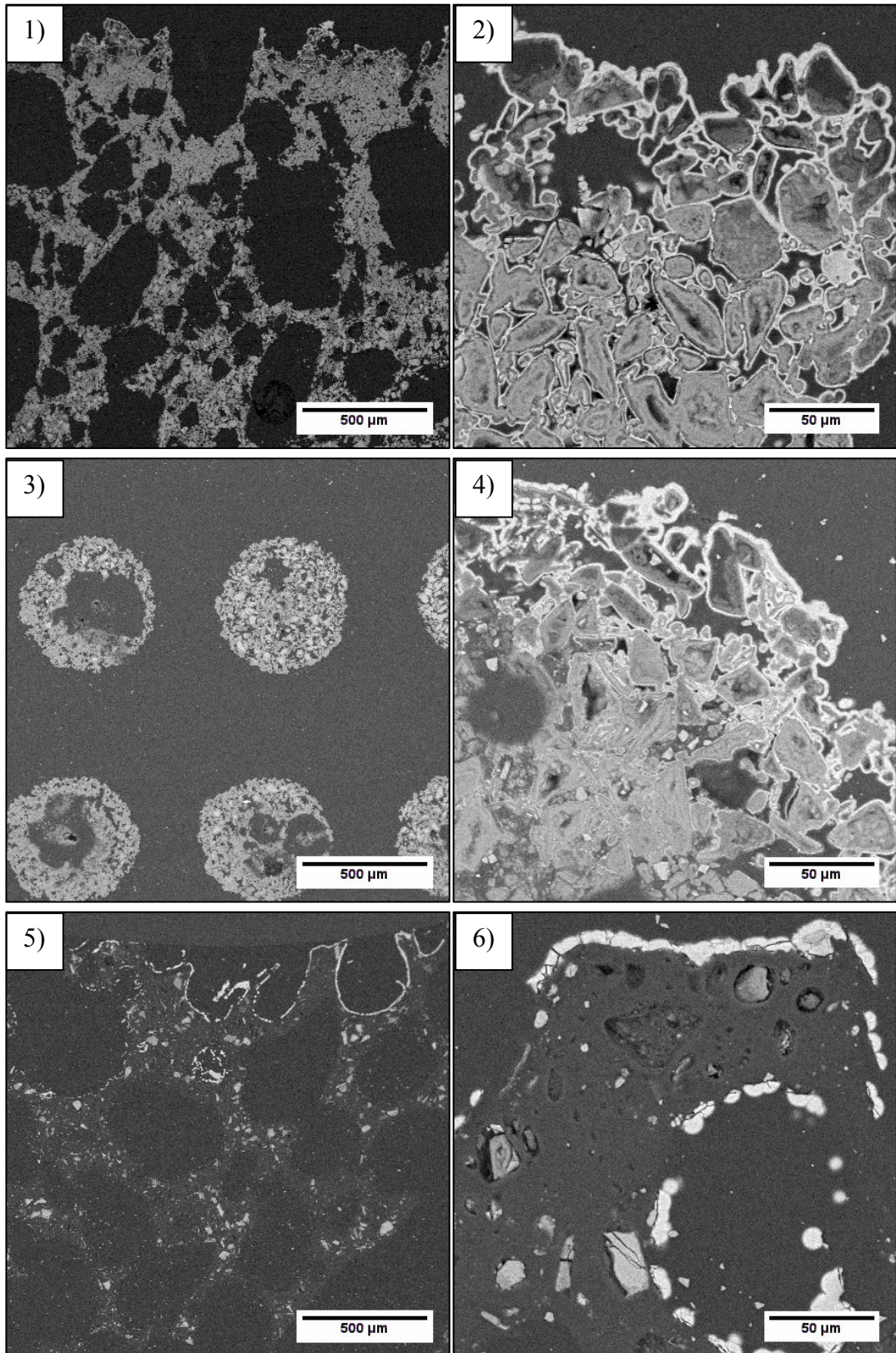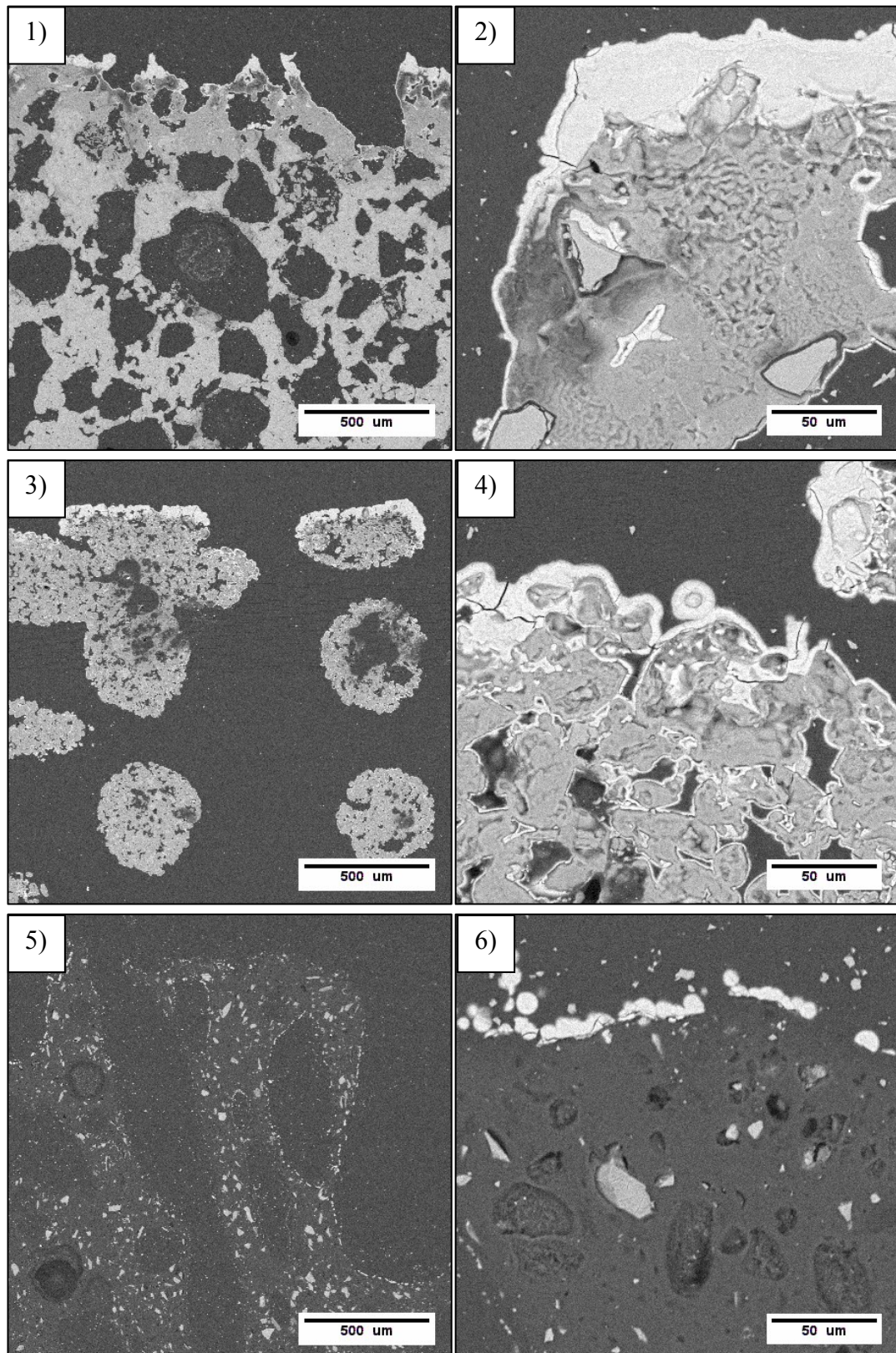
1)
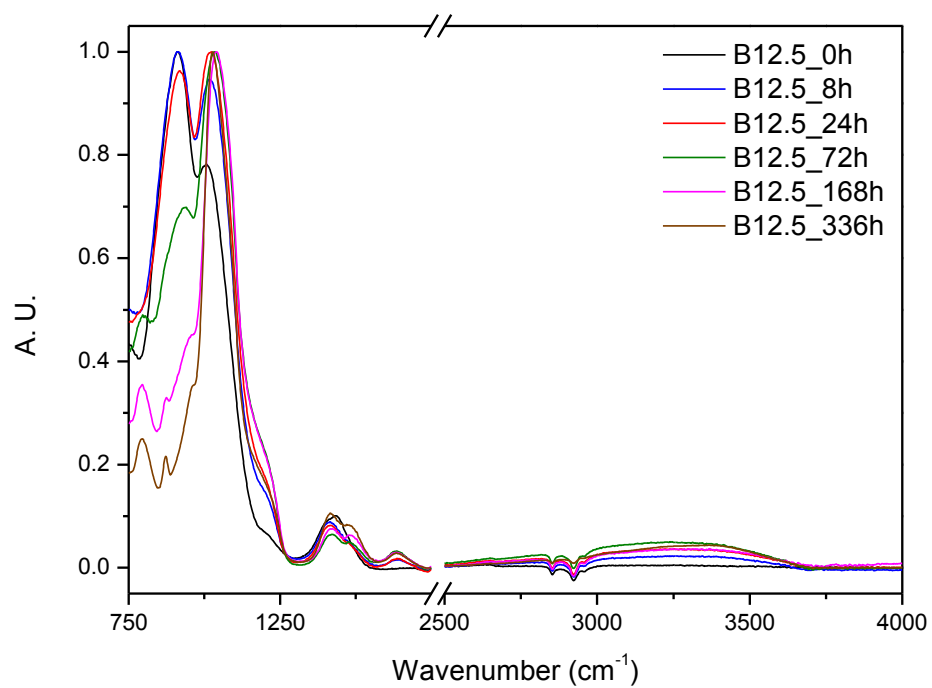
2)
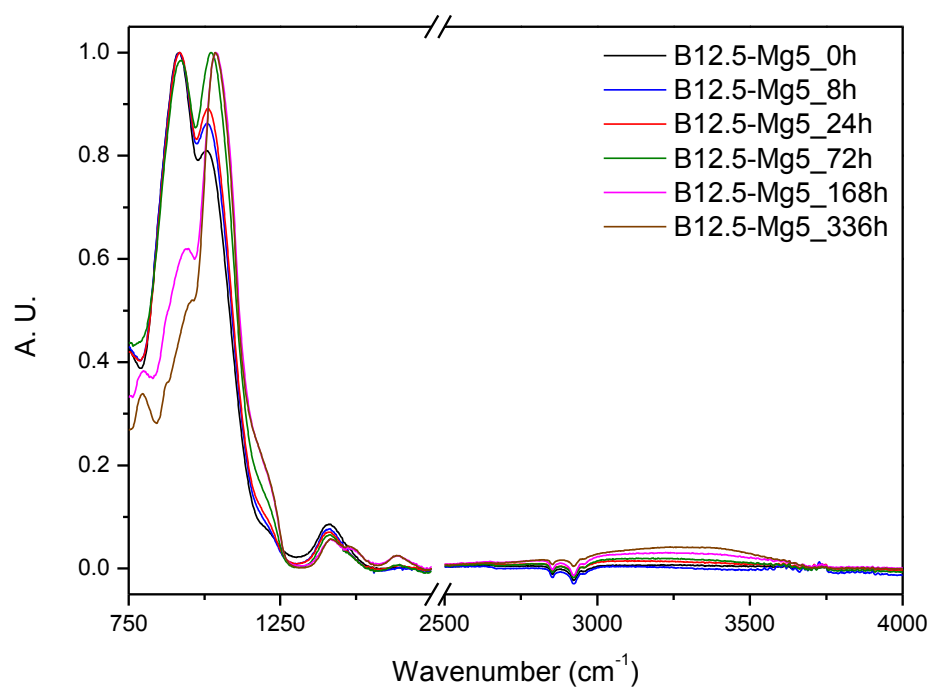
3)
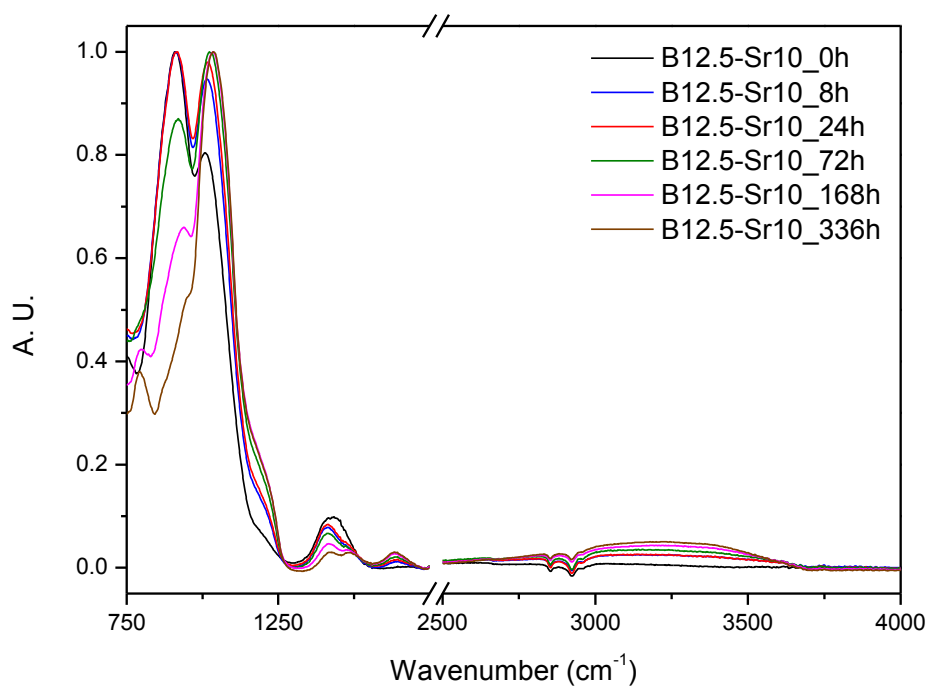
4)
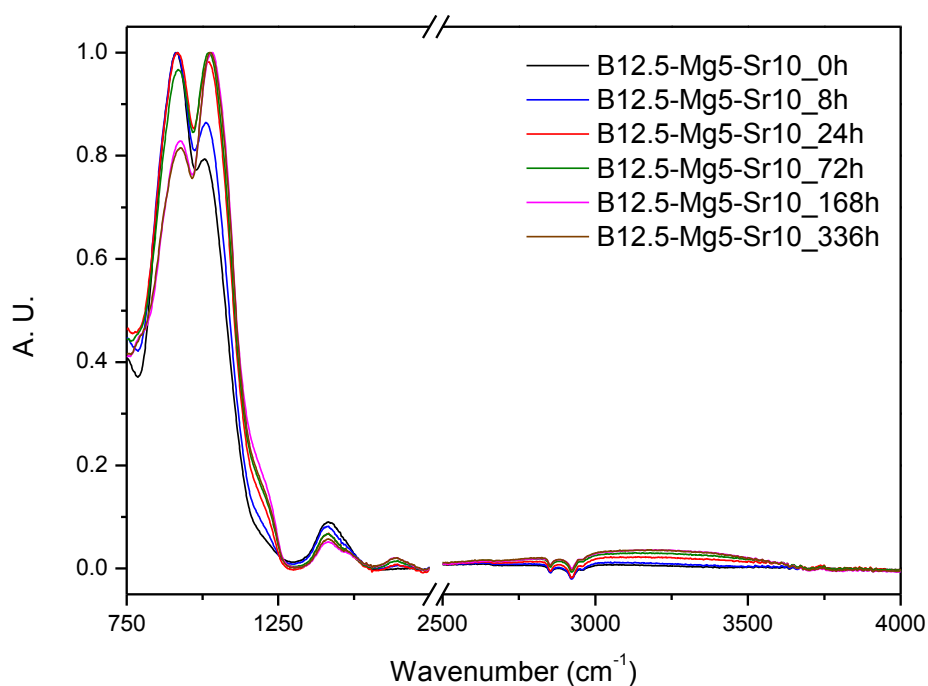
Figure E.2. *FTIR spectra of 1) B12.5, 2) B12.5-Mg5, 3) B12.5-Sr10 and 4) B12.5-Mg5-Sr10 scaffolds produced via robocasting after different SBF immersion times.*
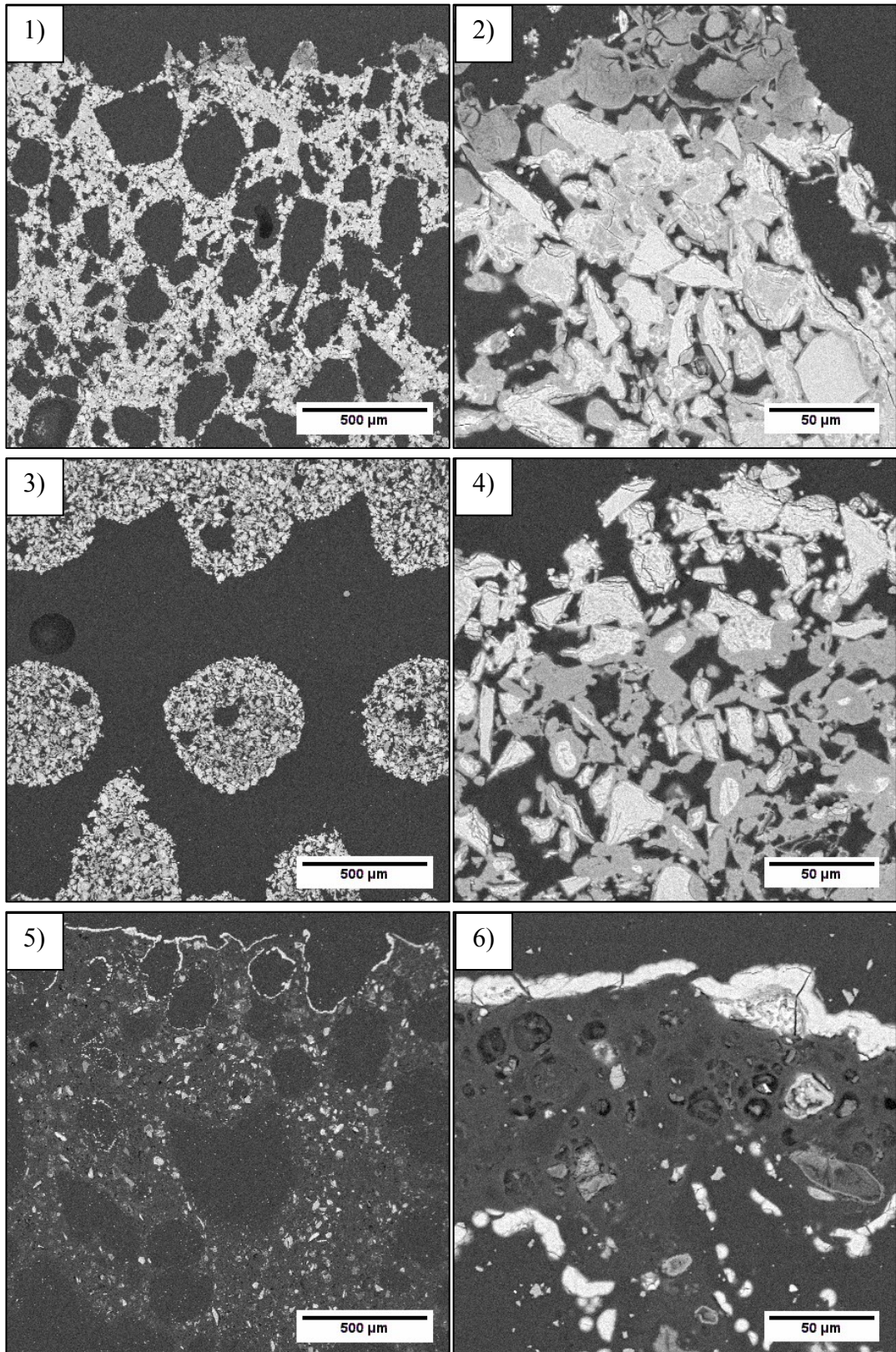
APPENDIX F: SEM IMAGES

Figure F.1. *SEM images of B12.5 scaffolds produced via porogen burn-off (1, 2), ro-bocasting (3, 4) and scCO$_2$ (5, 6) methods.*
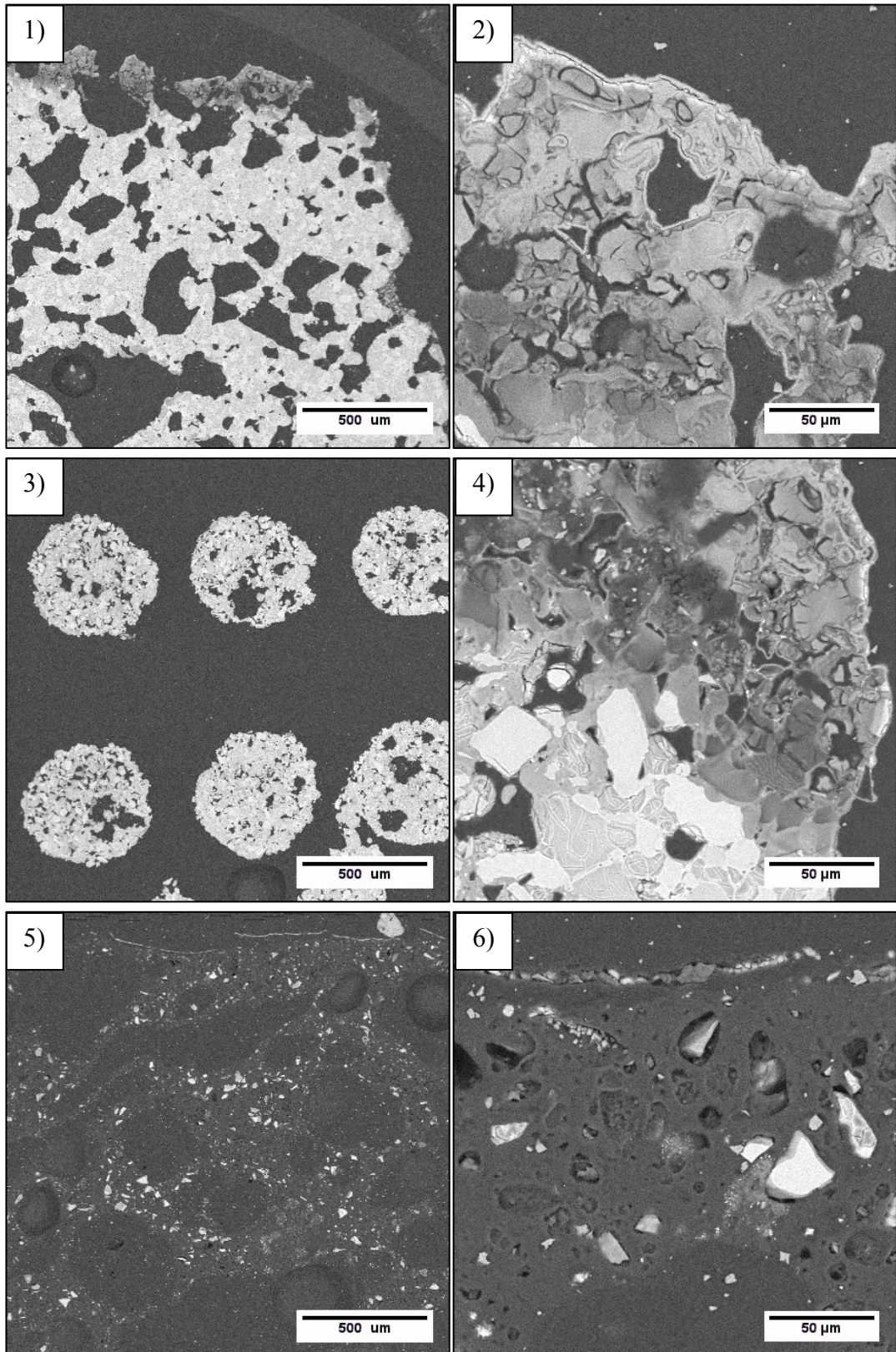
Figure F.2. *SEM images of B12.5-Mg5 scaffolds produced via porogen burn-off (1, 2), robocasting (3, 4) and scCO₂ (5, 6) methods.*

Figure F.3. *SEM images of B12.5-Sr10 scaffolds produced via porogen burn-off (1, 2), robocasting (3, 4) and scCO$_2$ (5, 6) methods.*

Figure F.4. *SEM images of B12.5-Mg5-Sr10 scaffolds produced via porogen burn-off (1, 2), robocasting (3, 4) and scCO$_2$ (5, 6) methods.*